ABSTRACT

Title of Dissertation:	TOWARDS AN UNDERSTANDING OF THE DEGRADATION MECHANISMS OF UHMWPE-BASED SOFT BALLISTIC INSERTS
	Zois Tsinas, Doctor of Philosophy, 2016
Dissertation directed by:	Professor Mohamad Al-Sheikhly, Department of Materials Science and Engineering

The objective of this work is to advance the field of lightweight and soft ultra-high molecular weight polyethylene (UHMWPE) inserts used in ballistic resistant-body armor, through the evaluation of chemical and physical degradation, and provide critical insight into the mechanisms involved. These inserts are comprised of non-woven UHMWPE fibers, foil-matrix low density polyethylene (LDPE), and a binder resin. Degradation of these components can be initiated by mechanical stress induced by routine use of the armor, thermal exposure due to storage and wear, and exposure to humidity and oxygen. Degradation of this system may include C-C and C-H bond ruptures resulting in C-centered radicals, thermo-oxidative reactions, as well as changes in the degree of crystallinity and the crystalline morphology of the UHMWPE

fibers. This is the first comprehensive study on degraded UHMWPE-fibers extracted from body armor that have been subjected to accelerated aging. Previous studies have only focused on oxygen uptake and changes in the tensile strength of virgin UHMWPE fibers as markers of degradation.

This work extends beyond oxygen uptake, to examine changes in the topography, the degree of crystallinity, and the crystal phases of UHMWPE fibers. Mechanical stress was found to be the main cause of kink band formation in UHMWPE fibers. Additionally, oxidation products and molecular oxygen were found to be at higher concentrations in the kink bands compared to other parts of the fiber. This suggests a synergistic effect between mechanical stress induced kink bands and oxidative degradation. The degree of crystallinity of the fibers did not change significantly, however morphological changes of the crystalline phases and changes in the orientation of the crystals were observed. Finally, this study investigates, for the first time, the degradation of the binder material that retains the fibers together in the laminates. The binder resin used in the laminates was identified to be a copolymer of polystyrene and polyisoprene, which undergoes oxidative degradation accompanied by a decrease in the weight-average molecular weight.

TOWARDS AN UNDERSTANDING OF THE DEGRADATION MECHANISMS OF UHMWPE-BASED SOFT BALLISTIC INSERTS

by

Zois Tsinas

Dissertation submitted to the Faculty of the Graduate School of the
University of Maryland, College Park, in partial fulfillment
of the requirements for the degree of
Doctor of Philosophy
2016

Advisory Committee:
Professor Mohamad Al-Sheikhly, Chair
Professor Christopher Jewell
Professor Peter Kofinas
Professor Amde M. Amde
Dr. Amanda L. Forster

Dedication

This thesis is dedicated to my dear grandparents Zois and Chariclia Tsinas.

Acknowledgements

First, I would like to acknowledge my advisor, Professor Mohamad Al-Sheikhly. If it was not for his continued support, enthusiasm for science, and guidance, I would not have been able to reach higher and to tackle all the difficulties during my time in the Ph.D. program. Thank you from the bottom of my heart for your trust, advice, and encouragement, I have learned so much.

I would also like to thank my supervisor at NIST, Amanda Forster, for the many hours she spent guiding and encouraging me. Without our fruitful conversations, and her technical assistance, this thesis would have never been possible. Acknowledgements are due to Professor Amde M Made and Professor Christopher Jewell for agreeing to serve on my thesis committee and for sparing their invaluable time reviewing this thesis. Also, special thanks to Professor Peter Kofinas for his support, guidance, and advice throughout all these years here at the University of Maryland.

I would like to thank my colleagues in the Lab for their support, patience, and limitless help: the postdoc, Dr. Ileana Pazos; the graduate students, Travis Dietz, Donald Jenket, Najlaa Hassan, Kevin Mecadon, Azadeh Farzaneh, Salimeh Gharazi, and Matt LeBlanc; all the undergraduate students who contributed to this work, Rohan Mittal, Miriam Silton, Aphrodite Strifas, and Harris Tsinas. All your hard work does not go un-noticed. Thank you for all that you have taught me, and all the memories and experiences you have shared with me. I will never forget our time together inside and outside of the lab.

Lastly, but not the least, I'd like to thank my dear family: Dad, Mom, Harris, and Maria. Without you all, I would not be the person I am today, and would not have been able to achieve what I have, so far from my comfort zone. Thank you all for your love and support.

Table of Contents

List of Figures

Chapter 1: Introduction to UHMWPE Soft Ballistic Protective Inserts

1.1 Chapter Overview

In this chapter, the use of high strength polymer fibers in body armor applications and especially ultrahigh molecular weight polyethylene (UHMWPE) fibers, is introduced. The components of UHMWPE body armor are identified and their synthesis, structure, morphology, and properties are discussed.

1.2 History of Polymers as Ballistic Inserts

High strength polymeric fibers produce light weight and flexible body armor. Historically, little emphasis was placed on the long-term performance of armor materials. However, there was a renewed effort to understand the body armor failure mechanisms based on an incident on June 23, 2003, where the armor of a police officer was penetrated by .40 caliber rounds that the vest was rated to stop [1]. After this incident, the law enforcement community focused immediately on the materials used to make that specific type of armor. The armor was made from poly(p-phenylene-2,6-benzobisoxazole), also known as PBO. After several years of research, it was determined by the law enforcement and research community that the use of PBO fibers in ballistic resistant body armor faced some major challenges. These challenges were due to the susceptibility of the material to degradation from environmental and wear conditions. Specifically, it has been shown that oxazole ring opening is a major indicator of hydrolysis and chain scission of PBO. As a result, deterioration of mechanical properties and a reduction in ballistic performance occurs [2-5]. Therefore, it is of major importance to study the effects of elevated temperature, mechanical stress, and oxygen solubility and diffusion into other commonly used materials comprising soft

ballistic inserts, and work towards better understanding the potential degradation mechanisms involved [1, 6, 7].

1.3 UHMWPE Soft Ballistic Inserts

Modern body armor is commonly designed using flexible, ballistic-resistant fabrics made from UHMWPE due to its ability to be processed into fibers with high tensile strength to weight ratios. [8, 9]. These soft ballistic inserts are comprised of UHMWPE fibers, foil-matrix low density polyethylene (LDPE), and resin material (e.g., polyisoprene), which serves as a binder [10, 11]. In this work we evaluate the long term stability of the UHMWPE fibers and the binder extracted from body armor subjected to accelerated aging.

1.3.1 Polyethylene Background

Polyethylene is produced from chain polymerization of the monomer ethylene (C_2H_4) that consists of only carbon and hydrogen atoms. Ethylene is a gas having a molecular weight of 28 g/mol and can be polymerized using different conditions of temperature and pressure, as well as in the presence or absence of catalysts (Figure 1) and produce a wide variety of polyethylenes $(C_2H_4)_n$ (where n is the degree of polymerization) with different properties [12].

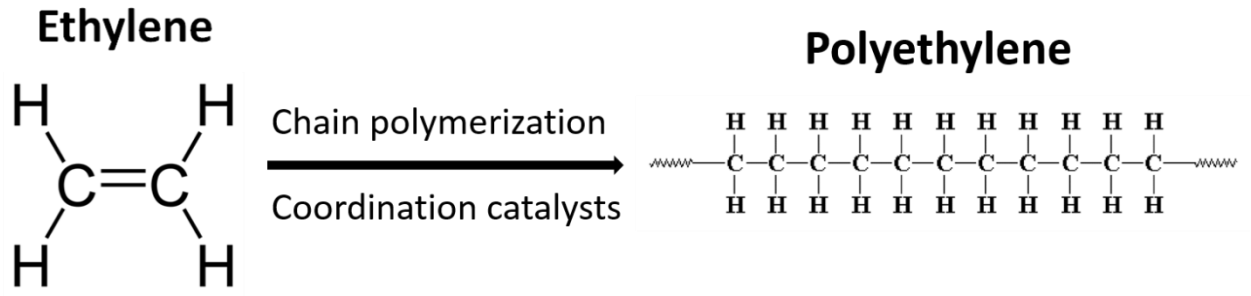

Figure 1. Free radical polymerization of ethylene in the presence of Ziegler-Natta catalysts results in linear polyethylene.

The molecular weight of the polyethylene polymer affects its mechanical properties. However, there are cases where a series of polyethylene samples of the same molecular weight have significant differences in their properties. This is attributed to their degree of crystallinity [12]. In some cases, such as in free radical polymerization of ethylene, the percent crystallinity of the polymer produced is low. During free radical polymerization, the monomers can form long side chains, known as branches, producing low-density polyethylene (LDPE) with a crystallinity between 40 and 60% and density between 0.91 and 0.93 g/cm^3 [13]. Increasing the crystallinity of the polymer can significantly increase the melting point, the density of the polymer, and enhance its mechanical properties [12]. Therefore, alternative methods of polymerization allowing for the production of polymers with higher crystallinity were developed. The addition of coordination catalysts, also known as Ziegler-Natta catalysts, prevents the branching that occurs in free radical polymerization of ethylene. This results in linear polyethylene with a crystallinity ranging from 70 to 90% depending on the molecular weight of the polymer and post treatment methods used [14]. Also, the density has a much smaller range compared to LDPE, between 0.94 and 0.97 g/cm^3.

Ultimately, polyethylene produced with coordination catalysts has higher molecular weight compared to LDPE [13, 15, 16].

The addition of coordination catalysts, mainly comprising of a transition metal compound (Ti, Cr etc.) and a metal alkyl (usually Al) are used to produce an organometallic complex that serves as the active site for polymerization. Polymerization using these catalysts results in the absence of termination reactions leading to a "living" polymerization (Figure 2). Living polymerization means the polymerization continues until the ethylene monomer in the reaction is entirely depleted. This type of polymerization produces linear polyethylene which could be high density (HDPE), when the average molecular weight of the polymer chains is between 20,000 and 200,000 g/mol, or ultrahigh molecular weight (UHMWPE) when the average molecular weight is above 2 million g/mol, depending on the amount of ethylene available.

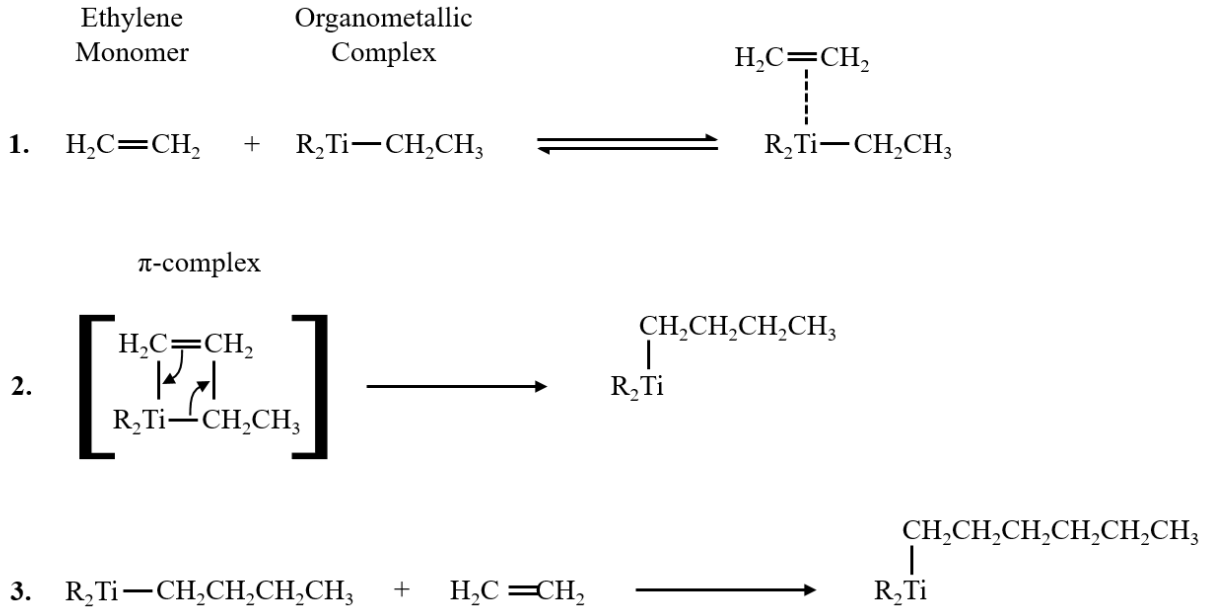

Figure 2. Reaction scheme for the transition metal catalyzed living polymerization of ethylene. During the second step of the reaction the Ti d-orbitals interact with the π electron cloud of ethylene. The chain propagation continues until the ethylene monomer is consumed.

The difference between HDPE and UHMWPE processes mainly rely on optimizing the usage of properly tailored catalysts and the polymerization conditions. The catalyst used in the process is of paramount importance. The most recent catalysts used for the production of UHMWPE are metallocenes catalysts based upon metal complexes of cyclopentadienyl, such as titanocene dichloride $(C_5H_5)_2TiCl_2$, followed by activation with aluminum alkyls, such as $Al(CH_3)_3$ [17]. The activation begins with alkylation of the titanium center, followed by coordination of the remaining chloride to the aluminum [18]. The final ratio of Al/Ti and the percentage of each oxidation state of Ti (Ti^{4+}, Ti^{3+}, and Ti^{2+}) will affect the molecular weight of the resulted polymer. The precise ratio of Al/Ti varies according to the pressure conditions and the present of trivalent titanium in the catalyst system [19, 20]. Additionally, in 1980, Kaminsky reported that upon adding water to the catalyst system the ethylene polymerization was dramatically increased [21, 22]. The water was determined to react with trimethyl aluminum to produce methylamunioxane (MAO), that worked as a cocatalyst to increase the activity of ethylene polymerization. Briefly, the methyl groups of the MAO displace two of the chlorine atoms from the metal complex, then one of the methyl groups is eliminated and the active polymerization catalyst forms a π-complex into witch the ethylene monomer is inserted, as shown in Figure 3 [23].

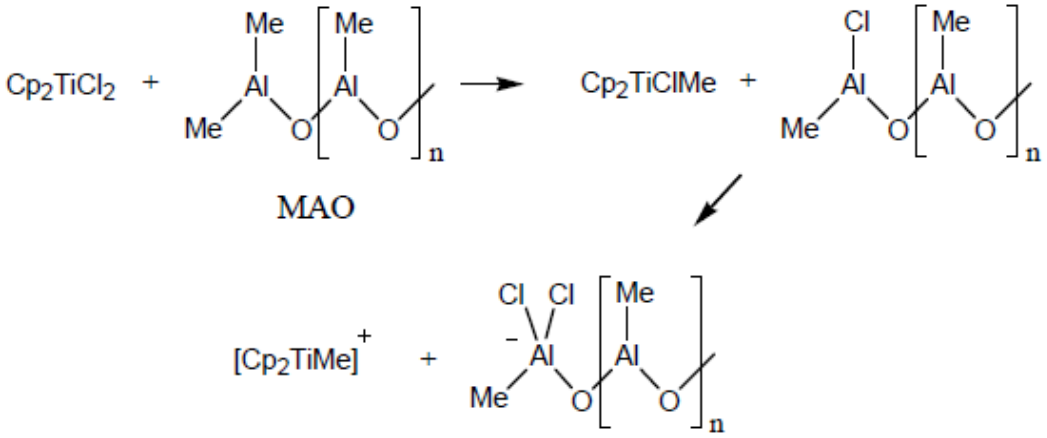

Figure 3. Mechanism of MAO activation [24].

The most recent processes for the production of UHMWPE involve the addition of hydrogen into the reaction along with the monomer that will lead to chain transfer reactions and help control the polymerization reaction and increase the conversion of ethylene to polyethylene, leading to a higher molecular weight product [19]. Also, inert solvents are used in the process to dissipate heat (as this is a highly exothermic reaction) and control the solubility of hydrogen and ethylene. Solvents that increase the solubility of ethylene will increase the rate of the polymerization reaction, by increasing the concentration of the monomer in solution, leading to higher molecular weight products [20]. Another important parameter is the temperature. As the temperature increases, the rate of the polymerization reaction increases. However, if the temperature is too high, spontaneous chain transfer can occur and abstract the catalyst from the polymer chain, prematurely terminating the polymerization. Therefore, it is important to finely tune the temperature of the reaction to increase the molecular weight of the polymer.

HDPE and UHMWPE can have the same density, but the molecular weight of UHMWPE is much higher. In general, high crystallinity in polyethylene can be achieved by a slow cooling rate of the polymer melt and post processing methods, such as drawing. In addition, branching will adversely affect the degree of crystallinity [15, 16, 25]. The typical crystal structure of UHMWPE is shown in Figure 4. The crystals in polyethylene orient in structures known as crystalline folded lamella with a typical thickness of 10 – 50 nm and length of 10 – 50 μm [26]. The lamellae are separated by amorphous regions that are approximately 50 nm in length [27].

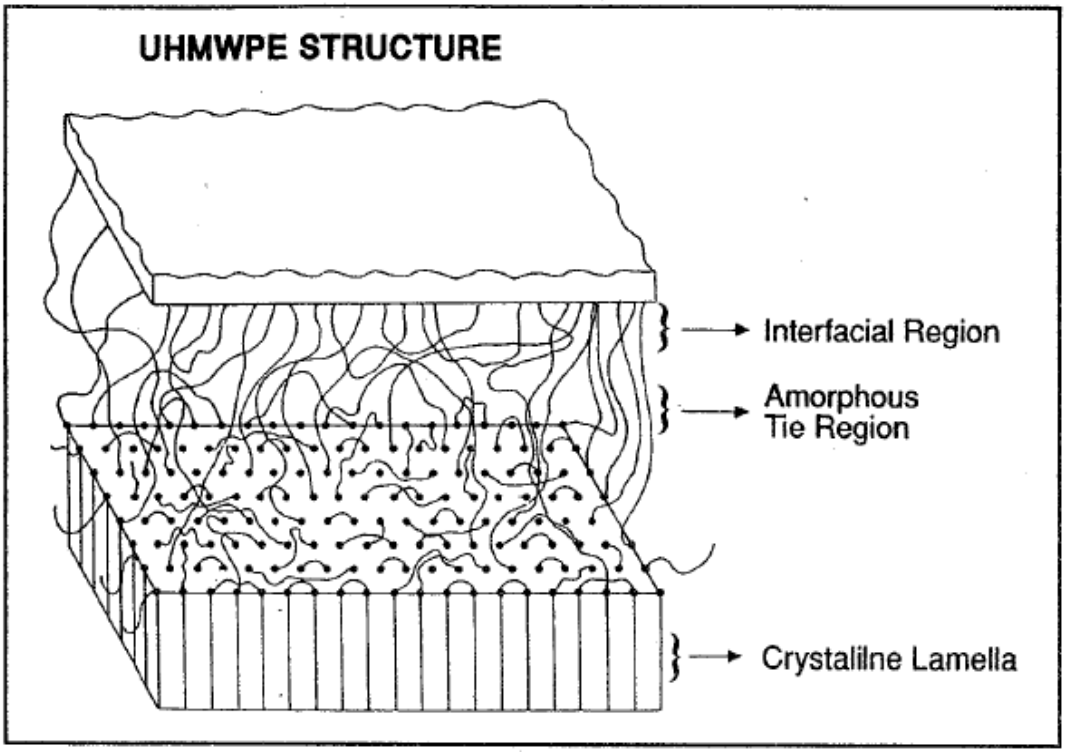

Figure 4. Schematic representation of the semi-crystalline structure of UHMWPE. A polymer chain can tie in the small crystalline lamellae and transverse the amorphous regions into the next crystallite [28].

It is important to note that one UHMWPE chain can exist in the amorphous phase as well as orient in many crystalline lamellae separated by tie molecules, all of which are part of the same polymer chain, as shown in Figure 5 [25]. Tie molecules are segments of the polymer chain which initiate in one crystalline domain, cross the amorphous region and connect to adjacent crystalline domain providing strength to the semi-crystalline structure. They are responsible for polyethylene properties such as high elongation, toughness, and environmental stress cracking.

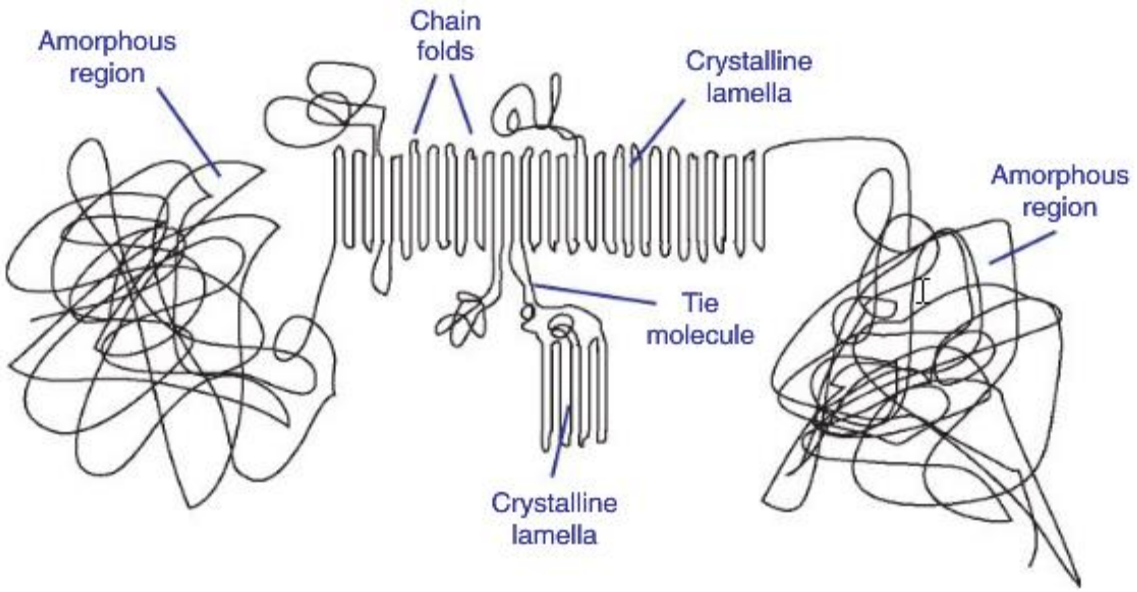

Figure 5. The different morphological structures that one UHMWPE polymer chain can exist [25].

The properties of polyethylene can be described by the average molecular weight, crystallinity, branching, density and oxidation products formed during post-processing. Properties of polyethylene that concern only slight movements of portion of the samples relative to each other, such as the melting point, softening point under low load, Young's modulus in tension, bending modulus, yield point (tension to cause cold-drawing), and surface hardness are all strongly dependent on crystallinity and very little on average molecular weight [12]. The degree of crystallinity affects the extent of the intermolecular secondary bonding (van der Waals interactions). In the crystalline regions of a semi-crystalline polymer in which molecular chains are tightly packed, extensive secondary bonding exists between adjacent chain segments. This secondary bonding is much less present in the amorphous areas. Thus, properties such as hardness, Young's modulus, and bending modulus increase significantly with degree of crystallinity [29]. Conversely, properties that involve more extensive movement, and rupture of the samples, such as

tensile strength, tear resistance, and low temperature brittle point can be mainly attributed to the average molecular weight of the polymer and to a lesser extent on crystallinity [12]. The effects of percent crystallinity and molecular weight on the physical properties of polyethylene are summarized in Figure 6.

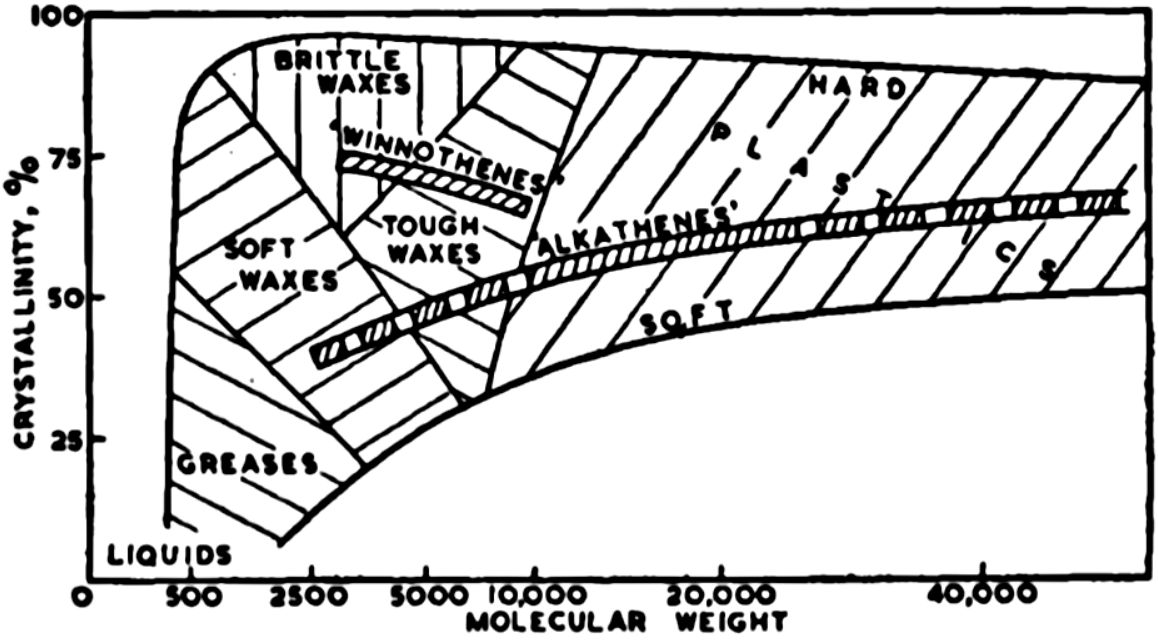

Figure 6. The influence of degree of crystallinity and molecular weight on the physical properties of polyethylene [12].

1.3.2 Manufacture of UHMWPE Fibers

UHMWPE has been commonly used to produce high strength fibers with superior fatigue, corrosion, and chemical resistance as compared to other materials [30-33]. UHMWPE fibers are commercially manufactured by two companies, DSM and Honeywell, who market their fibers as Dyneema and Spectra, respectively. The technique used to produce these fibers is known as gel

spinning (Figure 7), in which UHMWPE resin is dissolved in a solvent at low concentration and elevated temperature, and is then extruded through a spinneret into a water bath, for coagulation [34, 35].

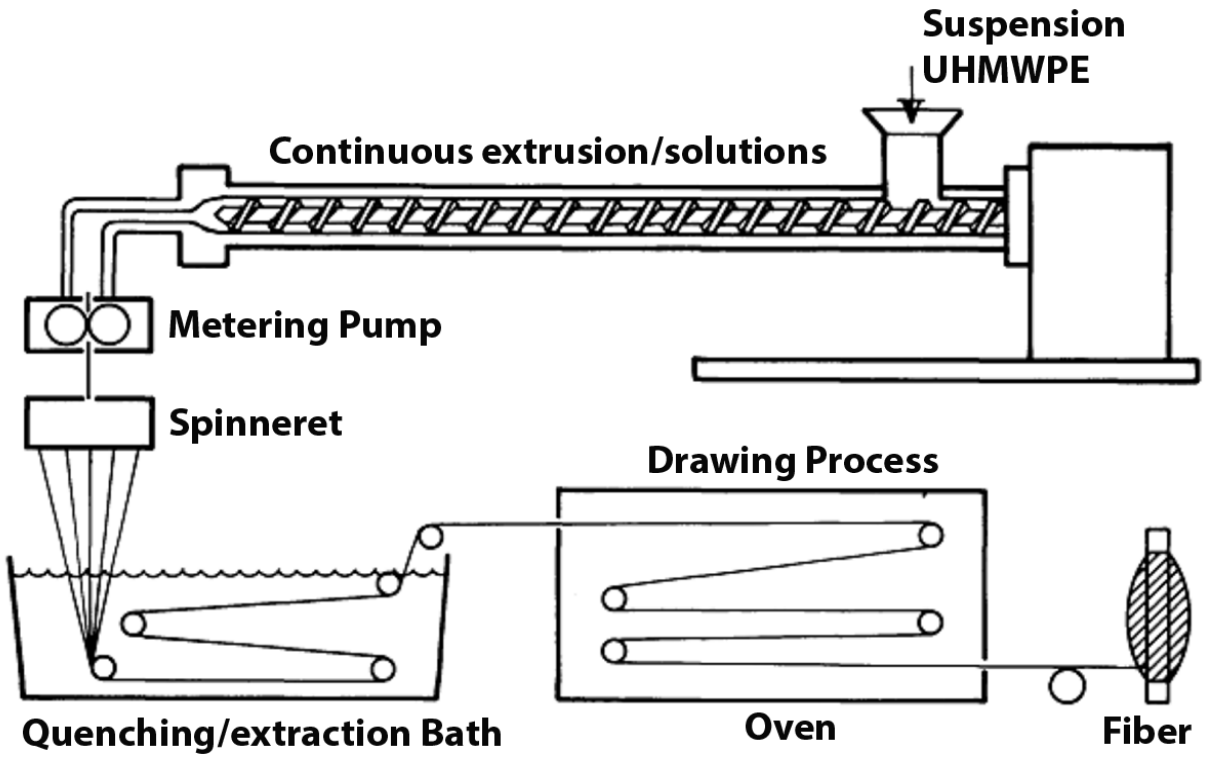

Figure 7. Schematic of the gel spinning and drawing process. Figure taken and modified from Yao et al. [36].

The resulting fibers are transported to an oven to remove any residual solvent and then treated with dilute solution to disentangle the polymer chains and prepare them for orientation through a process known as "super-drawing". This process involves extending the filaments 50 to 100 times their original length to produce highly-oriented fibers with a crystallinity of approximately 85% [37, 38]. According to a model proposed by Peterlin et al., during the drawing process, blocks of folded chains are extracted from the crystalline lamellae and extended to be

incorporated in the growing fibril, as shown in Figure 8 [39, 40]. A large portion of the lamellar structure of UHMWPE converts to extended orthorhombic, monoclinic, and hexagonal crystals during this process, the ratio of which varies according to the specific conditions (drawing ratio, and temperature) used during the drawing process [41, 42]. In general, as the drawing ratio increases, the amorphous region of the polymer decreases, the lamellar crystals decrease and the percentage of extended orthorhombic crystals increase, while an increase in the temperature during the drawing process leads to the formation of a hexagonal crystal phase [43].

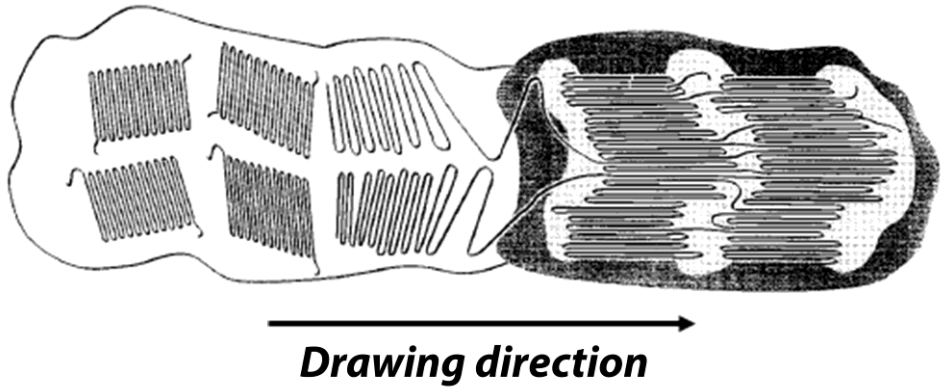

Figure 8. Schematic of the drawing process of UHMWPE fibers according to Peterlin et al. [39].

1.3.3 Structure of UHMWPE Fibers

There are several different theories as to the structure of highly oriented UHMWPE fibers. Generally, each UHMWPE fiber is around 10 to 12 μm in diameter and is considered to consist of about 150 macrofibrils. The diameter of these macrofibrils ranges from 0.5 to 2 μm [44]. Three models can be found in the literature to describe the microstructure of a macrofibril. In the first model, a macrofibril is believed to consist of highly extended and oriented chains forming crystalline microfibrils. According to this model, one macrofibril consists of about 2,500 microfibrils, each with a diameter of ~20 nm, as shown in Figure 9 [44].

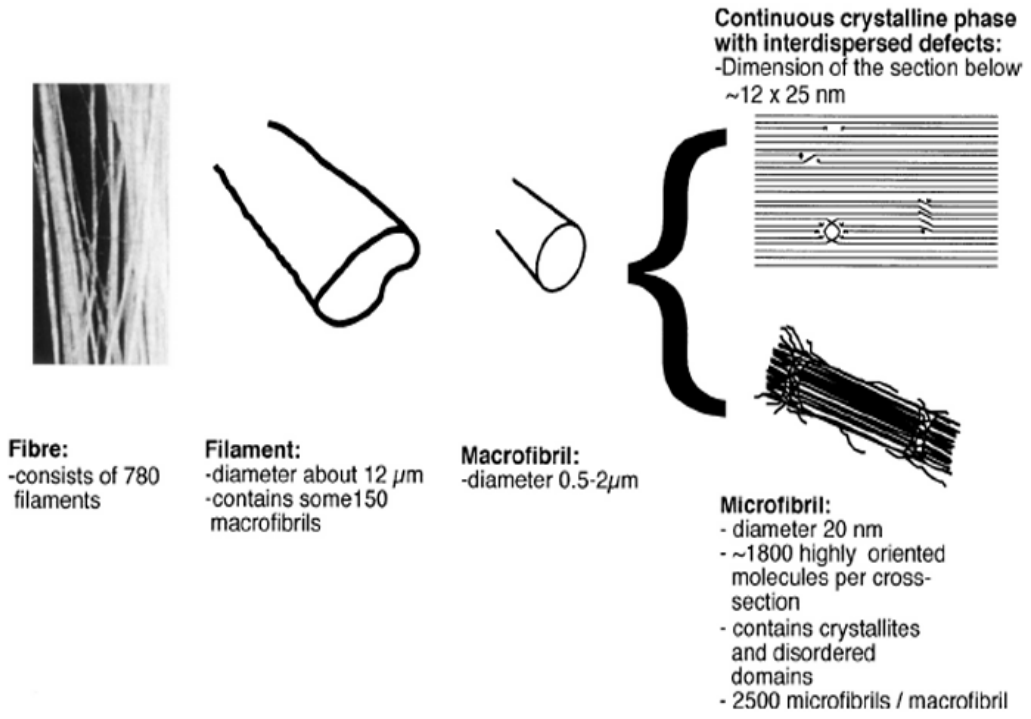

Figure 9. Macroscopic and microscopic structure of UHMWPE fibers [44].

The second model, also known as the continuous crystalline model, suggests that macrofibrils are comprised of a mostly continuous crystalline phase with rare, dispersed defects (amorphous areas) [44]. These two structural models transfer the intensity of lateral stress differently, since microfibrils behave as structural entities only in the case where lateral interactions are smaller than the intra-microfibrillar cohesion [44]. A third model combines aspects of the two previous models and it is known as the crystalline bridge model [44]. According to this model, macrofibrils consist of highly oriented crystalline regions, interfibrilar zones, and non-crystalline regions that contain more or less taut tie-molecules. A schematic representation of this model is shown in Figure 10.a [44]. This model allows for stronger lateral interactions across a microfibrillar interface through crystalline regions, and a much weaker interactions with the non-crystalline regions [44]. A similar, but more detailed model is proposed by Hu, et. al. in 2000, as

shown in Figure 10.b. According to Hu, in every microfibril the crystalline phase is continuous but each individual polymer chain is not in a continuous crystal. The amorphous phase is dispersed in the crystalline phase and most of the chains are alternately crystalline and amorphous. There are voids between the fibrils and the segments of the polymer chains on these surfaces are highly mobile [45]. Five morphological components were identified in the study: 83% crystal core, of which 80% is orthorhombic and 3% monoclinic, with a thickness of ~100nm; 5% disordered all-trans interfacial and/or tie molecules; 11% amorphous regions with diameters around 10 nm; and 1% highly mobile segments, probably at void surfaces or traversing voids [45].

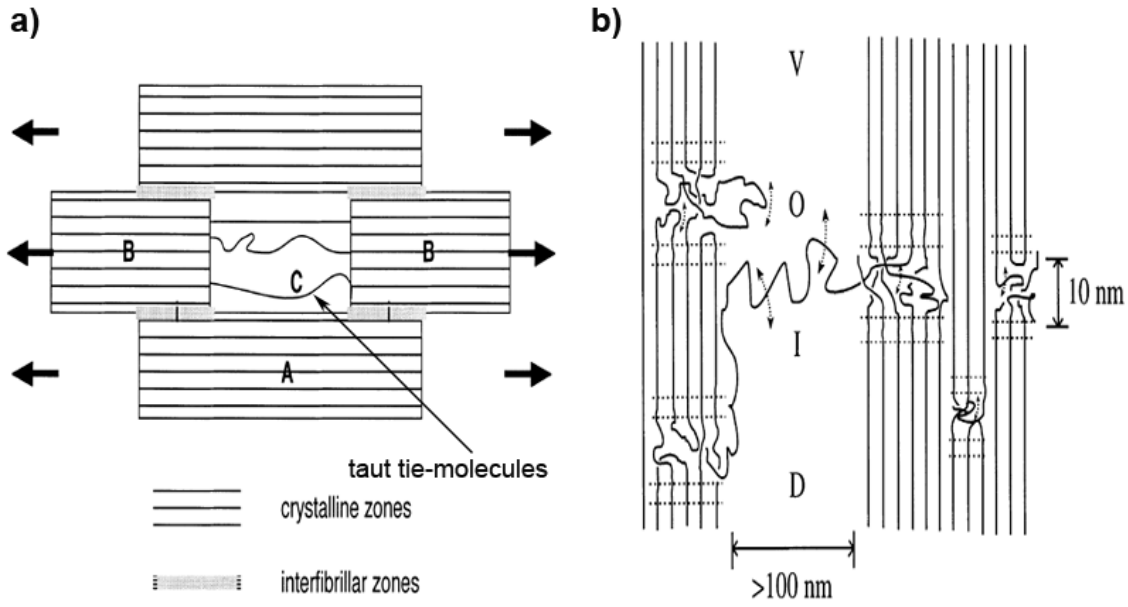

Figure 10. (a) The crystalline bridge model, depicting the crystalline regions (A and B), the interfibrilar zones (marked i), and the tie-molecules (C) [44]. (b) The fibril structure model by Hu et al., show the continuous crystalline phase with polymer chains alternately traversing crystalline and amorphous regions, voids between the fibrils, and highly mobile segments on the surface of the voids or traversing them [45].

Highly oriented UHMWPE fibers are generally believed to contain four morphological phases: a rigid orthorhombic phase, a monoclinic phase, an amorphous phase, and an intermediate phase also known as oriented crystal-amorphous transition area with low molecular mobility [46, 47]. Within the amorphous phase two areas with slightly different properties can be further identified, including a very small oriented amorphous phase with intermediate mobility, and an amorphous phase with high mobility due to chain ends, defects, and nano-voids [47]. Orthorhombic crystals (Figure 11) can exist in two conformations, folded lamellae (kebab) and extended chains (shish) [46].

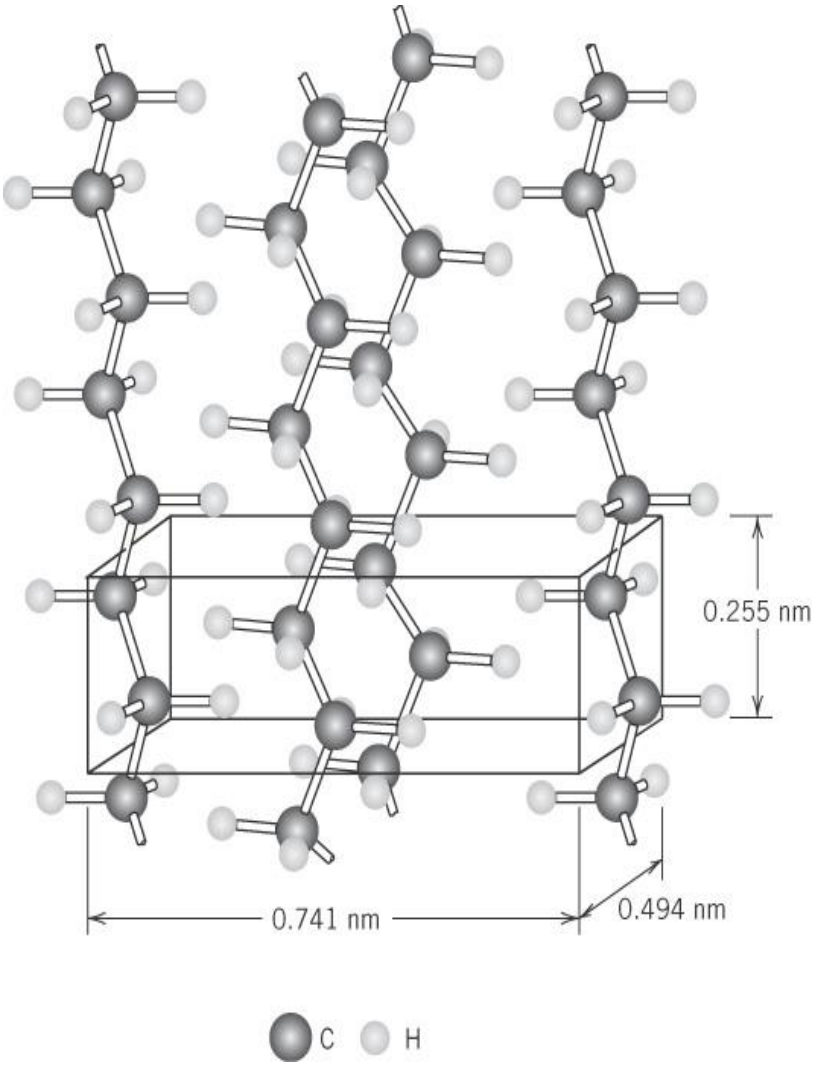

Figure 11. Unit cell of orthorhombic crystals in polyethylene [48].

Processing of UHMWPE fibers at high draw ratios leads to fibers with an increased overall orientation of their chains [47], primarily comprised of orthorhombic crystals in the extended-chain conformation [46, 49]. Higher draw ratios produce fibers with better mechanical properties mainly due to an increased extended chain orthorhombic phase, as this phase is responsible for the axial high-strength due to the C-C backbone being aligned in the fiber direction [46]. Also, higher draw ratios lead to a smaller fraction of monoclinic crystallites [46]. Finally, when heated at higher temperatures, close to the melting temperature, under constraint, UHMWPE fibers can form a hexagonal crystalline phase [43]. The differences between the unit cells of orthorhombic, monoclinic, and hexagonal crystals are shown in Figure 12. Finally, the behavior of the UHMWPE fibers during different drawing ration and temperatures is shown in Figure 13.a and 13.b respectively [43, 49].

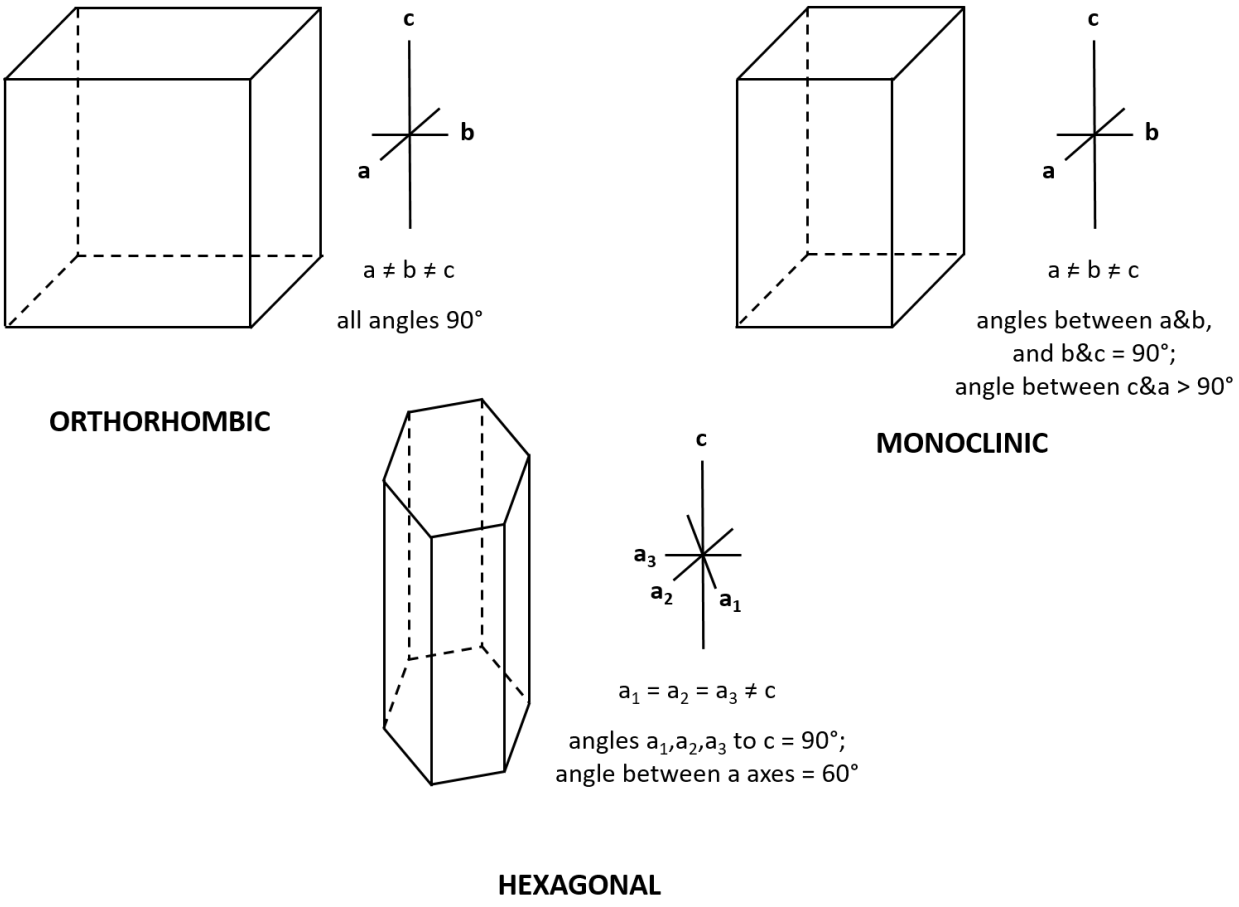

Figure 12. Unit cells of orthorhombic, monoclinic, and hexagonal crystal phases in UHMWPE.

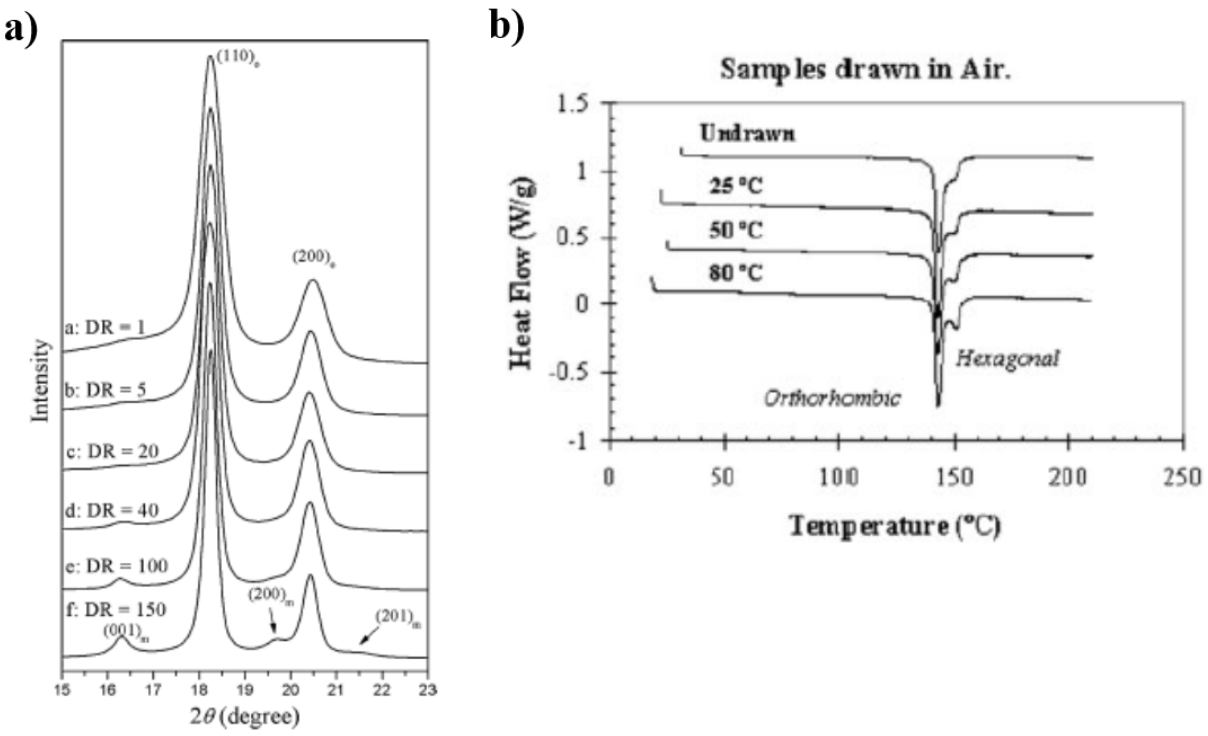

Figure 13. (a) Increase of the orthorhombic crystal phase and the appearance of the monoclinic crystal phase as the drawing ratio of the fibers increases [49]. (b) Formation of hexagonal crystal phase as temperature increases during the drawing process [43].

1.3.4 Structure of UHMWPE Body Armor

Many light-weight ballistic protective armor systems are currently constructed using high modulus and high strength polymeric fibers such as oriented polyethylene fibers (e.g. Spectra®, Dyneema®, etc.), which provide outstanding ballistic resistance [50, 51]. These fibers are used in combination with an elastic resin material, that can penetrate to the filament level, and holds them together to form a non-woven unidirectional tape. Two, or sometimes four layers of the unidirectional tape are laminated together in a crisscross pattern, where each layer is placed at a 90^{o} angle from the layer above and below to form a panel, as shown in Figure 14. A thin film of

low density polyethylene is added on both sides of each laminate, with a thickness of 0.35 mm, to prevent adjacent laminates from sticking together when they are layered on top of each other in the soft body armor [8, 52]. The fibers should at least occupy the 80% of the total weight of the armor in order to maintain its structural integrity. If the percentage of resin, and low density polyethylene exceeds 20%, the anti-ballistic properties of the laminate structure begin to degrade. Therefore, a representative UHMWPE-based material used in body armor usually consists of 80% UHMWPE fibers, 13% resin, and 7% LDPE [52, 53].

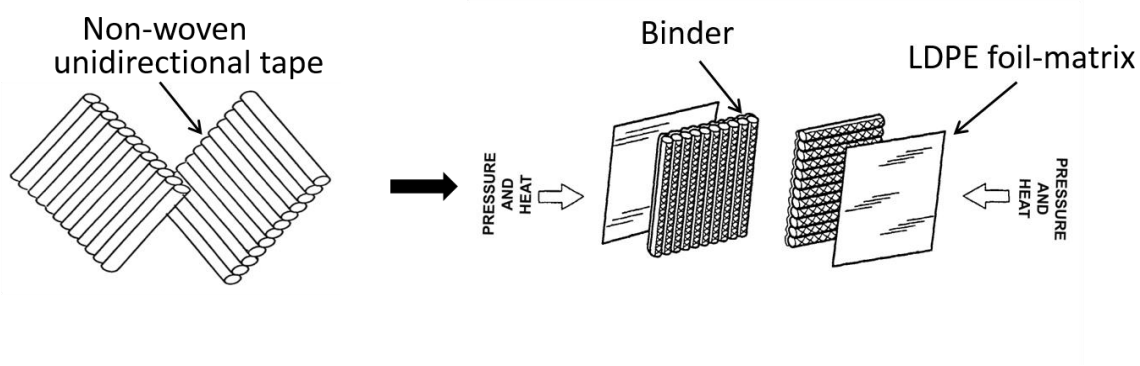

Figure 14. Two unidirectional UHMWPE tapes, a binder material, and two LDPE films are used to produce one armor panel.

The number of panels within the armor varies depending on the application. Usually, for protection against hand gun rounds, the armor contains anywhere between 10 and 60 panels, whereas in the case of high velocity rifle round protection the number of panels should be at least 40 and could be increased up to 150 [53].

1.3.5 Structure and Properties of Binder Resin

The binder is a very important component of the armor, since it keeps the UHMWPE fibers properly oriented and tightly packed inside the laminates [52]. It is preferably an elastomer based material with a very low tensile modulus. Materials commonly used as binders in body armor applications have a tensile modulus between 2,500 and 6,000psi, measured at about 23 °C [54]. Their glass transition temperature should be less than 0 °C and preferably below -50 °C [54]. These materials usually have an elongation to break at around 50% and elastomers used with superior performance are reported to have an elongation to break as high as 300% [54]. Furthermore, the binder material used in body armor applications should demonstrate good adhesive properties in order to keep the fibers together and give some elastic properties to the overall system. Upon degradation of these elastomer materials delamination may occur [54]. Thus, the degradation of the binder material is equally important to the degradation of the fibers and needs to be carefully studied, since upon degradation of the binder, UHMWPE fibers in the laminates can lose their original configuration, which is designed to protect against projectiles.

Chapter 2: Degradation Mechanisms

2.1 Chapter Overview

In this chapter, the mechanisms of degradation of UHMWPE are discussed. In body armor applications the long term stability of the materials, especially of the UHMWPE fibers that provide the antiballistic properties, is of major importance. The degradation of these materials under normal wear and daily use conditions needs to be fully understood prior to conducting any experiments. The effect of mechanical strain, elevated temperatures (up to 65 °C), and oxygen along with the potential mechanisms of mechanical, thermal, and oxidative degradation of UHMWPE is discussed in detail in this chapter.

2.2 Mechanical Degradation of UHMWPE

Mechanical energy transferred to a polymer molecule can be relieved by non-destructive processes, without inducing chemical changes, or destructive processes, such as chemical bond scission [55]. These two processes through which polymers can dissipate strain energy are in competition with each other. The probability for bond scissions increases as the relaxation processes are impeded [55]. In linear crystalline polymers, such as UHMWPE, that consists of glassy, rubbery, and crystalline states (with the crystalline state being the most abundant one) more bonds should be ruptured since the rigidity of the material is high [55].

To better understand bond scission in macromolecules, one must first understand how non-destructive relaxation processes occur, since the two compete to relieve the strain energy in polymers. The non-chemical relaxation processes can occur through slippage of the chains relative

to the surrounding molecules (enthalpic relaxation) and through changes of chain conformation (entropic relaxation) [55]. The first, enthalpic portion, originates from the intermolecular forces between segments of the same polymer chain and its surrounding molecules, which through rotational motion of the C-C bonds in the backbone of the polymer results in chain slippage. During this process, known as c/2 translation of the polymer chain, a 180° twist of the chain is performed resulting from a smooth twist that propagates from one side of the crystal to the other, as showing in Figure 15 [14]. Usually the criteria for enthalpic relaxation to occur are as follows: small or no pendant side groups, short repeating units, and weak intermolecular forces [14]. In the case of UHMWPE, which is comprised of -(C_2H_4)- monomers, these interactions are mainly weak Van der Waals forces.

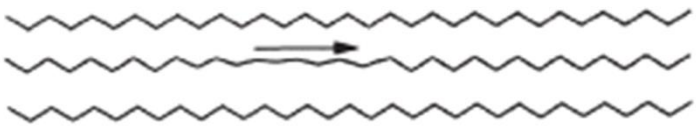

Figure 15. 180° rotation of C-C bonds and a c/2 translation of the polymer chain along its own axis to keep the chain in register with surrounding chains [14].

The second, entropic portion of this process, is a result of the enthalpic portion due to the resultant change in conformational freedom of the polymer chain after the chain slippage occurs, as shown in Figure 16 [14, 55]. Constrained chains have low entropy and high energy, whereas chains with higher freedom of motion and more physical arrangements available have a higher entropy and lower energy [14, 55].

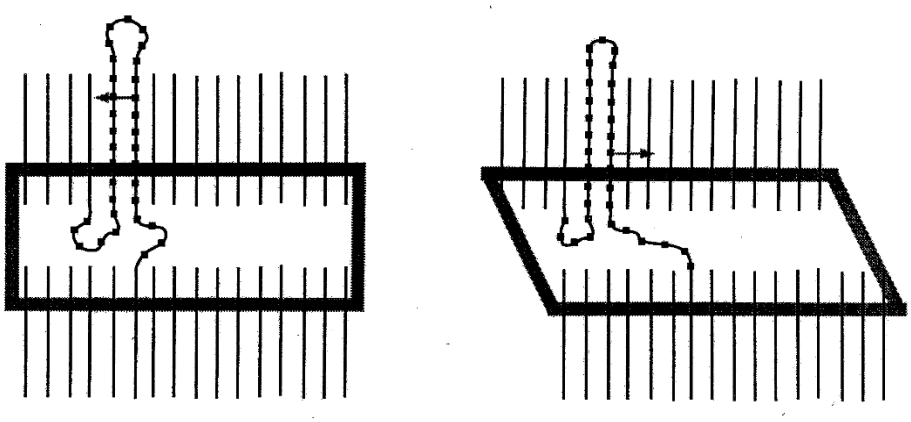

Figure 16. Mechanical relaxation process and chain slippage in polyethylene [14].

At this point it must be noted that the critical conditions for bond rupture depend on two major parameters. The first one is the amount of elastic energy stored in a polymer chain, and the second one is the time the chain remains in the strained state. The non-destructive relaxation processes frequently occur rapidly and appear to be the controlling factor with respect to bond rupture [55]. That means, if the time for bond scission is kept constant, an increase in the relaxation time will result to a higher yield for bond rupture and vice versa. One should note that the amount of energy stored should be equal or greater than the bond dissociation energy, where in the case of PE consisting of C-C and C-H bonds, is estimated to be around 260-400 kJ/mol for a C-C bond and 320-420kj/mol for a C-H bond, at room temperature (25 °C) [55]. As previously mentioned, UHMWPE fibers used in body armor applications are typically very highly drawn. The drawing of the fibers results in straight tightly packed UHMWPE chains that are aligned closely to each other, thus limiting their conformational freedom. When strain is imposed on these fibers, the limited mobility of the polymer chains will increase the relaxation time and prevent the slippage mechanism from being able to relief the strain energy. Therefore, the mechanical energy absorbed will be dissipated through the bond scission mechanism [14, 55].

Furthermore, under the influence of shear stress, individual linear polymer chains are extended in the direction of the stress, according to various theoretical approaches on how bond ruptures occur in linear crystalline polymers, such as UHMWPE [55-57]. Therefore, it is expected that the bonds in the middle of the chains are strained the most, while the remainder of the polymer chains are less affected. This means that there is a higher probability of bond scissions to occur in the middle portion of the polymer chains rather than the areas closer to the chain ends. Also, it is assumed that the rate of bond rupture increases significantly as the molecular weight of the polymer increases [55]. According to these theoretical approaches, UHMWPE fibers with chain molecular weight anywhere between 3 and 5 million Daltons are expected to have a high probability of bond scission under a strained state.

Lastly, if tensile stress is applied to polymers consisting of amorphous and crystalline regions (semi-crystalline), such as UHMWPE, and the mechanical energy transferred to the system is sufficient, initially main-chain bonds will be ruptured almost exclusively in the amorphous phase of the polymer (Figure 17). This is a result of elastic deformation of semi-crystalline polymers, which usually occurs at low stress levels [29]. The polymer chains in the amorphous regions elongate in the direction of the applied tensile stress These amorphous areas of the polymer connect the crystalline regions through “tie molecules” [55].

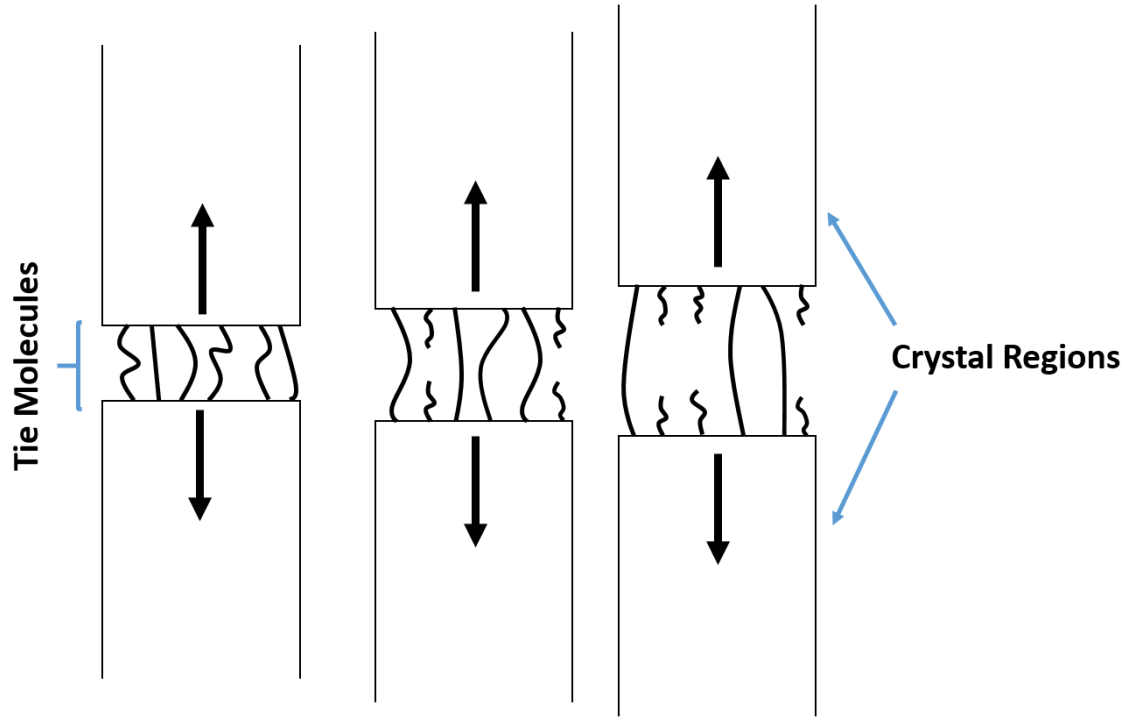

Figure 17. Bond rupture in the "tie molecules" in the amorphous regions of semi-crystalline polymers.

When bond rupture occurs, the molecular weight of the polymer decreases and carbon centered free radicals form in the polymer [55]. In polyethylene it was experimentally proven that the concentration of free radicals increases drastically which increases strain, but no radicals were detected when the amorphous areas of the polymer were eliminated via pretreatment with HNO_3 [55]. This result validates the idea that in UHMWPE bond scission mainly occurs in the amorphous areas of the polymer. However, at very high strain rates free radicals can also form in the crystalline regions, but to a lesser extent [55].

2.3 Thermal Degradation of UHMWPE

Temperature plays an important role in the stability of organic macromolecules such as polyethylene. Organic molecules are stable only below certain temperatures usually ranging from 100 °C to 200 °C. If the temperature is increased to 1,000 °C or higher, bond scissions take place and these molecules decompose into small fragments. This process is known as "depolymerization" [55]. However, at ambient temperatures, thermal energies correspond to values around $kT \approx 2.4$ kJ/mol, which compared to the C-C and C-H bond dissociation energies discussed in the previous section is insufficient to cause bond rupture [55]. UHMWPE fibers used in body armor applications are not exposed to these extreme temperatures, and are typically exposed to their most extreme temperatures during wear and storage conditions, with maximum temperatures of approximately 67 °C [58], where bond scission is not feasible. However, in condensed systems vibrational energy is rapidly dissipated among all molecules and bonds, which can lead to highly excited vibrational state of bonds in some molecules. The population of these highly vibrational excited bonds increases with increasing temperature, and could potentially lead to a repulsive energy level and bond breakage even at lower temperatures [55].

Although temperature alone should not result into bond scission in the case of UHMWPE fibers used in body armor applications, it has a synergistic effect with mechanical stress. When strain is applied and temperature increases close to the range of α-relaxation temperature (80 °C) [59], polymer chains will attempt to increase their entropy by folding back on themselves [14]. Rotational motion of the C-C bonds in the backbone of the UHMWPE chains can occur more easily, thus increasing the free volume of the chains and making them more mobile [14]. As a result, there is a higher probability for chain slippage to occur instead of rupture of chemical bonds

when strain is applied [55]. Therefore, at low strain, a small increase in temperature could be beneficial for the material and prevent bond scissions. Conversely, at high strain rates and low temperatures the mechanism of chain scission is expected to dominate. Finally, as temperature increases (up to 150 °C), various chemical reactions, such as oxidation reactions, can be further promoted and induce bond rupture decreasing even more the molecular weight of UHMWPE fibers, though mechanisms that will be discussed in the following section [55, 60].

2.4 Oxidative Degradation of UHMWPE

As discussed in the previous sections of this chapter, mechanical stress and elevated temperatures can induce scission of C-C bonds along the backbone of an UHMWPE chain, almost entirely in the amorphous regions that connect the crystalline regions [55]. The rupture of these bonds results in the formation of C-centered free radicals. These free radicals can undergo various reactions which in general, depend on the presence of oxygen in the amorphous areas of the UHMWPE, the concentration of oxygen present, the temperature, the water content, the presence of antioxidants in the material, and the degree of crystallinity [55, 61, 62].

2.4.1 Formation of Free Radicals and Consequent Reactions

The chemical composition of UHMWPE is simple and consists of singe carbon-carbon, and carbon-hydrogen bonds. The energy of a single carbon-carbon bond (C−C) is known to be 346 kJ/mol and that of a carbon-hydrogen bond (C−H) is 411 kJ/mol [63]. When energy, greater than the mean energy of these bonds, is transferred to the UHMWPE polymer, scission of C−C and C−H bonds can occur [55, 64]. This bond scission will result to the formation of hydrogen atoms

(H), primary carbon centered free radicals (C•), and secondary carbon centered free radicals (C•) as shown in the following reactions (where R represents the polymer chain) [55, 64, 65].

$$PEH \xrightarrow{k_1} PE\bullet + H \quad (1)$$

$$PE{-}PE' \rightarrow PE\bullet + PE'\bullet \quad (2)$$

Reaction (1) represents the breaking of a C−H bond to produce hydrogen atoms, and secondary alkyl free radicals, whereas reaction (2) refers to chain scission on the backbone of the polymer through a breaking of a carbon-carbon bond producing two primary alkyl free radicals. In the case of reaction (1) the secondary alkyl radicals forming can involve in very fast intermolecular reactions, which are thermodynamically favored with a ΔH = -288 kJ/mol, to produce vinylene double bonds and molecular oxygen (H_2) [64, 66, 67]. Also, secondary alkyl radicals can migrate along the polymer chain via H transfer and form allyl and polyenyl radicals (Figure 18), which are more stable due to the formation of conjugated bonds and can survive even for a few years in the polymer's backbone, at room temperature [68]. This process can occur at a high rate even at room temperature, since it has a very low activation energy of only ΔH = 40 kJ/mol [27].

Secondary Alkyl Free Radicals	Allyl Free Radicals	Polyenyl Free Radicals
$-CH_2-\dot{C}H-CH_2-$	$-CH=CH-\dot{C}H-$	$-CH_2-(CH=CH)_N-\dot{C}H-$

Figure 18. Chemical structure of the different types of free radicals in polyethylene.

Another reaction that secondary alkyl radicals can undergo is β-scissions where the secondary free radical breaks two carbons away producing an ethylene and a primary alkyl free radical (Figure 19) [27]. These reactions are endothermic reactions (ΔH = 88 kJ/mol) and are

extremely unlikely to occur at room temperature [27]. However, in the absence of oxygen β-scission can happen when the temperature is close to 200 - 250 °C [27].

Figure 19. β-scission reaction of secondary alkyl free radicals.

The hydrogen atoms formed during reaction (1) are very small in size (diameter of 0.1 nm) and can diffuse easily in the polymer mass, even in the crystalline phase of polyethylene, where the distances between two carbon atoms are around 0.4 nm [27]. These hydrogen atoms have a very high probability to extract other hydrogen atoms intramolecularly, producing new secondary alkyl free radicals and molecular hydrogen [69]. This reaction is exothermal (ΔH = -30 kJ/mol) and it is favorable to occur even at room temperature [69].

Finally, the primary alkyl free radicals formed in reaction (2), have been shown to exist only for short period of times, in the order of 24 h. It is assumed that this type of free radical can undergo termination reactions, such as recombination reactions, in both amorphous and crystalline phase, giving back a C−C bond, as shown in reaction (3). The recombination reactions are exothermal and the energy produced is dissipated in the polymer mass [27].

$$PE\bullet + PE'\bullet \xrightarrow{k_2} PE - PE' \qquad (3)$$

In addition, secondary alkyl free radicals can undergo termination reactions, such as crosslinking (Figure 20), or disproportionation reactions where one free radical molecule will act as an acceptor while the other will act as a donor [55, 70]. During a disproportionation reaction, a hydrogen atom is abstracted by the acceptor and the donor undergoes an elimination reaction to from a double bond (Figure 21) [55].

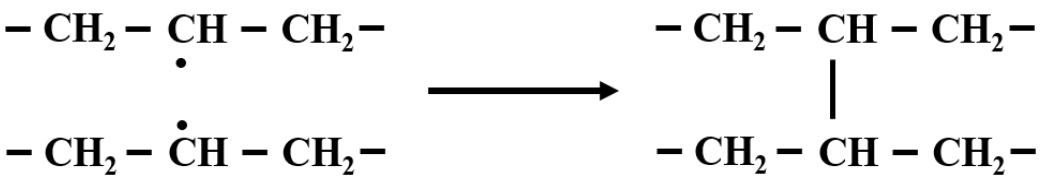

Figure 20. Formation of crosslinks in UHMWPE by the recombination of C-centered radicals located on adjacent chains.

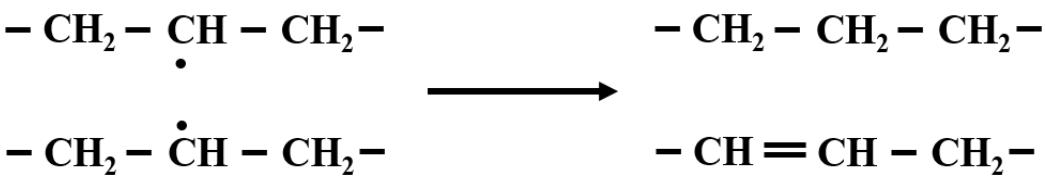

Figure 21. Termination thorough disproportionation reaction and formation of double bond.

In some cases, primary alky free radicals in the crystalline phase of the polymer can rapidly retract from each other due to axial chain stresses, preventing them from recombining. These radicals then can convert to secondary free radicals through transfer of a hydrogen atom [70]. The hydrogen transfer process can occur along the same polymer chain (radical migration along the polymer chain) (Figure 22), or a hydrogen atom can be abstracted from a neighboring chain (hydrogen hopping across chains) (Figure 23) resulting in a transfer of the radicals to a mid-chain position [71, 72].

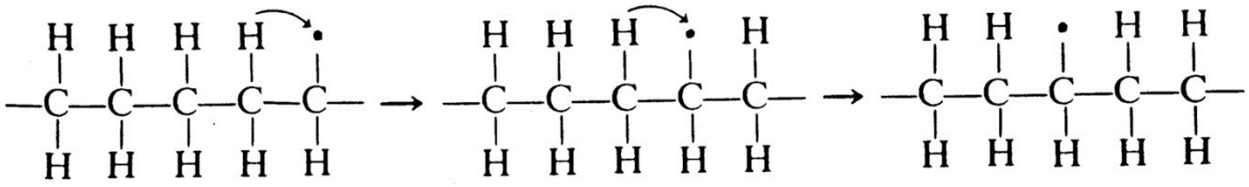

Figure 22. Hydrogen transfer mechanism along the same polymer chain.

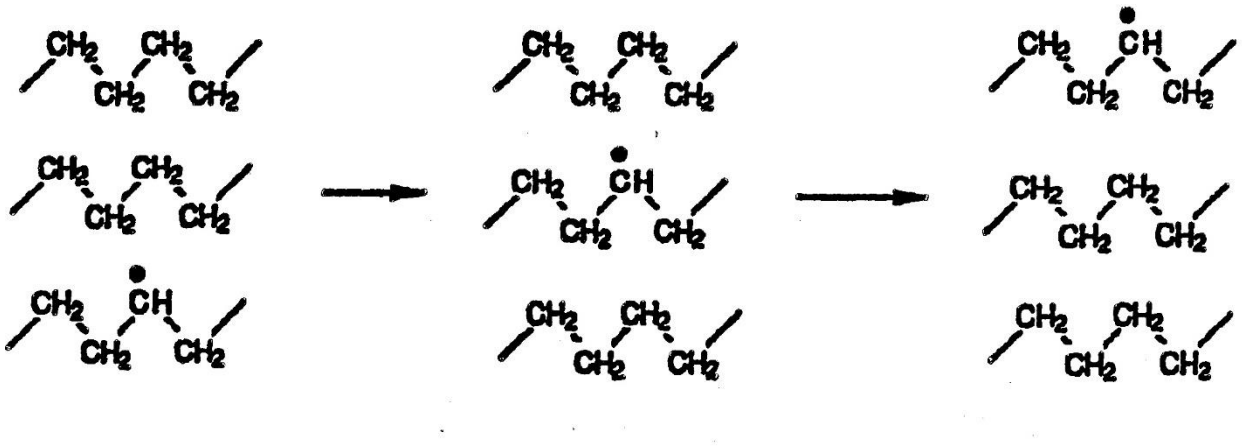

Figure 23. Hydrogen hopping mechanism across adjacent polymer chains.

These reactions produce secondary alkyl radicals and new chain-end groups (CH_3) leading to a reduction of the molecular weight of the polymer and the decrease of the mechanical properties of the UHMWPE [55, 72]. Also, through these hydrogen transfer mechanisms C-center free radicals can migrate from the crystalline regions of the polymer to the amorphous regions where oxygen is present and undergo oxidation reactions [55].

2.4.2 Oxidation Reactions

In the presence of oxygen solubilized in the amorphous phase of UHMWPE, alkyl free radicals will involve in a series of reactions that can further decrease the molecular weight of the polymer and result in products such as ketones, carboxylic acids, alcohols and esters [55, 73, 74]. These products will give the polymer hydrophilic properties, to a certain extent, making it susceptible to water, which can in turn penetrate into the polymer and induce more oxidation over time [55].

Oxygen can be both initially present in the material as well as diffuse into the polymer over time [61]. During industrial processing of the material, oxygen can become entrapped in the structure and it is practically impossible to obtain a totally oxygen-free polymer, even in the presence of an inert gas [75, 76]. Furthermore, the solubility and the diffusion of oxygen into the surface of the material and towards its interior adds more complexity to the kinetics of the oxidation reactions. The oxygen solubility and diffusivity are functions of temperature [77]. In general, the solubility decreases slightly, whereas the diffusivity increases with temperature [77]. In the case of highly oriented UHMWPE fibers, oxygen transport takes place almost exclusively through the amorphous regions of the polymer and the crystalline regions provide barriers to impede oxygen flow [78]. The extent of these barriers and their influence on the diffusion of oxygen through the amorphous regions of the polymer depend on the molecular orientation of the polymer chains and their packing density in the highly drawn fibers [78]. As a result, at higher drawing ratios, oxygen permeability and diffusion into the UHMWPE fibers through the sparse amorphous regions is more restricted [79]. More recent results have shown that there is a linear correlation between the solubility of oxygen and the amorphous volume fraction of the polymer, which provides the carrier for the diffusion process, while the permeability and diffusion coefficient demonstrate a more complex behavior which relates to the detailed morphology of the crystalline and amorphous regions, such as their distribution and size [80]. Also, the permeability and diffusion coefficient depend on the size of the diffusant molecule, which in this case is oxygen molecules with a diameter of about 0.35 nm [80]. Therefore, the calculation of these two parameters is relative and needs to be calculated case by case. An estimated value of oxygen's diffusion coefficient in UHMWPE was calculated by Daly et al. to be around 1.14×10^{-7} cm^2/s [81]. On the other hand, the specific solubility of oxygen in the amorphous phase of highly oriented

UHMWPE does not vary significantly and was estimated to be around 0.00970 cm^3 (STP)/cm^3 atm (cubic centimeters of gas at STP per cubic centimeters of solid at a pressure of 1 atm) [80]. This value is very close to the one Daly et al. calculated for UHMWPE as a whole and not specifically for the amorphous regions of the polymer, which was 0.00881 mL (STP)/mL atm [81]. These values of oxygen specific solubility can be useful to approximate the concentration of oxygen in UHMPE fibers, assuming we have a pressure of 1 atm, thorough the following equation:

$$[O_2] = \frac{S \times P_{O_2} \times \rho_{UHMWPE}}{MW_{O_2}}$$

Where, S is the specific solubility of oxygen, P is the pressure, ρ is the density of UHMWPE (0.930 g/mL), and MW is the molecular weight of oxygen (32.0g/mol).

The various alkyl macroradicals R• mainly present in the amorphous regions of the UHMWPE will rapidly react though a thermodynamically favored reaction with the oxygen molecules present in these amorphous regions to form peroxy radicals (PEOO•), as shown in reaction (4) [55, 76, 82].

$$PE\bullet + O_2 \xrightarrow{k_3} PEOO\bullet \qquad (4)$$

The peroxy radicals formed are relatively stable in highly oriented UHMWPE, in spite of the readily available hydrogen atoms in the polymer. This is confirmed by studies showing that peroxy radicals in polyethylene are still present after many weeks of storage at room temperature in air [76]. Also, this is further supported by the high activation energy needed for hydrogen extraction from a nearby UHMWPE molecule by peroxy radicals, which at room temperature was calculated at 108 kJ/mol [76]. However, an increase of only 10 °C can almost double the rate of the hydrogen extraction reaction and this results in the formation of hydroperoxides and newly formed alkyl macroradicals, as shown in reaction (5) [55, 70, 82, 83].

$$PEOO\bullet + PE'H \xrightarrow{k'_4} PEOOH + PE'\bullet \quad (5)$$

In addition, peroxy radicals can participate in termination reactions either by reacting with alkyl macroradicals present to produce peroxides, reaction (6), or combining with each other to produce peroxides and molecular oxygen, reaction (7) [61, 82]. This last reaction is known as the Russell reaction between two peroxy radicals. This biomolecular termination reaction is strongly disfavored at room temperature due to the relative immobility of the highly crystalline UHMWPE and the relative stability of the peroxy radicals, as mentioned above [71]. On the other hand, reaction (6) is more thermodynamic feasible and it is not kinetically inhibited, since the alkyl macroradicals can migrate along the polymer chain and can find the peroxy radicals to react with and produce peroxides [71]. Finally, peroxy radicals can undergo oxygen elimination reactions to produce super oxide ions ($O_2^{\bullet -}$). These super oxide ions can then react with hydronium ions (H_3O^+) and produce water and hydroperoxyl radicals ($HO_2^{\bullet}$).

$$PEOO\bullet + PE'\bullet \xrightarrow{k_5} PEOOPE' \quad (6)$$

$$PEOO\bullet + PE'OO\bullet \xrightarrow{k_6} PEOOPE' + O_2 \quad (7)$$

Furthermore, the hydroperoxides formed by reaction (5) are thermally unstable [76]. When temperature increases from room temperature to 70 °C and above, hydroperoxides undergo decomposition reactions [76, 82]. UHMWPE fibers used in personal body armor applications can be exposed to temperatures of approximately 67 °C or higher during normal wear and storage conditions, as previously mentioned [58]. This results in thermal oxidation decomposition reactions that can further induce the degradation of the fibers, since hydroperoxides will decompose to produce very reactive •OH and RO• radicals, or ketones (R_2CO) and H_2O molecules, as shown in reactions (8) and (9) respectively [61, 76, 82].

$$PEOOH \rightarrow PEO\bullet + \bullet OH \quad (8)$$

$$PEOOH \rightarrow PECOPE + H_2O \quad (9)$$

Reaction (8) is a very important propagation reaction of thermal oxidation, since it produces new highly reactive species, the alkoxy radicals (RO•), which can give β-scission to produce new primary alkyl radicals and carbon monoxide (CO) through reaction (10), as shown in Figure 24 [61, 76, 82]. The activation energy for this reaction is relatively low, around 50 kJ/mol and can occur even at room temperature [76].

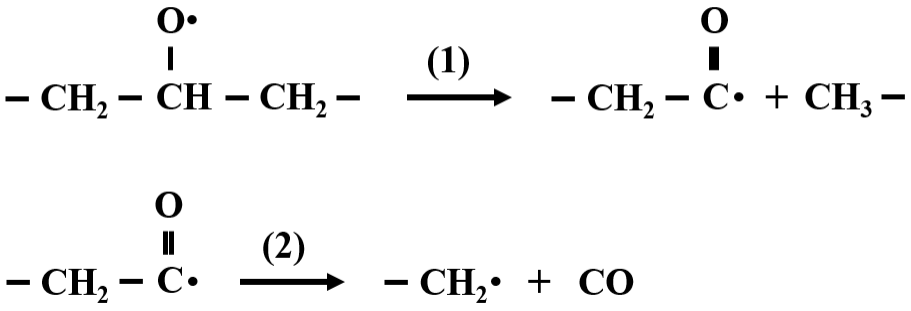

Figure 24. β-scission of alkoxy radical (reaction 10).

In addition to the β-scission reaction, alkoxy radicals can abstract hydrogen molecules from the polyethylene chain to produce alcohols and new alkyl macroradicals, reaction (11) [55, 61, 76, 82].

$$PEO\bullet + PE'H \rightarrow PEOH + PE'\bullet \quad (11)$$

The hydroxyl radicals (•OH) formed previously from reaction (8) during the thermal decomposition of hydroperoxides are highly reactive species, as well, and can easily abstract hydrogen molecules from the polymer chain to produce new alkyl macroradicals and H_2O molecules, as shown in reaction (12) [61, 76, 82].

$$PEH + \bullet OH \rightarrow PE\bullet + H_2O \quad (12)$$

Finally, during oxidative degradation of polyethylene, besides the formation of ketone and alcohol groups, ester groups can also be produced mainly through the decomposition of primary peroxides. However, the precise mechanism of ester group formation is not yet completely understood [84].

An approximation of the kinetics of these oxidation reactions, utilizing the initiation reaction (1), the propagation reactions (4) and (5), and the biomolecular termination reactions (3), (6), and (7), described above, has been applied to the oxidation of polymers [65]. For this oxidation model a steady-state analysis was used along with the assumption that a high number of propagation cycles occur before the termination reactions take place, and that $k_5^2 = 4k_2k_6$ for the reaction rates of the bimolecular termination reactions [65]. It has been estimated that, in the presence of oxygen, one free radical generates, on average, 12 carbonyl and 5 hydroxyl groups before decaying [55, 65]. Therefore, the oxygen consumption rate was obtained from standard kinetic analysis to be as follows [65, 85]:

$$\frac{dO_2}{dt} = \frac{C_{1b} \times [O_2]}{1 + C_{2b} \times [O_2]}$$

where the constants $C_{1b} = \frac{k_3 \times {k_1}^{0.5}}{(2k_2)^{0.5}}$ and $C_{2b} = \frac{k_6 \times {k_3}^{0.5}}{{k_2}^{0.5} \times k_4}$ and $k_4 = k_4' \times [PE'H]$

The aforementioned oxidation reactions in UHMWPE are summarized in Figure 25. The ultimate result of these reactions is a material with reduced molecular weight, which directly affects its mechanical properties, as well as the formation of groups such as esters, ketones, and alcohols that increase the hydrophilicity of the UHMWPE fibers making them more susceptible to water and oxygen penetration, further inducing the deterioration of the material.

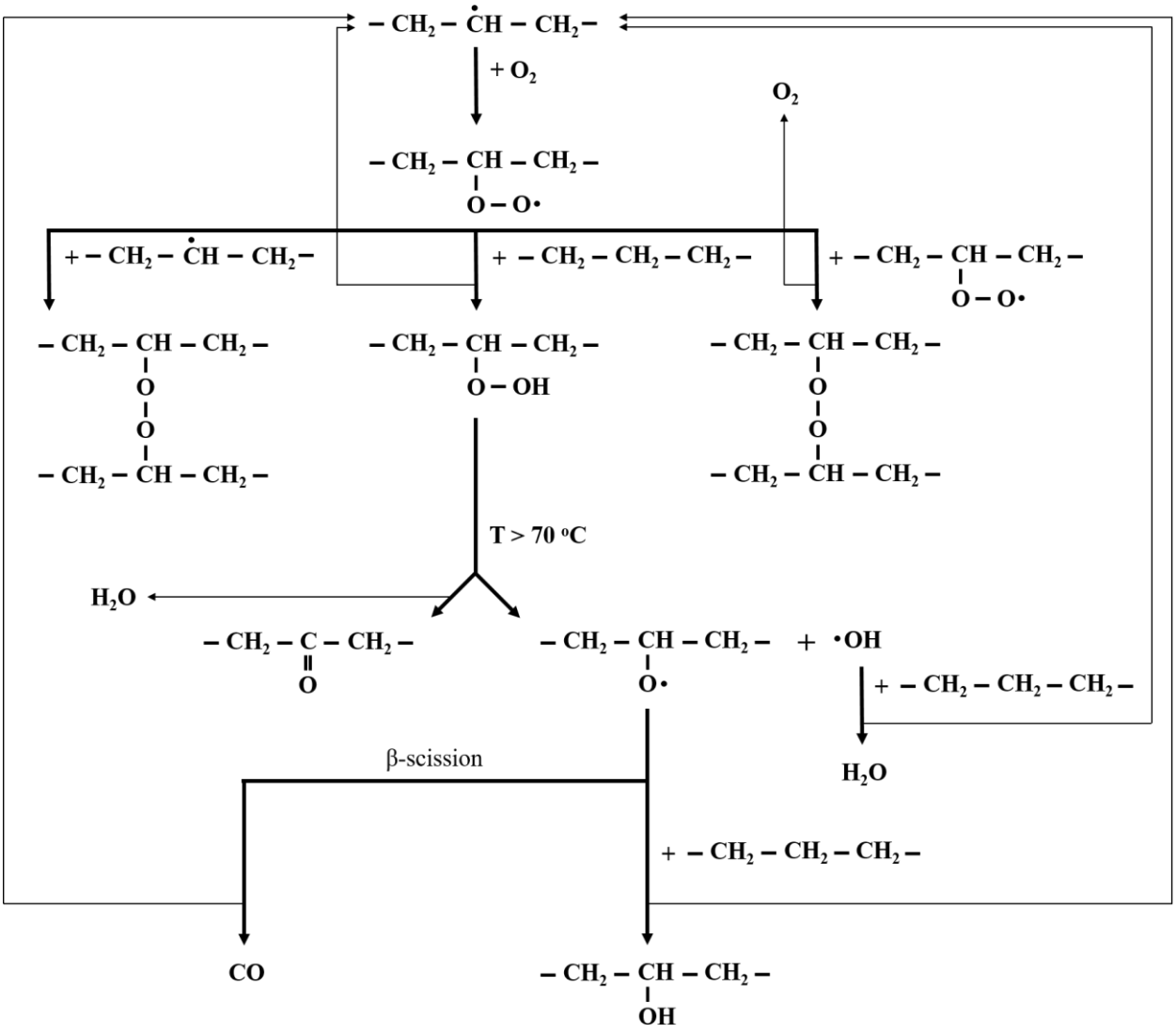

Figure 25. Oxidation reactions of UHMWPE free radicals in the amorphous regions.

2.4.3 Antioxidants

Commercial polyethylene usually contains phenolic antioxidants such as Vitamin-E when used in bio applications, or Irganox [86-90]. Also, special stable oxygen centered free radicals, such as nitroxides (TEMPOL and TEMPO) are commonly used in polyethylene materials [91, 92]. These reagents are used as scavengers for free radicals and induce the termination reactions of C-

centered free radicals in PE. As previously discussed, C-centered free radicals will react with available oxygen to produce peroxy radicals. However, in the presence of phenolic antioxidants the following reactions are in competition:

a) Vitamin-E as antioxidant:

$RO_2\bullet + \alpha\text{-TOH} \rightarrow ROOH + \alpha\text{-TO}\bullet$

b) Irganox as antioxidant, reactions shown in Figure 26 [93]:

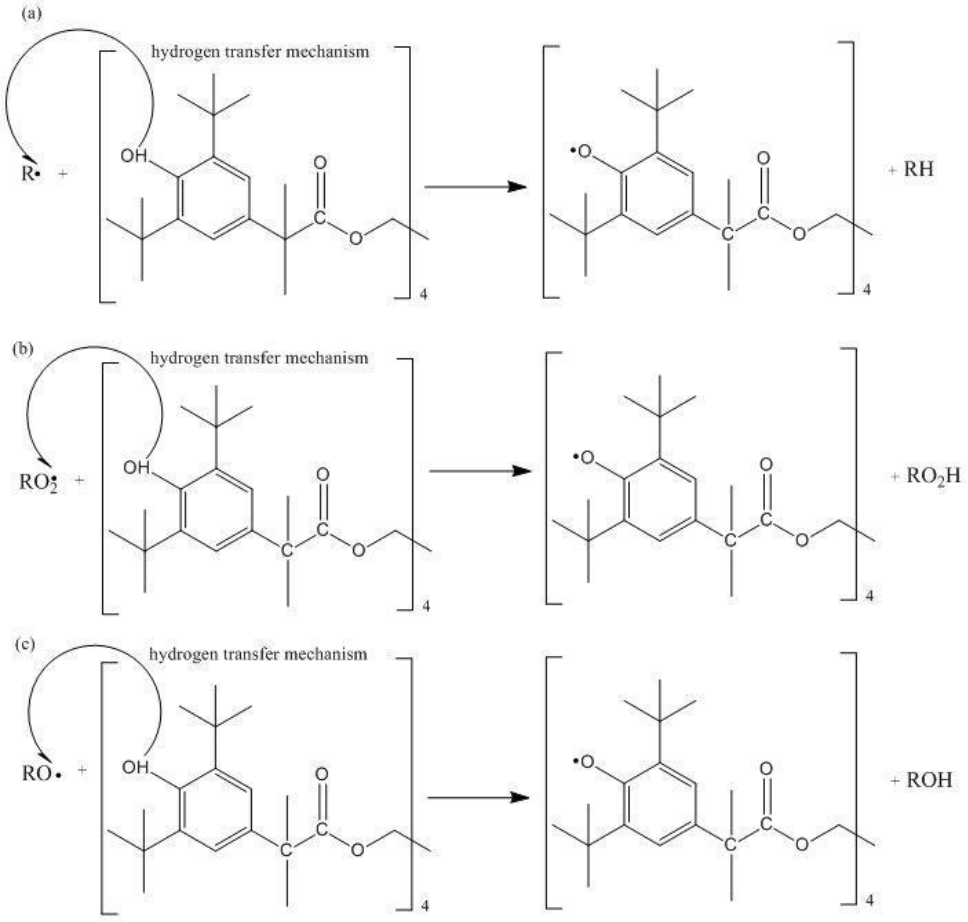

Figure 26. Reactions of Irganox 1010 with C-centered, peroxy, and alcoxy free radicals [93].

Nitroxides, can also work as C-centered radical scavengers via the following reactions:

$R\bullet + >NO\bullet \rightarrow >NOR$

$RO_2\bullet + >NO\bullet \leftrightarrow \text{intermediate} \rightarrow >N^{+}=O + RO_2^{-}$

The kinetics of the oxidation reactions described in the previous section will change in the presence of antioxidants, since C-centered free radicals can not only react with oxygen, but also with these scavenger reagents. In this case, the oxidation reactions including their reaction rate constants are as follows:

$R\bullet + R\bullet \rightarrow R\text{-}R$ (reaction rate constant, k_1)

$R\bullet + O_2 \rightarrow RO_2\bullet$ (reaction rate constant, k_2)

$R\bullet + \text{Ant-OH} \rightarrow RH + \text{Ant-O}\bullet$ (reaction rate constant, k_3)

According to the above reactions we can calculate the consumption rate of C-centered free radicals from the equation below:

$$-d[R\bullet]/dt = k_1[R\bullet] + k_2[R\bullet][O_2] + k_3[R\bullet][\text{Ant-OH}]$$

In addition to these reactions, the peroxy radicals formed can be terminated by the antioxidant, as shown in the reactions below:

$RO_2\bullet + \text{Ant-OH} \rightarrow RO_2H + \text{Ant-O}\bullet$ (reaction rate constant, k_4)

$RO_2\bullet + RO_2\bullet \rightarrow ROOR + O2$ (reaction rate constant, k_5)

$RO_2\bullet + R\text{-}H \rightarrow RO_2H + R\bullet$ (reaction rate constant, k_6)

The consumption rate of peroxy radicals can be calculated using the following equation:

$$D[RO_2\bullet]/dt = k_2[R\bullet][O_2] - k_4[RO_2\bullet][\text{Ant-OH}] - k_5[RO_2\bullet]^2 - k_6[RO_2\bullet][R\bullet]$$

Finally, in the presence of oxygen and antioxidants, the probability of C-centered radicals reacting with oxygen will be lower than that in the absence of antioxidants, as can be seen from the equation below:

$$\text{Probability} = \frac{k_2[R\bullet][O_2]}{k_1[R\bullet]^2 + k_2[R\bullet][O_2] + k_3[R\bullet][\text{Ant-OH}]}$$

In this study, the presence of Irganox-type hindered phenol antioxidants is suspected due to results from previous work conducted on the same generation of virgin UHMWPE fibers manufactured by the same company [93]. However, the results of this study did not show evidence of the existence of such scavenger molecules.

Chapter 3: Materials and Methods

3.1 Chapter Overview

To assess the long term stability of UHMWPE-soft ballistic inserts, a number of analytical methods were utilized. The description of these methods is located here for easy reference, since they are used in the subsequent chapters. A discussion of the materials used in this study, and the instrumentation used to investigate the changes in the chemical and physical structure of UHMWPE fibers and the binder resin can be found below.

3.2 Materials

The UHMWPE-soft ballistic resistant armor panels used in this study were provided from DSM company and the fibers utilized in these vest inserts are characterized by the company as Dyneema SK76 UHMWPE fibers. No description of the LDPE film or the binder resin used was provided by the company. The body armors were stored in dark ambient conditions prior to or after having been subjected to accelerated aging conditions. In this work, the ballistic vests were aged according to the protocol described in NIJ Standard 0101.06 [58, 94]. Briefly, the vests were placed into specially designed chambers at 65 °C, 80% relative humidity, and 5 rpm tumbling for a two-week period of time. A series of temperature/relative humidity data loggers were used to monitor the consistency of the chamber conditions during the exposure time. In addition to this protocol, a folding protocol was developed and used in this study to allow for the evaluation of the isolated effect of mechanical stress on the UHMWPE fibers when part of the laminated structure. Briefly, laminates from a new body armor were folded and constrained in half (180° fold), and then placed in into an oven at 80 °C, under ambient pressure and humidity conditions for a period

of two weeks. A thermocouple was used to monitor the consistency of the oven temperature during the exposure time. Solvents, including chloroform (HPLC grade, ≥99.9%), deuterated chloroform (99.8 atom % D), and tetrahydrofuran (HPLC grade, ≥99.9%) were purchased from Sigma-Aldrich (St. Louis, MO).

3.3 Extraction Protocol of UHMWPE and Binder Resin

The materials used in this study were all initially incorporated into ballistic vests. In order to be able to study each individual component of the vest, an extraction protocol had to be developed and used. The goal was to effectively break down the laminated structure of the vest and isolate the UHMWPE fibers as well as the binder resin without affecting their chemical composition and physical structure, or inducing any type of degradation to the materials during this process. To achieve this, sections of the material removed from the laminates were completely immersed in beakers containing chloroform. Mild agitation by hand was performed periodically, until the laminates were visually observed to separate. Then, the samples were left overnight into the chloroform solution to allow for the binder resin to fully dissolve in the chloroform. The UHMWPE fibers and the LDPE film do not dissolve in chloroform and will precipitate in the bottom of the beaker. Filtration was performed to separate the UHMWPE fibers and LDPE film from the chloroform solution containing the binder resin. Next, to eliminate any residual traces of resin from the surface of UHMWPE fibers, the fibers were transferred back to the beaker and more chloroform was added and left overnight. This process was repeated two more times for a total of 4 days. This protocol successfully separated the body armor materials from each other. At the end of the fourth day, all the chloroform solutions containing the binder resin were combined and let under the hood overnight to allow for the solvent to evaporate. The resin was then collected from

the bottom of the beaker and stored in air tight vials. The UHMWPE fibers were also air dried and stored in zip-lock containers inside a desiccator. Materials were extracted from the center part as well as the edge of laminates from various parts of the body armor.

3.4 Characterization of Surface Morphology of UHMWPE Fibers

The shape and the surface morphology of the UHMWPE were characterized by scanning electron microscopy (SEM) using Hitachi S-2400 variable pressure SEM equipped with an X-ray detector that allows for elemental analysis through energy dispersive spectroscopy (EDS). The fibers were evenly spread over slabs and left under vacuum overnight to eliminate any traces of humidity and oxygen bound to the surface of the fibers prior to analysis. The analysis was conducted using variable pressure mode at 15 keV.

3.5 Oxidation Measurement

Oxidation of UHMWPE fiber samples and binder resin material was measured using Fourier Transform Infrared Spectroscopy (FTIR). A Thermo Nicolet NEXUS 670 FTIR equipped with an attenuated total reflectance (ATR) accessory was used to measure the oxidation of the materials. The final spectrum of each sample represent the average of 128 individual scans with a resolution of 2 cm^{-1} between 650 cm^{-1} and 4000 cm^{-1} wavenumbers. A background was collected and subtracted prior to each sample run. Three replicated were prepared for each sample. Spectra analysis, including baseline correction and normalization, was carried out using the instrument software package provided (Omnic ESP). The spectra were baseline corrected and normalized using the peak at 1472 cm^{-1}, which was attributed to the CH_2 bending. Typical standard uncertainties for spectral measurement are 2 cm^{-1} in wavenumber and 5% in peak intensity. To

evaluate the degree of oxidation, the overlapping peaks between 1712 cm^{-1} and 1735 cm^{-1} assigned to the oxidation products (ester and ketone groups) were deconvoluted using Origin Pro software.

3.6 Crystallinity Determination

Differential scanning calorimetry was carried out using a TA Q2000 differential scanning calorimeter (DSC) (TA Instruments). UHMWPE fibers extracted from new and treated vests were coiled around a wire and placed at the bottom of aluminum hermetic pans. The typical weight of the samples was kept between 3 and 5 mg to increase resolution. Samples were held at 25 °C for 5 min and then heated to 180 °C at a rate of 10 °C/min. The measurements were conducted under flowing nitrogen at a flow rate of 25 mL/min. The melting curves of the crystals were deconvoluted into 4 peaks, using the Origin Pro software, which were assigned to the melting of different crystal phases. The melting points were characterized by the temperature of the peak maximum, and the area under each peak was intergraded to assess the crystal composition of the material. Also, the heat of fusion was determined by integrating the entire area under the melting curve to calculate the total percent crystallinity of each sample. Each sample was tested in triplicate.

3.7 Characterization of Morphological Changes in UHMWPE Fibers

Wide angle X-ray scattering (WAXS) measurements were conducted using a Xenocs Xeuss SAXS/WAXS small angle X-ray Scattering System. The instrument was equipped with a 300K Dectris Pilatus detector for SAXS analysis with a minimum Q=0.0045 $Å^{-1}$, an100K Dectris Pilatus detector for WAXS analysis (up to about 45° 2θ) and a Linham stage controlling temperature from about -100 °C to 250 °C. The incident beam, diffracted beam and sample chamber were kept under vacuum. The fibers were mounted across a small groove formed by a

copper block used along with the heating stage to acquire data at various temperatures, as shown in Figure 27. The bundle of fibers was mounted horizontally, perpendicular to the direction of the X-ray beam. In these experiments silver behenate was used as a control and each sample and condition was tested in duplicate. Briefly, the purpose of this experiment was to identify the various crystal phases of the fibers and the morphological changes of the crystals occurring at elevated temperatures. This data will supplement the DSC data obtained and give better insight into the morphological changes of each crystal phase as a function of temperature.

Figure 27. Bundle of UHMWPE fibers mounted on the heating stage for WAXS diffraction.

3.8 Molecular Weight Determination

To determine the extent of chemical degradation of the binder resin material, the molecular weight (Mw) of the resin extracted from new (control) and aged vests was measured through gel permeation chromatography (GPC). The samples were dissolved in tetrahydrofuran (THF), resulting in solutions of 3 mg/mL. Then the solutions were processed using positive filtration through a Whatman 0.2 μm pore-size filter ((polytetrafluoroethylene membrane; PTFE) from Thermo Fisher Scientific (Waltham, MA). The number average and weight average molecular weight, as well as the polydispersity index of the samples was determined using polystyrene standards and the instrument software package provided.

3.9 Determination of the Binder Resin Material Used

To identify the material used as a binder in these body armors the resin was dissolved in deuterated chloroform ($CDCl_3$) and the ^{13}C and ^{1}H two-dimensional nuclear magnetic resonance (NMR) spectra (HSQC and HMBC) were acquired on a Bruker AVIII-600MHz spectrometer. The ^{13}C NMR spectra of the samples in $CDCl_3$ were acquired using proton decoupling. A total of 44,023 data points were acquired at a spectral width of 31 kHz, corresponding to an acquisition time of 1.4 sec, and 4,348 scans were averaged. The ^{1}H NMR spectra were acquired with homo-nuclear decoupling during the acquisition time. Sixteen scans were acquired, each with 24,576 data points at a spectral width of 8 kHz, corresponding to an acquisition time of 3.1 sec. A pulse delay of 1 sec was used in both cases.

Chapter 4: UHMWPE Fibers Extracted from Body Armor

4.1 Chapter Overview

In this chapter, the long term stability of the UHMWPE fibers extracted from body armor is evaluated. The effect of mechanical stress on the surface morphology of the fibers and the oxidative degradation is studied. Additionally, changes in the crystallinity and the morphology of the crystalline phase is evaluated.

4.2 Surface Morphology of UHMWPE Fibers and Elemental Analysis

Fibers extracted from body armor, after being artificially aged through the NIJ protocol and the folding protocol described in the previous chapter, were subjected to surface analysis via scanning electron microscopy. Imaging revealed that fibers removed from aged body armor exhibit some morphological deformations, also known as kink bands. These defects on polymeric fibers were previously observed and characterized by Takahashi et al. [95]. Kink bands appear as a series of successive bands at an angle of 50-60° to the fiber axis, as shown in Figure 28 [95].

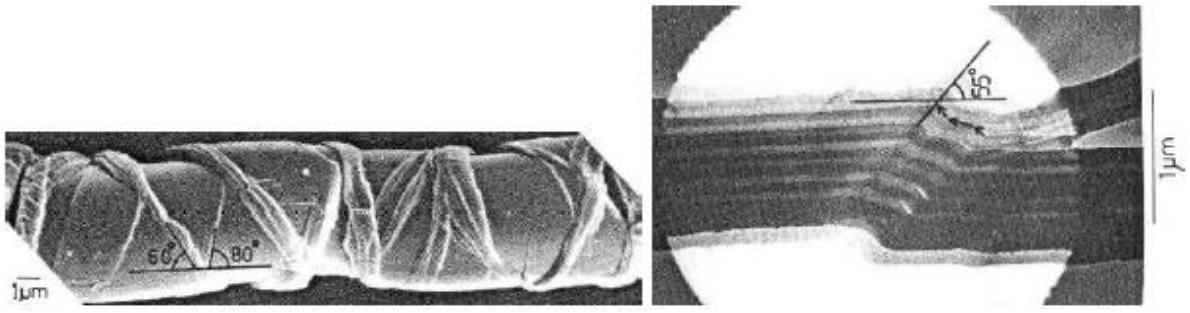

Figure 28. Kink bands on PPTA fibers characterized by Takahashi et al. [95].

These bands form a narrow triangular, or wedged-shaped area on the fiber where the orientation of the polymer chains suddenly changes. A model for the kink band formation has been proposed by Edmunds et al. and is shown in Figure 29 [96]. In this model kink bands are assumed to be made from straight limbs and sharp corners, based on a previous work by Hunt et al. [97]. According to this model, the orientation of kink band deformation (angle β) remains constant and the kink band angle α is the one changing. All of the fiber layers are compressed transversely and have the same thickness. When angles α and β are equal, the thickness of the layers within the kink band increases to the original uncompressed thickness. Then, when $\alpha = 2\beta$ all the layers whether they are internal or external to the kink band have the same thickness. Finally, as α increases, the internal layer thickness in the kink band decreases more than the thickness of the external layers.

All in all, bending or compression forces are required for a kink band to form. As compressive forces increase, deformation increases and begins to propagate from the surface to the fiber axis, and simultaneously new kinks begin to form along the fiber axis. With further increased compression bands intersect with each other and the outer region of the fiber, opposite to the compressed kink banded region, the fiber will fracture under tension to form a kink band break [95, 98, 99]. The process of a kink band break, also known as knuckle formation, is not reversible and voids are formed within the kink band as a result of lateral splitting between the polymer chains [100].

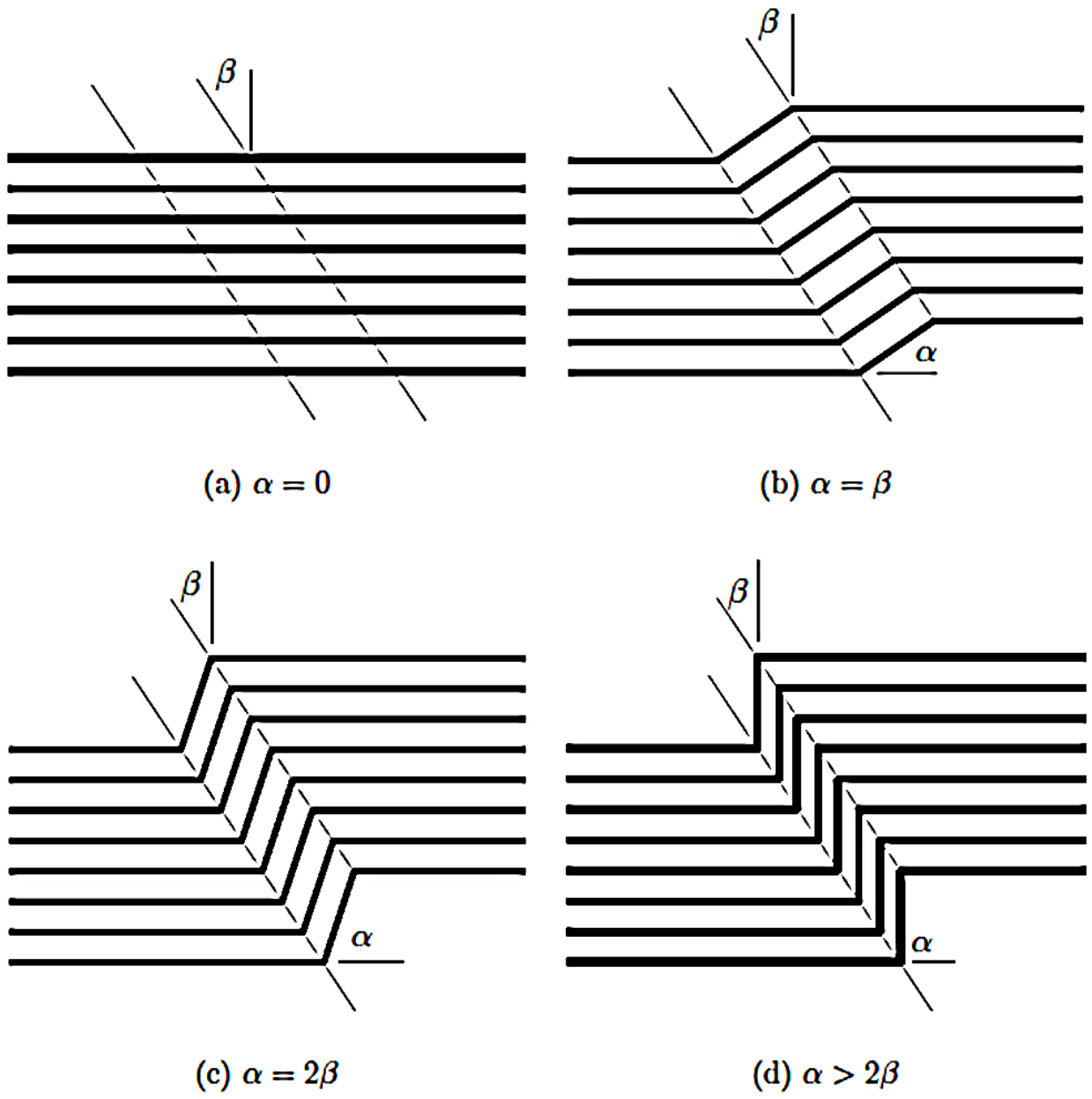

Figure 29. Model for kink band formation on PPTA fibers due to compressive forces [96].

Kink band formation on high strength polymer fibers used in body armor applications has been previously reported and characterized in other high strength fibers [95, 98-100]. However, the formation of kink bands in UHMWPE fibers used for ballistic protection has not been fully characterized yet. The imaging of the fibers in this study indicates that the kink bands formed in

UHMWPE fibers have similar morphological characteristics to those fibers made of PBO or PPTA (Figure 28). Our results, as can be concluded by the images shown in Figure 30, suggest that mechanical stress transferred to the fibers during bending of the body armor is translated to compressive and tensile stress onto the fibers leading to the formation of kink bands. UHMWPE fibers extracted from new body armor did not reveal any kink bands (Figure 30.a) and that was also the case for the fibers extracted from vest that were aged using the folding protocol, at areas away from the bending site (Figure 30.d). However, as can be seen in Figure 30.b, fibers extracted from aged (NIJ protocol) vests revealed the presence of kink bands, which were uniformly spread across the fibers of all the samples tested in this study. In addition, fibers extracted from laminates of the armor that were folded at an 180° angle (folding protocol) revealed severe kink band and knuckle formation at the bending point, as shown in Figure 30.c. These results clearly demonstrate that mechanical stress is the primary mechanism of kink band formation in UHMWPE fibers.

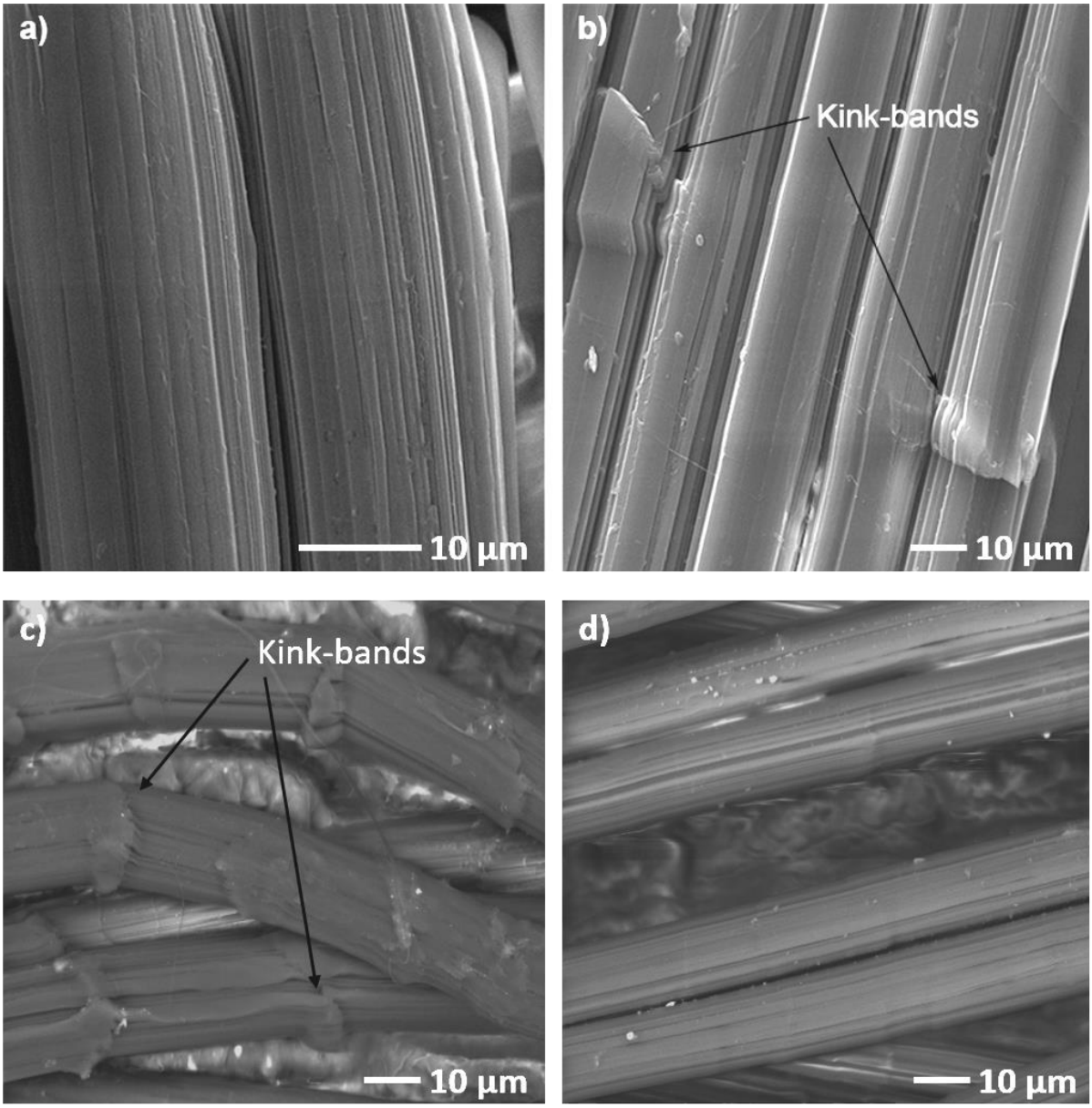

Figure 30. Scanning electron microscopy (SEM) images of UHMWPE fibers extracted from new (a), NIJ conditioned (b), and body armor aged via the folding protocol, 180° bending point (c) and non-bended areas (d) respectively.

In addition to these observations, energy dispersive spectroscopy (EDS) was used simultaneously to the imaging of the fibers to evaluate their chemical composition at various areas

including the kink bands. Fibers extracted from new body armor, conditioned with the NIJ protocol, as well as the folding protocol were tested in this set of experiments. The areas on these fibers that were analyzed via EDS to evaluate the oxygen concentration were the following: a) random areas on fibers extracted from new vests, referred as “New”, b) areas without kink bands and the kink band areas of fibers conditioned via the NIJ protocol, referred as “Normal-NIJ” and “Kink Band-NIJ” respectively, c) areas without and with kink bands on fibers conditioned via the folding protocol, referred as “Normal-Folding” and “Kink Band-Folding”. The results are summarized in Figure 31 below.

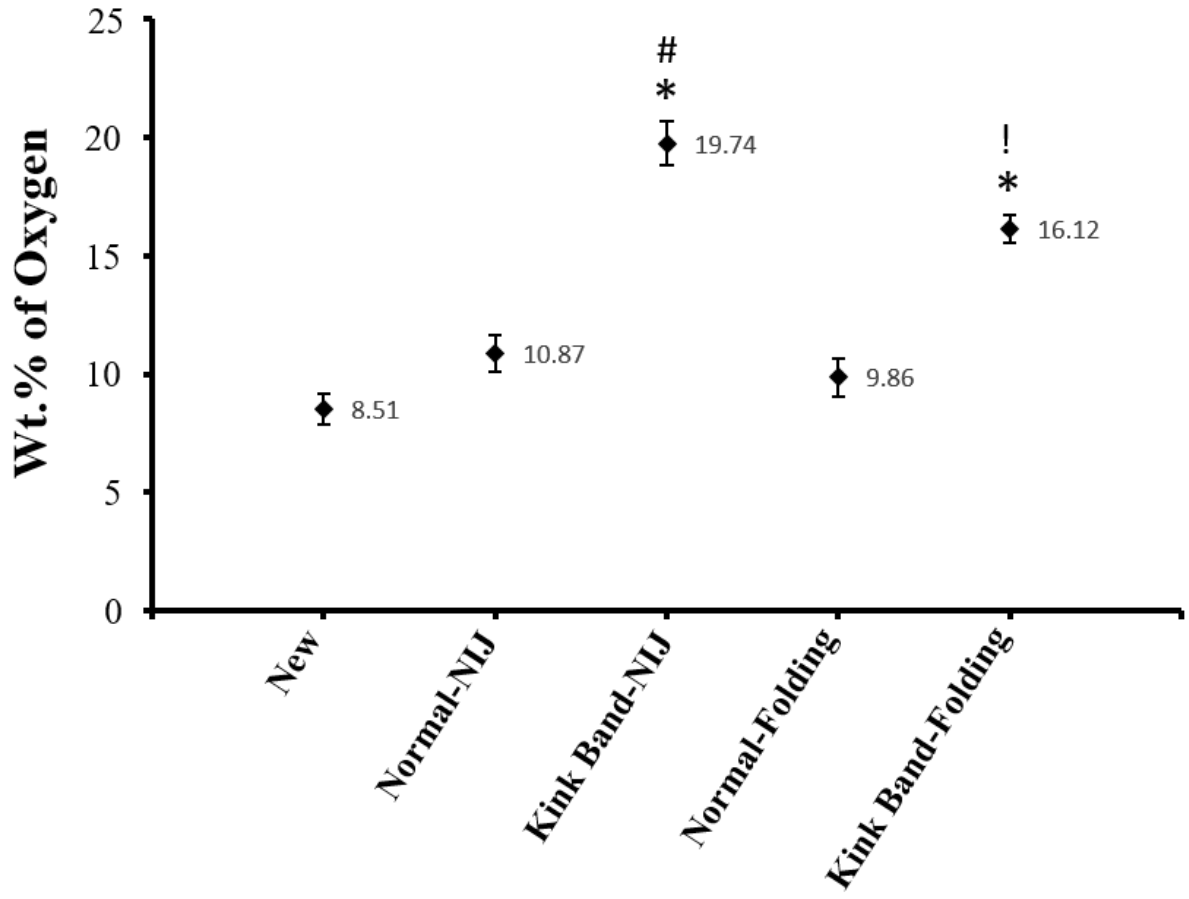

Figure 31. EDS analysis on UHMWPE fibers extracted from new, and conditioned body armor through the NIJ and Folding protocol. For each fiber sample the normalized wt.% of oxygen is reported. *p≤0.05, compares each fiber area to the new fibers, by Student's t-test. #p≤0.05 and !p ≤0.05 compares the "Kink Band-NIJ" and "Kink Band-Folding" data with the "No-Kink Band -NIJ" and "No-Kink Band -Folding" data respectively, by Student's t-test. Data are mean± S.E.M. (n≥50).

As can be seen from the Figure 31 above, there is a statistically significant increase in the oxygen concentration at the kink band areas of the UHMWPE fibers. This increase can be attributed to the formation of oxidation products, such as esters and ketones, or an increase of the

molecular oxygen concentration produced during the thermo-oxidative degradation of UHMWPE from reactions, such as the recombination reaction of peroxy radicals, as discussed in Chapter 2. Another important conclusion from this study is that areas on the aged fibers without kink bands show similar oxygen concentration to the new, non-treated, fibers. This result demonstrates that oxidation of the UHMWPE fibers is mainly occurring at the kink band areas. As previously mentioned, compression forces that produce kink bands in combination with tension forces generated on the opposite side of the fibers can potentially lead to bond scissions in the polymer chains and the formation of C-centered free radicals. These free radicals can consequently react with oxygen and result in oxidation reactions. Also, micro voids created by the kink bands could potentially induce the diffusion and solubility of oxygen into these areas of the fiber. All the above suggest that mechanical stress and the formation of kink bands in the material may have a major role in the initiation and propagation of the oxidative degradation of UHMWPE fibers.

4.3 Oxidation Analysis of UHMWPE Fibers

To further support the results of the previous section, and the conclusion that oxidation reactions in UHMWPE fibers initiate from the kink band areas, Infrared Spectroscopy (IR) experiments were conducted. First, the FTIR spectrum of UHMWPE fibers extracted from the center part of the 14th laminate of a new body armor (armor is comprised of 27 laminates) was acquired and used as a control in this study (Figure 32). The characteristic peaks at 2916 cm^{-1} and 2848 cm^{-1} are identified as sp^3 C-H symmetric and asymmetric stretching, at 1471 and 1461 cm^{-1} are assigned to C-H bending, and those at 731 and 717 cm^{-1} are in-phase and out-of-phase C-H rocking, respectively [101]. When oxidation takes place in UHMWPE, a new peak is formed at around 1700 cm^{-1}. This peak can be usually resolved into two individual peaks, one with a

maximum at 1735 cm^{-1}, which is assigned to an ester; and another one with a maximum at 1713 cm^{-1}, which is assigned to a ketone [58].

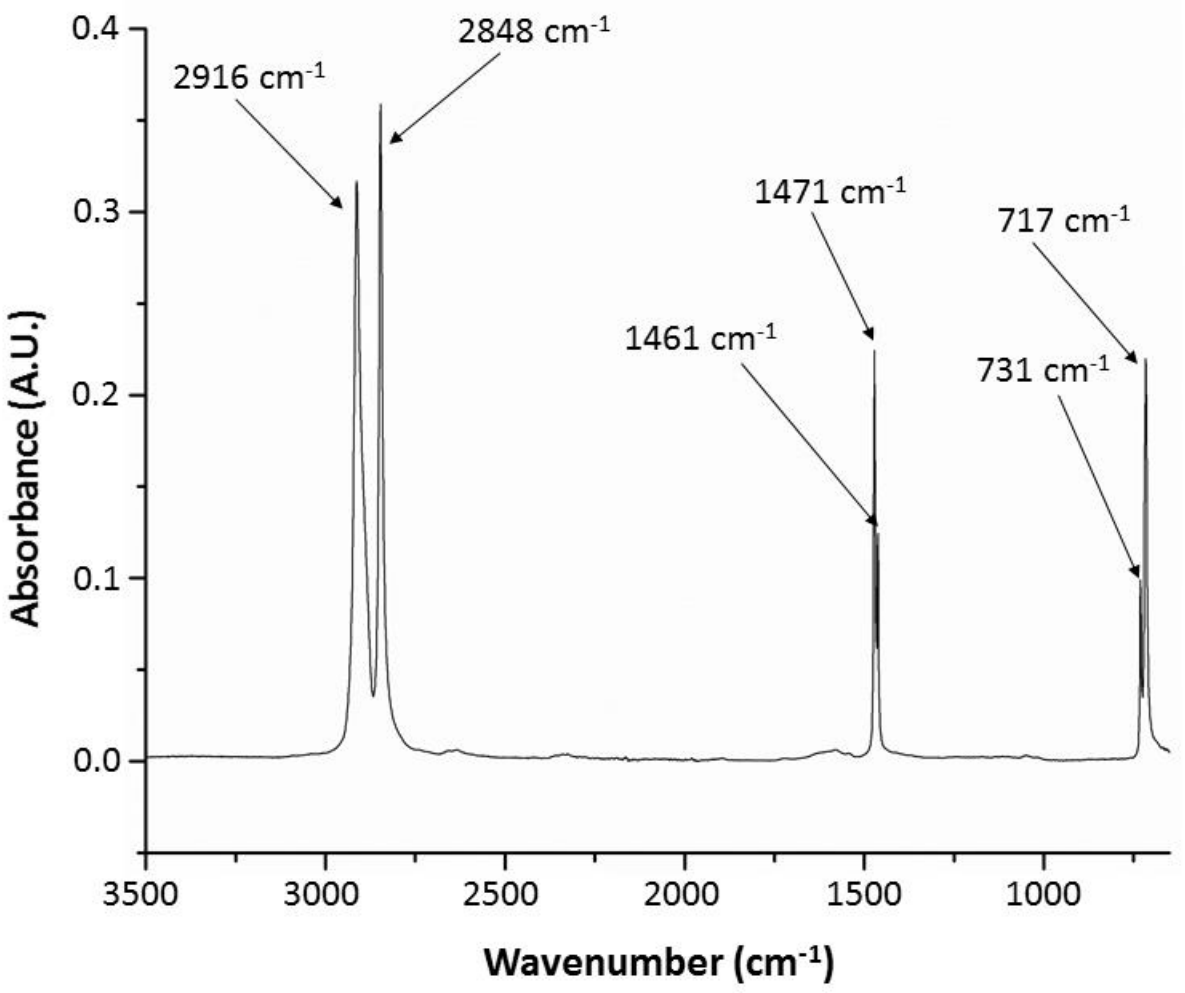

Figure 32. FTIR spectrum of control UHMWPE fibers, extracted from an unaged vest. The fibers used for the collection of this spectrum were isolated from the center part of the middle laminate of the body armor. The units of absorbance are arbitrary. The characteristic peaks of the spectrum are represented by arrows. The data are the mean values of 3 different fiber samples, each tested in triplicate.

In this study the degree of oxidation of the UHMWPE fibers tested was quantified by introducing the oxidation index (OI), as used in other artificial aging applications for UHMWPE materials [58, 84, 102]. For the purpose of this study, the peak at 1471 cm^{-1} was used as the reference peak. The OI was calculated by dividing the peak area at 1713 cm^{-1} by the peak area of the reference peak at 1471 cm^{-1}. In this study, OriginPro software was used to integrate the FTIR spectra collected. The following equation was used for the calculation of OI.

$$OI = \frac{A_{1713cm^{-1}}}{A_{1471cm^{-1}}}$$

In Figure 33, a representative FTIR spectrum of the oxidation peak at around 1700 cm^{-1} is shown for UHMWPE fibers extracted from the center part of the 14th laminate of a new body armor (Control Fibers), fibers extracted from the edge of the 1st laminate of a NIJ conditioned body armor (NIJ Conditioned Fibers), and fibers from the non-folded area (Folding Protocol – Non-Folded Area Fibers) and the folded area (Folding Protocol – Folded Area Fibers) of laminates conditioned using the Folding protocol. For each condition, more than three different fiber samples were tested and the spectrum of each sample was collected twice. After the integration of each peak, the mean values were used to calculate the oxidation index for each condition. As shown in Figure 33, the "NIJ Conditioned Fibers" demonstrate the most severe oxidation, since the area under the peak at 1713 cm^{-1} was the largest of the four. Also, the OI calculated for these fiber samples was 0.0719±0.0059, while the "Control Fibers" have an oxidation index of 0.0127±0.0016. This is a statistically significant 446% increase in the oxidation index between fibers extracted from new and NIJ conditioned body armor ($p \leq 0.05$, by Student's t-test). Furthermore, the area under the peak at 1713 cm^{-1} for the "Folding Protocol – Non-Folded Area Fibers" was slightly larger than that of the "Control Fibers" and their OI was calculated to be

0.0224±0.0063. These results are in accordance with the results acquired from the EDS analysis in the previous section, where the UHMWPE fibers from a non-folded area of the laminates conditioned with the Folding protocol have not shown a significant increase over the fibers extracted from a new vest. Finally, the area under the oxidation peak of the "Folding Protocol – Folded Area Fibers" was larger than that of the "Control Fibers" and the "Folding Protocol – Non-Folded Area Fibers" but lower that the "NIJ Conditioned Fibers". The calculated OI for these fibers was 0.0497±0.00582, which was statistically significant lower than 0.0719±0.0059 for the "NIJ Conditioned Fibers", but greater than the other two fiber samples in this set of experiments ($p \leq 0.05$, by Student's t-test).

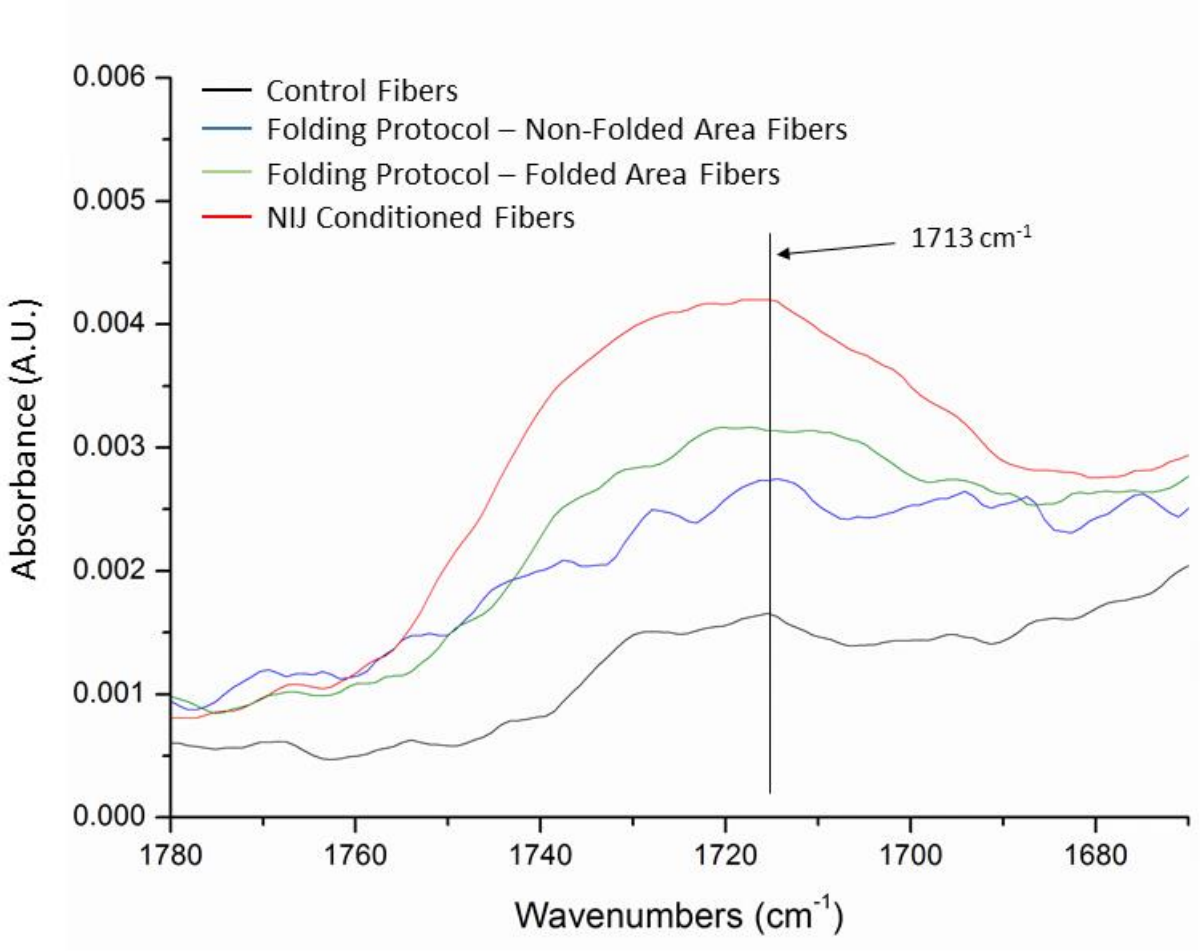

Figure 33. FTIR spectra of the oxidation peak at 1713 cm^{-1} wavenumber for different UHMWPE fiber samples. These peaks were integrated between 1690 and 1755 cm^{-1} and the areas calculated were used to calculate the OI of the samples.

All in all, the results of this set of FTIR experiments demonstrate that UHMWPE fibers without kink bands have low OI and show limited oxidation. This supports the idea that the thermal treatment of these fibers at 65 °C and the presence of oxygen in the surrounding environment do not have a major effect in the oxidation of UHMWPE fibers. However, when they are combined with mechanical stress and the formation of kink bands can drastically enhance the oxidative degradation of the material. The differences observed in the FTIR data and the OI of the fibers

extracted from the NIJ conditioned vests and the folded areas of the laminates conditioned with the Folding protocol may be attributed to the number of kink bands in the samples. Kink bands are abundant in the case of the NIJ conditioned fiber samples, whereas in the case of fibers from the Folding protocol they are isolated only at the bended area. Therefore, it can be concluded that fibers with a higher content of kink bands will oxidize more severely after a given period of time. These results further support the conclusions from the SEM-EDS analysis and the hypothesis that oxidation in UHMWPE fibers, when used in soft-ballistic inserts, is initiated and mainly occurring at the kink band areas and from there can potentially propagate easier along the fiber axis.

As previously mentioned, the body armor used in this study were comprised of 27 laminates. To evaluate the oxygen diffusion and the extend of oxidation among the different number of laminates in the body armor, including those in the outer most and the inner part of the armor, the following experiment was designed. UHMWPE fibers were extracted from the center and edge part of the following laminates of a vest conditioned via the NIJ protocol: laminate number 1, 7, and 14. This resulted in 6 different fiber samples, which are described below: "OV_Fiber_P1_Edge", which refers to fibers extracted from the edge part of the 1st laminate of a NIJ conditioned vest; "OV_Fiber_P1_Center", which refers to fibers extracted from the center part of the 1st laminate of a NIJ conditioned vest; "OV_Fiber_P7_Edge", which refers to fibers extracted from the edge of the 7th laminate of a NIJ conditioned vest; "OV_Fiber_P7_Center", which refers to fibers extracted from the center of the 7th laminate of a NIJ conditioned vest; "OV_Fiber_P14_Edge", which refers to fibers extracted from the edge of the 14th laminate of a NIJ conditioned vest; and "OV_Fiber_P7_Center", which refers to fibers extracted from the center of the 14th laminate of a NIJ conditioned vest. The control used in this experiment were fibers extracted from the center part of the 14th laminate of a new body armor "NV_Fibers_P14_Center",

as in the previous set of FTIR experiments. Figure 34 shows the OI calculated for each one of the aforementioned samples.

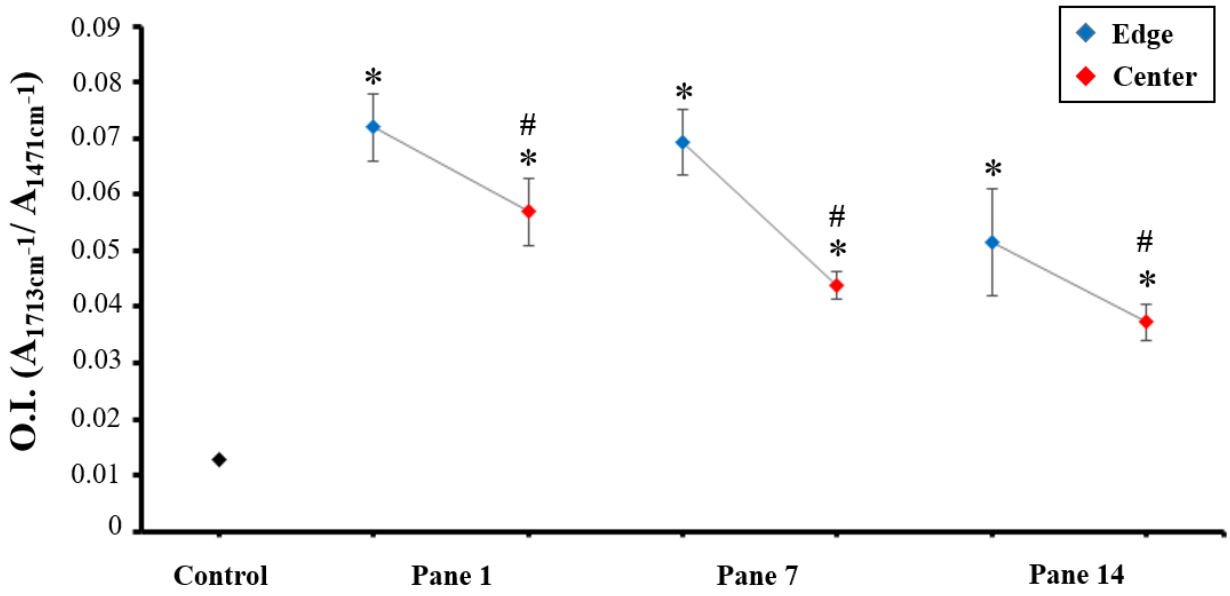

Figure 34. Changes in oxidation index (OI) for UHMWPE fibers extracted from various areas of NIJ conditioned body armor. The FTIR spectra of each sample were collected and the area under 1713 cm^{-1} was integrated and used to calculate the OI. *$p \leq 0.05$, compares each sample with the control; #$p \leq 0.05$, compares edge with center samples, by Student's t-test. Data are mean ± S.E.M. ($n \geq 3$).

The results presented in Figure 34 show that all of the UHMWPE fibers extracted from the NIJ conditioned vest are significantly more oxidized than the control fibers, which were extracted from a new vest. The most severe oxidation occurs on those fibers along the edge of the first laminate of the body armor. Conversely, the fibers residing in the center part of the fourteenth laminate appear to be the least oxidized ones. The oxidation of the fibers is shown to decrease when moving towards the inner part of the body armor. Also, the fibers extracted from the same

laminates showed a statistically significant decrease in the OI when moving from the edges to the center part of each laminate. These results clearly demonstrate the strong dependence of the oxidation reactions to the diffusion of oxygen into the material, as expected. Additionally, it should be noted that the edges of the laminates are more prone to bending during daily use of the body armor. This will result in a higher concentration of kink bands on fibers around the edge of the body armor, which can also contribute to the statistically significant higher degree of oxidation in these areas compared to the fibers reside in the center part of the laminates, as previously discussed.

4.4 Thermal Analysis and Crystallinity Determination

Thermal analysis of UHMWPE fibers was conducted using differential scanning calorimetry (DSC) to evaluate the effects of aging in the crystallinity of the material and investigate changes in the different crystalline phases. Representative DSC thermograms of UHMWPE fibers extracted from new and NIJ conditioned body armor are presented in Figure 35 and Figure 36, respectively. In both cases, the thermograms of UHMWPE fiber samples revealed broad melting peaks with a maximum at ∼147 °C. All melting peaks were treated as Gaussian functions and fitted by OriginPro software to predefine four different melting peaks as shown in Figure 37. The calculation of the total percent crystallinity of each sample was performed using the ASTM standard value for the theoretical heat of fusion of 100% crystalline polyethylene (289.3 J/g) [103]. However, for these UHMWPE fiber samples, the overall percent crystallinity as calculated by this method was nearly unchanged. Fibers extracted from a new vest revealed a total % crystallinity of 90±1.0 and those extracted from a NIJ conditioned vest have a slightly smaller value of 87.8±1.1. These numbers represent mean values with their standard error calculated by more than 6 thermograms per condition, produced from different fiber samples.

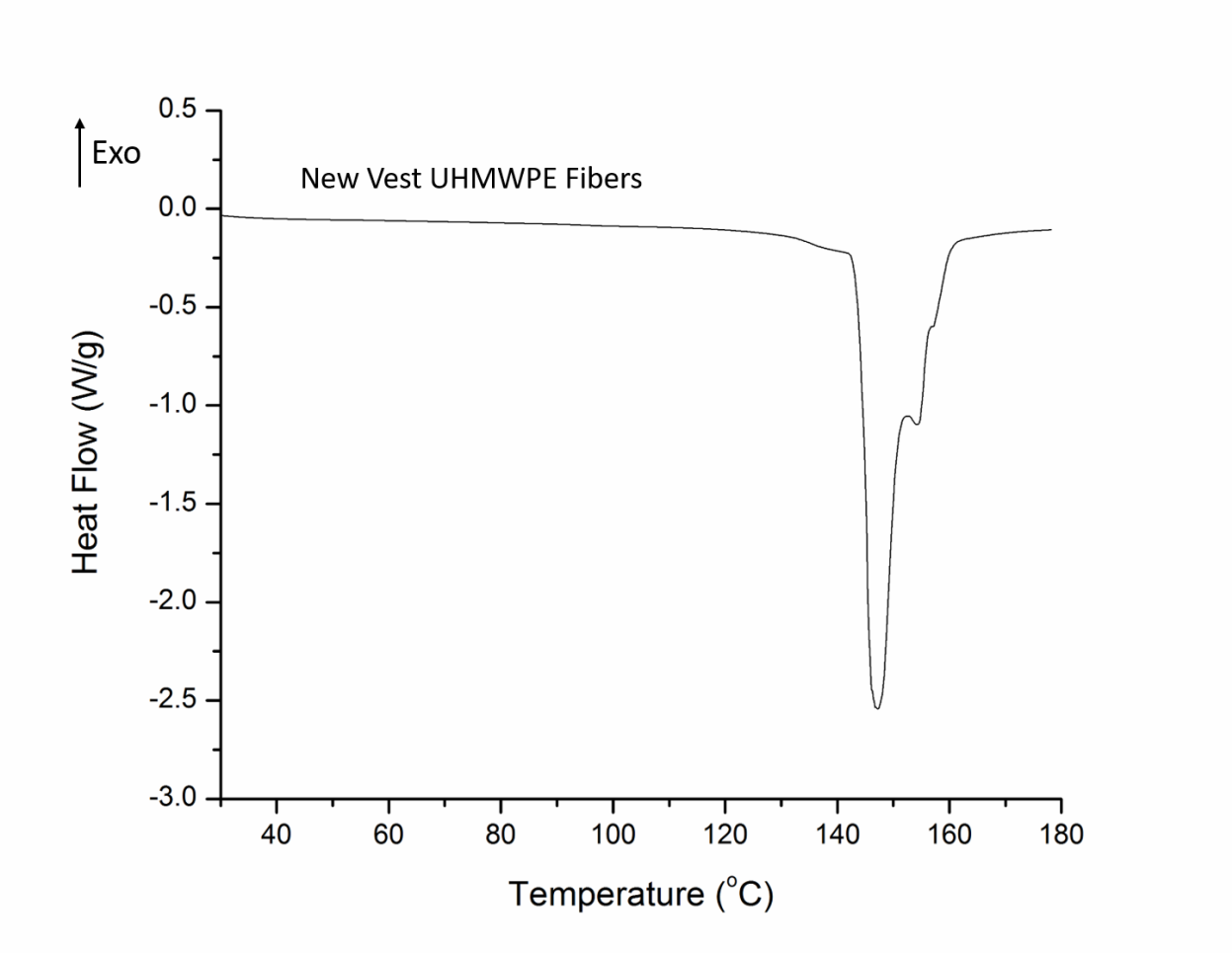

Figure 35. DSC thermogram of UHMWPE fibers extracted from a new body armor. Note the broad melting curve which can be resolved into four individual peaks with different maximum temperatures and different intensities. The more intense peak of the endotherm is at 147.3 °C. Standard uncertainties associated with the use of DSC in the measurement of these thermal properties are 5%.

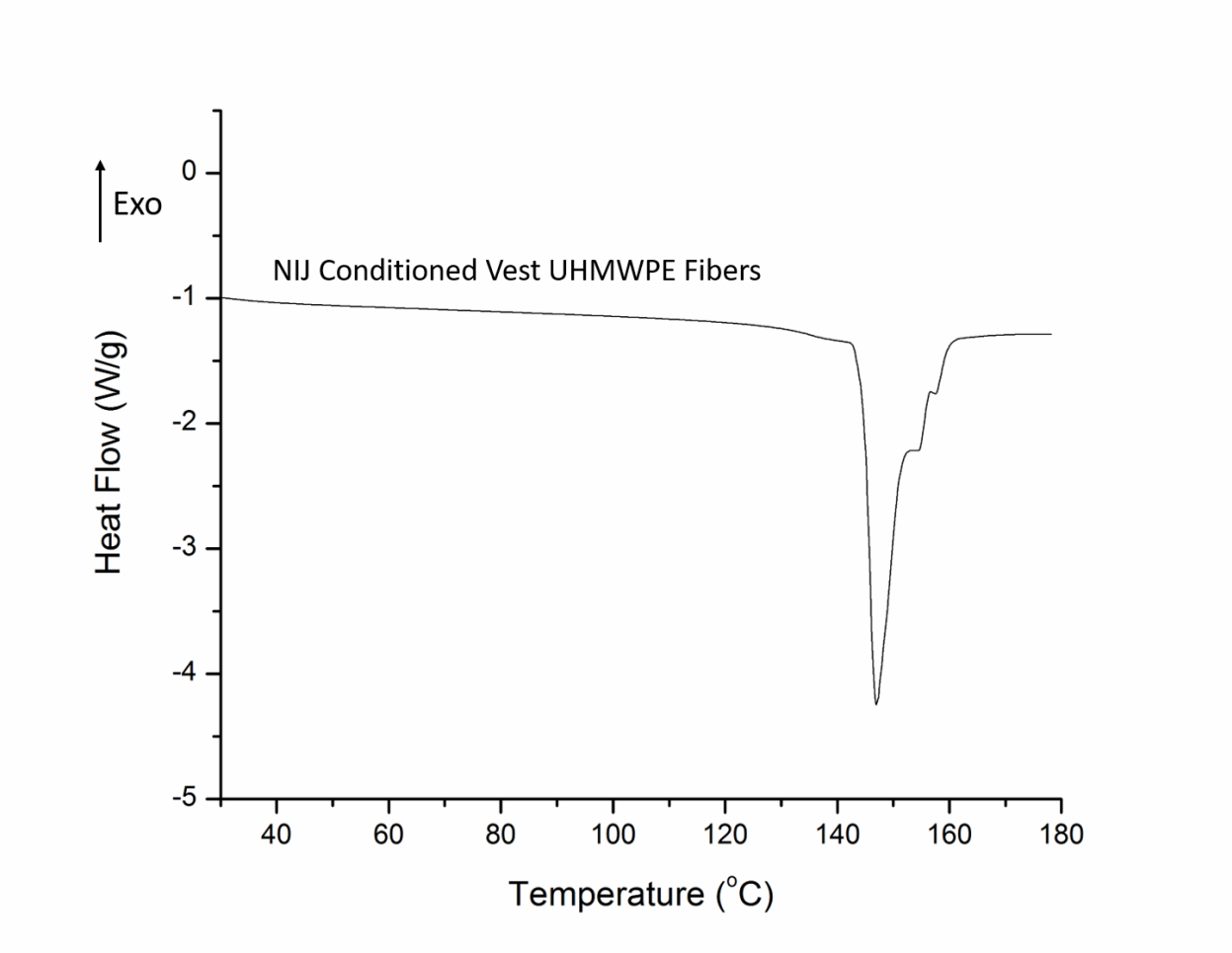

Figure 36. DSC thermogram of UHMWPE fibers extracted from a body armor conditioned with the NIJ protocol. Note broad melting curve which can be resolved into four individual peaks with different maximum temperatures and different intensities. The more intense peak of the endotherm is at 146.9 °C. Standard uncertainties associated with the use of DSC in the measurement of these thermal properties are 5%.

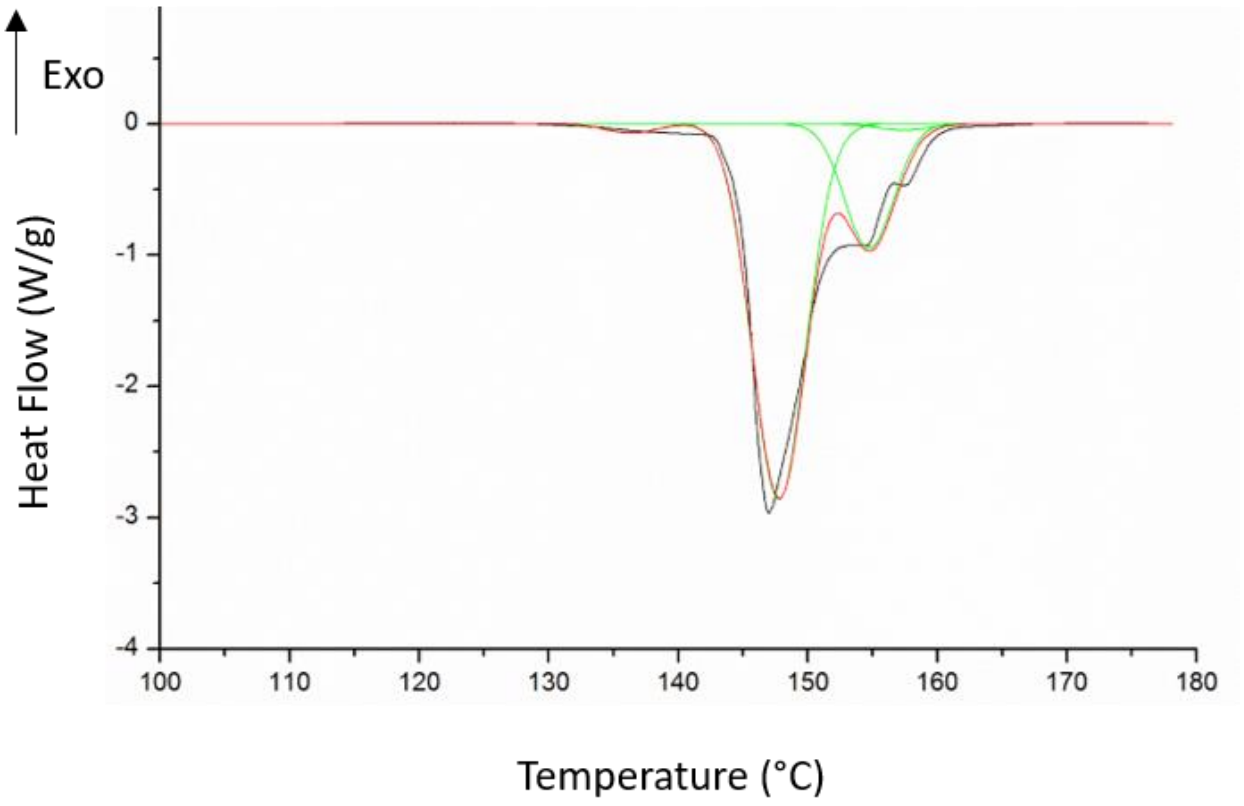

Figure 37. Resolved DSC thermogram of UHMWPE fibers extracted from a body armor treated with the NIJ protocol, scale enlarged to better show the deconvolution of the endotherm and the four peaks acquired through this process. Fitting was done using OriginPro software. The four peaks fitted in this endotherm had maxima at 136 °C, 147 °C, 151 °C, and 158 °C. Standard uncertainties associated with the use of DSC in the measurement of these thermal properties are 5%.

As can be seen from the figures above, the endotherm of the UHMWPE fibers used in this study was broad with overlapping regions between 136 °C and 162 °C. After the deconvolution of the endotherm into four peaks, as shown in Figure 37, these peaks were integrated to give four different areas, and the percentage of the area of the total melting endotherm was attributed to the area of each individual peak. Each one of the deconvoluted peaks corresponds to four different

melting points, the results are summarized in Figure 38. The lowest melting peak in the region of 136 °C is assigned as T_{m1}, and is relatively broad. This peak did not change significantly between new and aged vest fibers and is attributed to the melting of the monoclinic phase [10, 42, 104, 105]. The second melting peak T_{m2}, around the region of 147 °C is the strongest signal and is attributed to melting of the extended orthorhombic crystals to form pseudo-hexagonal crystals [10, 31, 42, 104, 106, 107]. This peak did not shift between fibers extracted from new and NIJ conditioned body armor. However, the percentage of peak area for the heat of melting decreased from 76.7% to 70.4% with aging (Figure 39). The third melting peak, T_{m3}, is located at around 154 °C and is hypothesized to be the melting of a pseudo-hexagonal mesophase [10, 31, 42, 104, 106, 107]. Finally, a fourth melting peak, T_{m4}, was observed at around 160 °C, which is identified to be the melting of the hexagonal crystal phase [10, 42, 104-106].

UHMWPE Fibers Conditioning	T_{m1} (°C)	T_{m2} (°C)	T_{m3} (°C)	T_{m4} (°C)	ΔH_f J/g	X_c %
New	136	147	153	159	260.4	**90**
65 °C, 80% relative humidity, 5 rpm, 14 days	136	147	154	158	254	**87.8**

Figure 38. Summary of melting points, heat of fusion, and crystallinity for UHMWPE fibers extracted from new and NIJ conditioned body armor. Note that the melting peaks and the total % crystallinity do not change significantly. Changes in the percentages of each crystal phase are observed with aging.

Overall, no major changes in the total % crystallinity, or the location of the melting peaks of the endotherms were observed between UHMWPE fibers extracted from new and NIJ

conditioned vests. Additionally, our results show that the percentages of the monoclinic and the hexagonal crystal phases do not change upon aging, as shown in Figure 39. According to the literature, the monoclinic crystals can form only at high drawing rations, whereas hexagonal crystals will only form when polymer chains in UHMWPE fibers are constrained when heated at elevated temperatures, such as in the case of fiber drawing at high temperatures [43, 49]. Therefore, the presence of these two crystal phases in our fibers further validates that the fibers been used in these body armors are highly drawn fibers with very highly oriented polymer chains. Also, conditioning of the body armor at 65 °C is not a high enough temperature to melt the monoclinic crystal phase, as shown by our DSC results. Thus, the percentage of this phase did not change in upon aging, as expected.

UHMWPE Fibers Conditioning	Crystal Phase Percentages			
	T_{m1}	T_{m2}	T_{m3}	T_{m4}
New	1.8%	76.7%	20.3%	1.2%
65 °C, 80% relative humidity, 5 rpm, 14 days	1.9%	70.4%	26.1%	1.6%

Figure 39. Summary of the crystal phase percentages for UHMWPE fibers extracted from new and NIJ conditioned body armor. Calculations were done by fitting and integrating the DSC endotherms using OriginPro software. Changes in the percentages of each crystal phase are observed with aging.

The most significant changes observed from the thermal analysis of these samples is the decrease of the orthorhombic crystal phase and the increase of what we hypothesize to be the pseudo-hexagonal mesophase after aging (Figure 39). Without any significant changes to the other two crystal phases identified (monoclinic and hexagonal), these results may suggest that during aging, some polymer chains originally in the orthorhombic crystal phase are losing their initial conformation. This allows these polymer chains to re-orient and convert easier into pseudo-hexagonal crystal phase, which is a mesophase between the transition of the polymer chains from the orthorhombic to the hexagonal crystals. This hypothesis could be explained if one takes into consideration the parameters of the formation of the hexagonal phase. Hexagonal crystal phase will form upon heating the polymer chains at high temperatures (e.g. 65 °, 80 °C, or higher) while constraining them at the same time [43]. Considering now that the highly drawn fibers in this study result in miniscule free volume between the polymer chains in the extended orthorhombic phase, upon heating of the fibers during the DSC analysis, the chains in the orthorhombic phase might not be able to fold back on each other, since they are constrained by the adjacent chains, and may form pseudo-hexagonal and hexagonal crystals, as shown by the DSC endotherms. However, as temperature increases in the DSC pan, the freedom of motion and free volume of the self-constrained polymer chains will increase. Therefore, the conditions are not optimum for the complete transformation of the orthorhombic to a hexagonal phase, and a new mesophase, which could have some orthorhombic and some hexagonal phase properties, can potentially form. Finally, to better support this hypothesis we need to conduct more experiments that are described in the future work and will help us to better understand the existence of this peak at 153 °C.

4.5 Crystal Morphology of UHMWPE Fibers

The UHMWPE fibers used in this study were shown to be very highly crystalline with about 90% total crystallinity. This results in very tightly packed and highly oriented crystallites within the fibers. To better understand the morphological changes that the crystals undergo in the material we need first to fully characterize the crystal morphology of these fibers. In this set of experiments WAXS analysis was performed on UHMWPE fibers extracted from new body armor to assess the different type of crystals initially present in these fibers, and complement the data obtained from the DSC analysis. WAXS data of the new fibers were collected at 25, 140 °C and the diffraction patterns are shown in Figure 40, and the diffractograms of intensity vs. 2θ° are shown in Figure 41 and Figure 42.

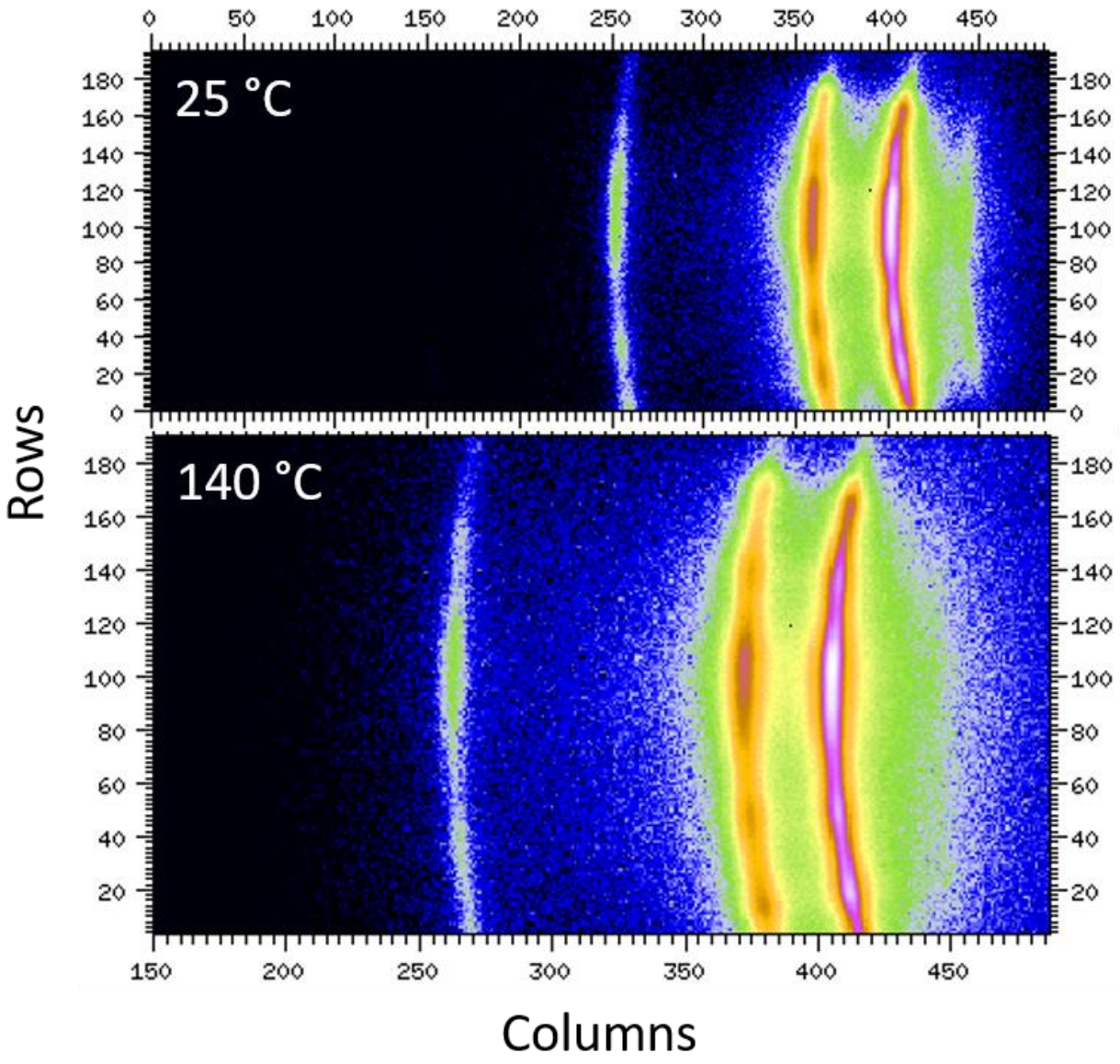

Figure 40. 2D WAXS patterns for UHMWPE fibers extracted from new vests at 25 and 140 °C. The scattering patterns were measured on a bundle of fibers placed horizontally, with their axis perpendicularly to the X-ray beam. Each condition was measured twice using different samples on different days.

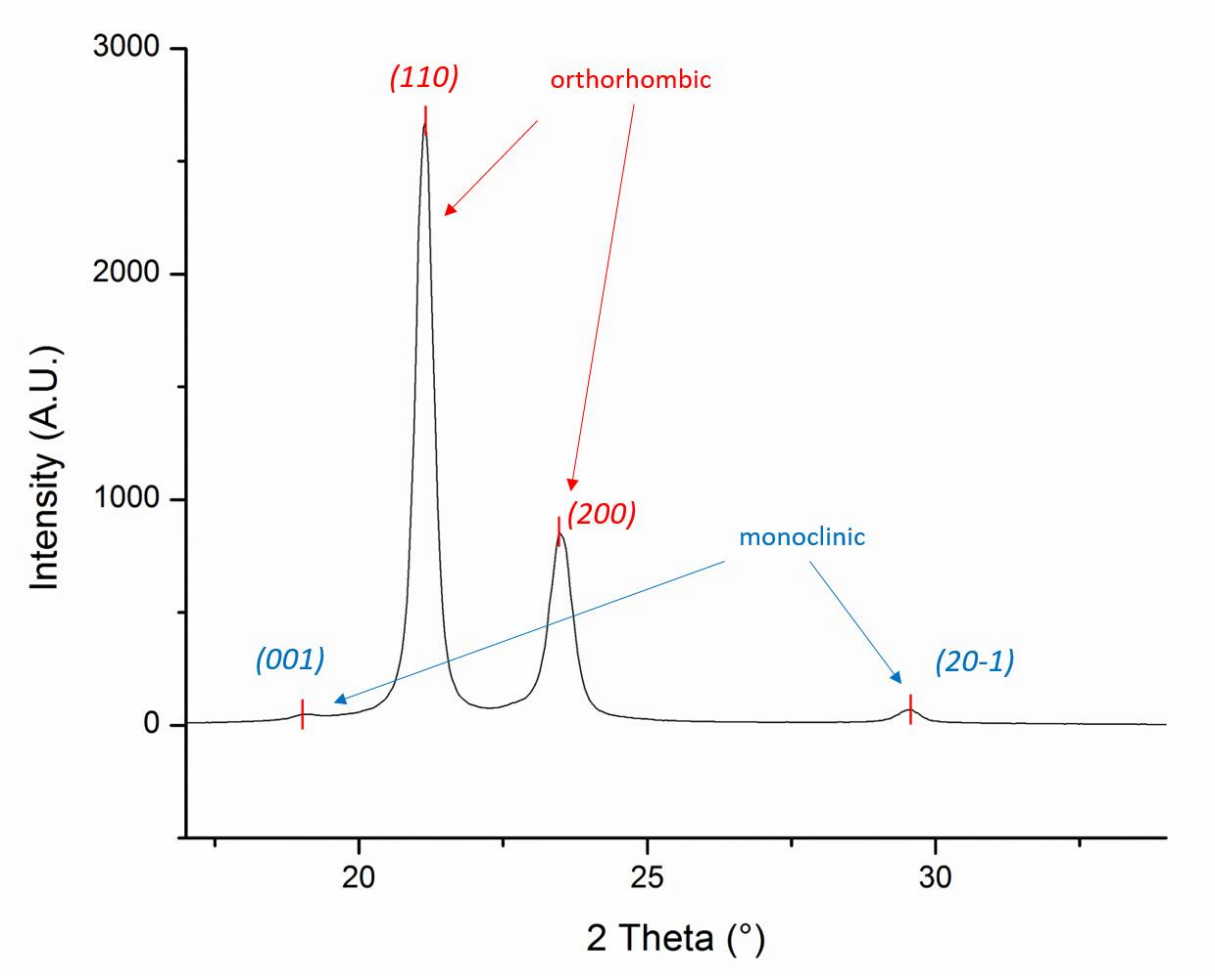

Figure 41. WAXS diffractograms of UHMWPE fibers extracted from new body armors. The diffraction was measured on a bundle of fibers placed horizontally, with their axis perpendicularly to the X-ray beam, at 25°C. The intensity peaks for the orthorhombic and monoclinic crystal phases are shown.

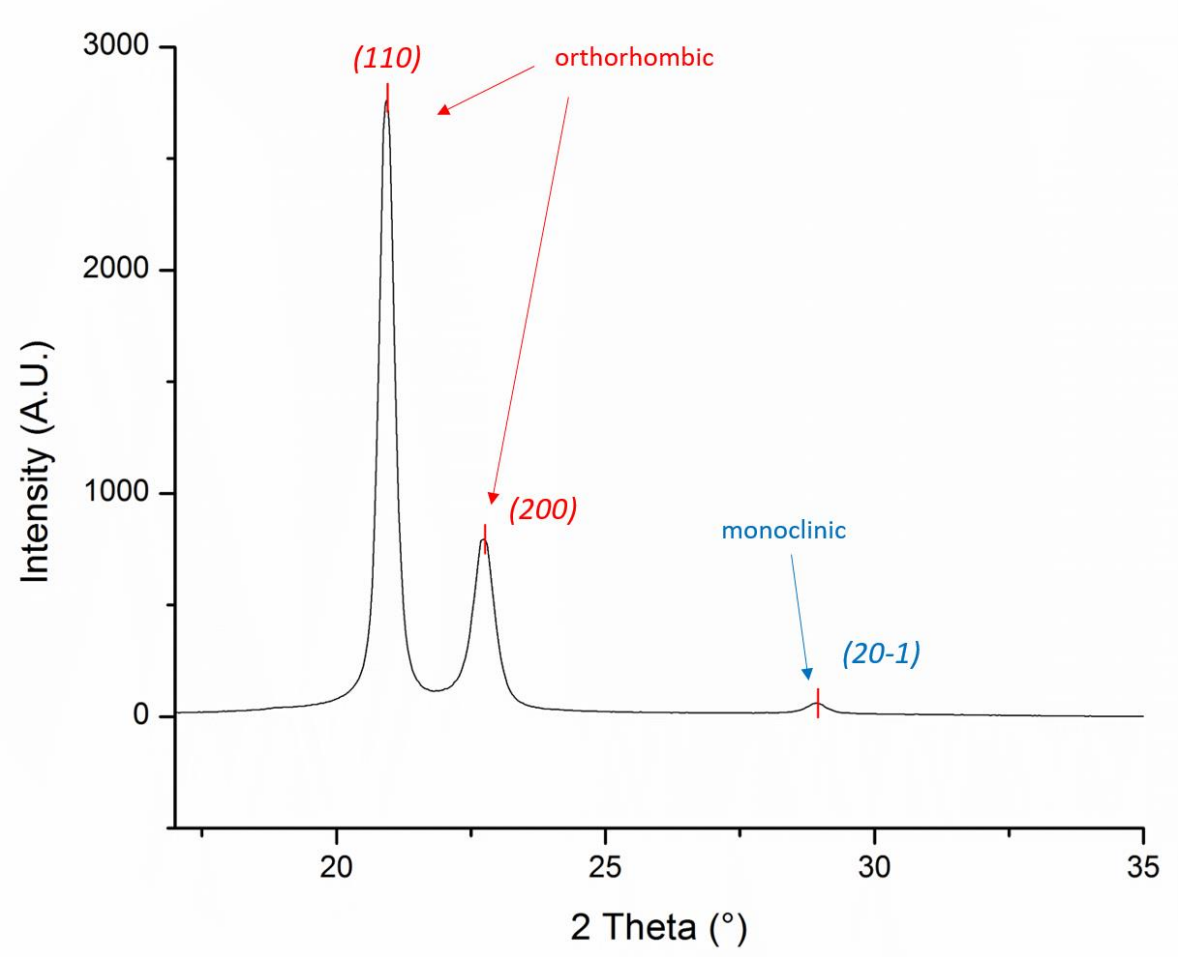

Figure 42. WAXS diffractograms of UHMWPE fibers extracted from new body armors. The diffraction was measured on a bundle of fibers placed horizontally, with their axis perpendicularly to the X-ray beam, at 140°C. The intensity peaks for the orthorhombic and monoclinic crystal phases are shown.

As can be seen from the figures above, two monoclinic peaks and two orthorhombic peaks are identified for the fibers extracted from new vests at 25 °C [47, 49, 105, 108]. As the temperature increase to 140 °C the monoclinic (001) diffraction peak can be barely detected, while the area under the (20-1) monoclinic peak decreases from 1.79%, in the 25 °C diffractogram, to 1.44%. Overall, the percentage of the monoclinic phase decreases from 2.22% to 1.44% as temperature

increases from 25 °C to 140 °C. This result indicated that at a temperature between this range something occurs to the monoclinic phase and it starts decreasing. These data support the DSC results where the melting peak for the monoclinic phase was found to be at 136 °C. Also at room temperature the amount of the monoclinic phase calculated by the deconvolution of the DSC endotherm was found to be ~2%, which is in agreement with the value of 2.22% calculated by the integration of the WAXS diffraction patterns of $(001)_m$ and $(20\text{-}1)_m$ at 25 °C. Finally, no hexagonal phase was observed in the WAXS diffractograms of the fibers, since the appearance of the WAXS diffraction peak of the hexagonal phase has been shown to occur at very high temperatures above 277 °C, when fibers are constrained [104]. It should be also noted, that the equatorial diffraction peak of the hexagonal phase is right at $2\theta = 20.5$ [105]. Since the diffraction peak of the (110) lattice plane of the orthorhombic crystals is at $2\theta = 21.5$, it might be very difficult to observe the diffraction peak of such a small percentage (only ~1%) of hexagonal phase due to overlapping of the two peaks. However, if WAXS analysis is conducted on constrained fibers at very high temperatures (above 160 °C), the diffraction peak of the hexagonal phase at $2\theta = 20.5$ will be strong and easily identified [104]. Additionally, the meridional diffraction pattern of the crystals when fibers are placed perpendicular to the X-ray beam, which could potentially reveal the existence of the pseudo-hexagonal phase, was not collected in this study due to lack of the appropriate mounting stage.

4.6 Summary

In this chapter the degradation of UHMWPE fibers extracted from body armor is characterized and discussed. The EDS results demonstrate that the oxygen concentration of the fibers is higher in the kink bands. These kink bands where shown to be produced by mechanical

stress. Also, the FTIR analysis of the fibers showed that the kink banded areas are significantly more oxidized than the rest of the areas along the fibers. The above results lead to the conclusion that there is a synergy between the mechanical induced degradation and the oxidation in these UHMWPE fibers.

Additionally, the crystallinity characterization of the material revealed that the total percent crystallinity did not change upon aging. This supports the idea that oxidation occurs in the amorphous regions of the polymer. DSC data demonstrate that the drawing process of these fibers was conducted at high drawing ratios, due the presence of a monoclinic melting peak identified on the endotherm, also supported by the monoclinic diffraction peaks $(001)_m$ and $(20\text{-}1)_m$ of the WAXS analysis. The percentage of this peak remains constant upon aging, however the percent of the orthorhombic crystalline phase decreases significantly from 62.1% to 45.8%. A melting peak was observed at 155 °C which is attributed to a pseudo-hexagonal mesophase. We hypothesize that right above the melting temperature of the orthorhombic crystals, the highly oriented self-constrained polymer chains of the extended orthorhombic phase will absorb enough energy, through heat, to transition to the hexagonal phase. However, the high heating rate (10 °C/min) during the DSC analysis will not allow these polymer chains to fully reconfigure into hexagonal crystals and they will form a transition mesophase, which will melt at around 155 °C, before the melting of hexagonal phase (160 °).

Finally, the WAXS results supplemented the DSC data results showing that the most abundant crystal phase in the fibers is the orthorhombic. Furthermore, the scattering from the monoclinic crystals at 25 °C prove that the percentage of this phase in the fibers is constant at ~2%. Also, combining the DSC with the WAXS data at 140 °C it can be clearly stated that the monoclinic phase is melting around 136 °C. No hexagonal phase was observed from the WAXS

analysis, since its formation requires constraining the polymer chains at higher temperatures than 140 °C. Finally, the pseudo-hexagonal phase was not observed in the WAXS diffractogram. This result suggests that the orientation of the pseudo-hexagonal crystals in the fibers that could result in a diffraction peak during WAXS analysis, is different than that of the monoclinic, orthorhombic, and hexagonal phases. Since the fibers were placed perpendicular to the X-ray beam, this result suggests that WAXS analysis should also be performed with the fiber axis placed parallel to the X-ray beam.

Chapter 5: Binder Resin Extracted from Body Armor

5.1 Chapter Overview

In this chapter the effects of accelerated aging in the degradation of the binder material used in the body armor is studied. The chemistry of the material extracted from the body armor is first identified and the molecular weight and oxidation were characterized as marker of degradation.

5.2 Identification of Binder Resin Material Used in Body Armor

The binder resin was initially extracted from new body armor and dissolved in deuterated chloroform for analysis through liquid NMR spectroscopy acquiring the ^{13}C and ^{1}H spectra. These non-aged samples were used as a control to help in the identification process of the material incorporated in the laminates. The ^{1}H NMR spectrum of the binder, as can been seen in Figure 43 (red spectrum), revealed the existence of a peak attributed to the phenyl groups (C_6H_5), which is a characteristic signal of polystyrene [109]. However, more signals were present in the spectrum that were attributed to polyisoprene, including the =CH-, -CH_2-, and -CH_3 as shown in Figure 43 (red spectrum) [110]. To support these findings polystyrene and polyisoprene samples were purchased and tested via NMR using the same parameters. The spectra collected are shown in Figure 43, blue and purple spectrum, respectively and the results obtained are in accordance with the literature [109, 110]. These results suggest that the binder used in the body armor could be a co-polymer of polystyrene and polyisoprene. Also, since the intensity of the peaks corresponding to polyisoprene have a higher intensity in the binder sample, than those found in the polystyrene spectrum we strongly believed that the copolymer used should have a higher polyisoprene

percentage. One of the commercially available 18% styrene-isoprene co-polymer is manufactured by Kraton Polymers. This elastomer was purchased and studied using NMR. Its proton NMR spectrum is almost identical to the binder spectrum, as shown in Figure 43 (green spectrum).

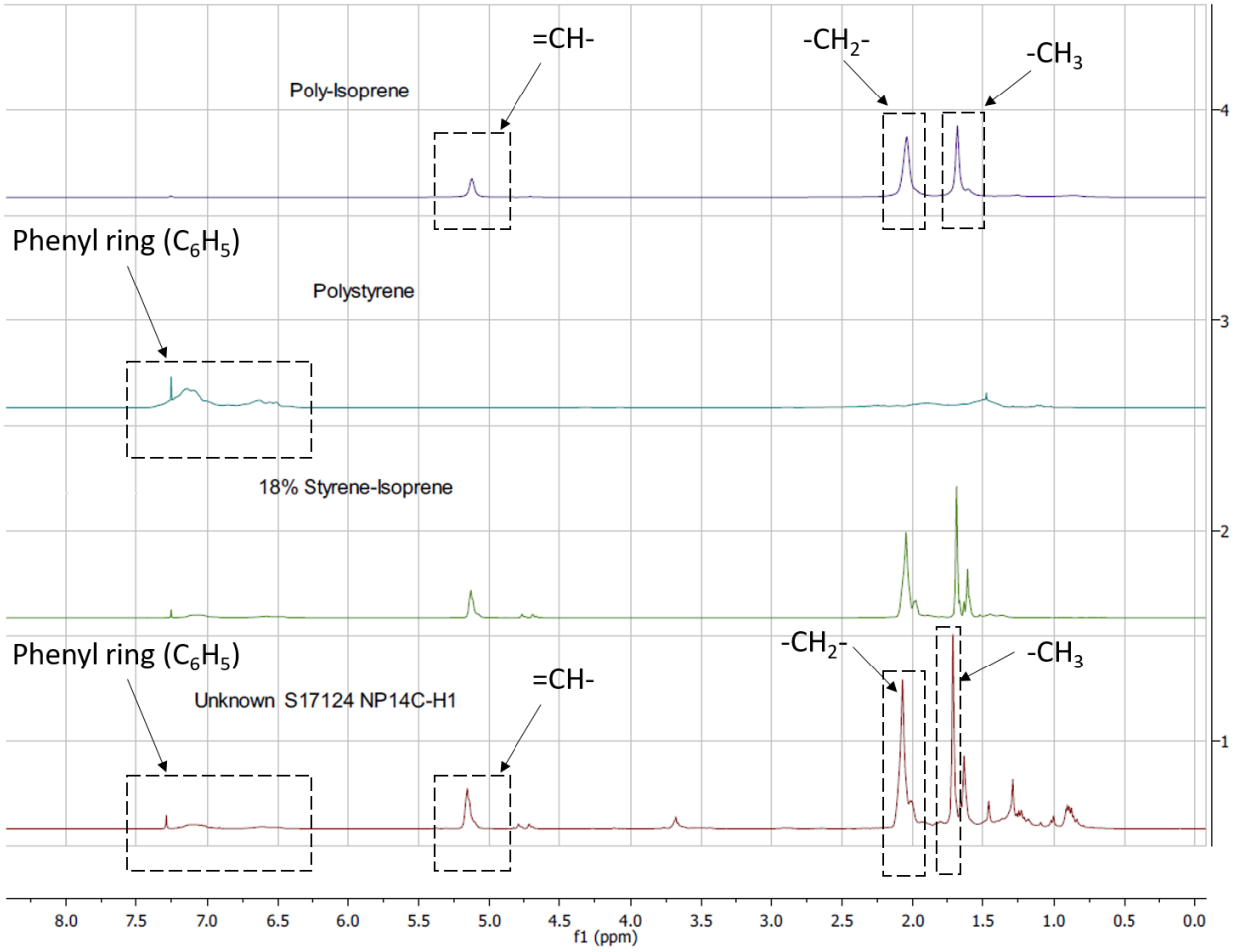

Figure 43. ^{1}H NMR spectra (in $CDCl_3$) of polyisoprene (purple spectrum), polystyrene (blue spectrum), 18% styrene-isoprene co-polymer (green spectrum), and binder resin (red spectrum).

To further validate these findings, the ^{13}C NMR spectra of the binder resin, polystyrene, polyisoprene, and 18% styrene-isoprene Kraton elastomer were obtained and represented in Figure 44. As can be seen from the spectra of the binder resin and the Kraton elastomer, the peaks produced for both materials are almost identical.

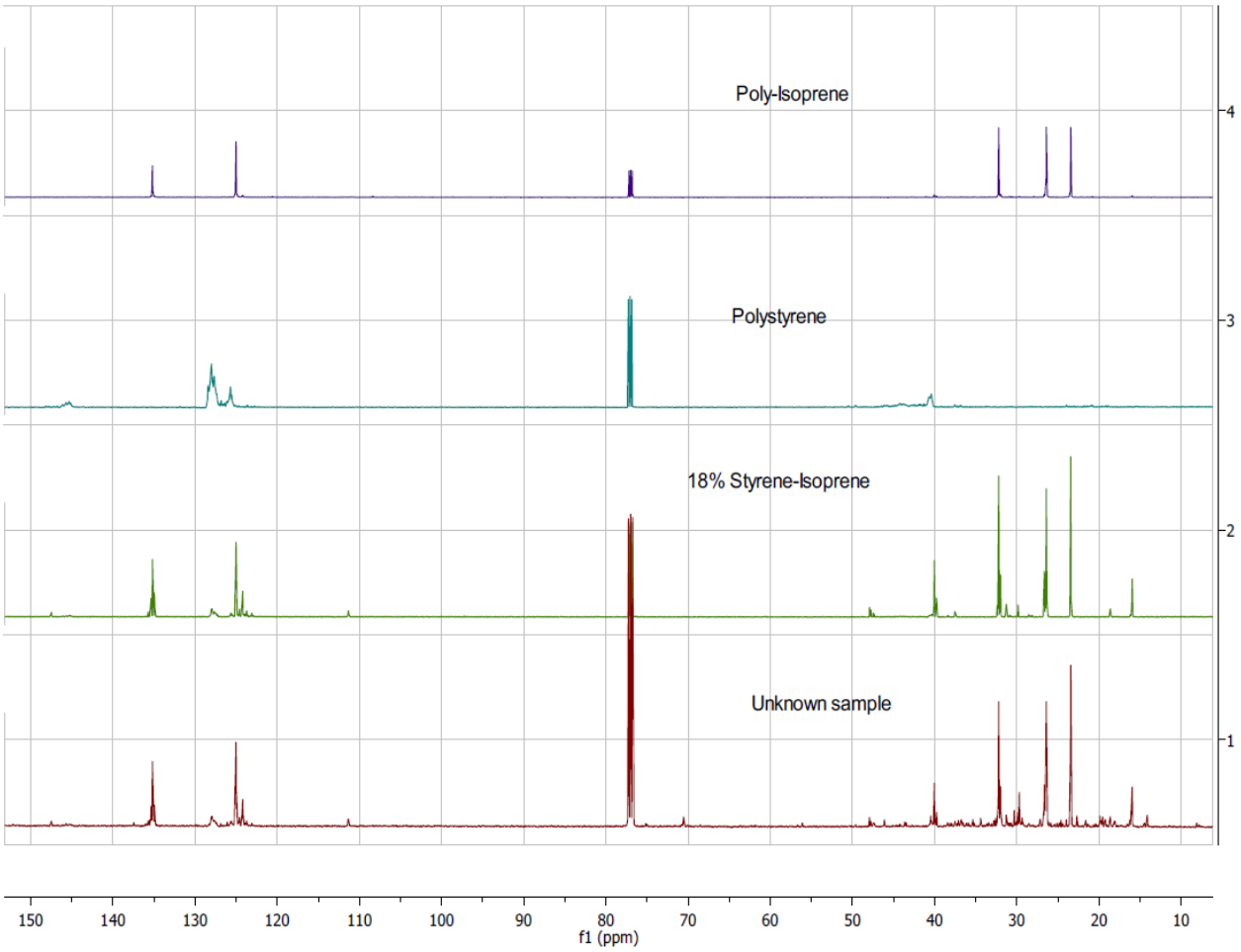

Figure 44. ^{13}C NMR spectra (in $CDCl_3$) of polyisoprene (purple spectrum), polystyrene (blue spectrum), 18% styrene-isoprene co-polymer (green spectrum), and binder resin (red spectrum). Note that the high intensity peak at around 77 ppm is produced by the $CDCl_3$.

5.3 Characterization of Oxidation

A representative FTIR spectra of the binder elastomer extracted from a new body armor is shown in Figure 45. The characteristic peaks at 2958, 2917, and 2850 cm^{-1} are identified as C-H stretching. the peak at 1631 cm^{-1} is assigned to C=C stretching, and the peaks at 1445 and 1375 cm^{-1} are identified as CH_2 and CH_3 stretching, respectively [111].

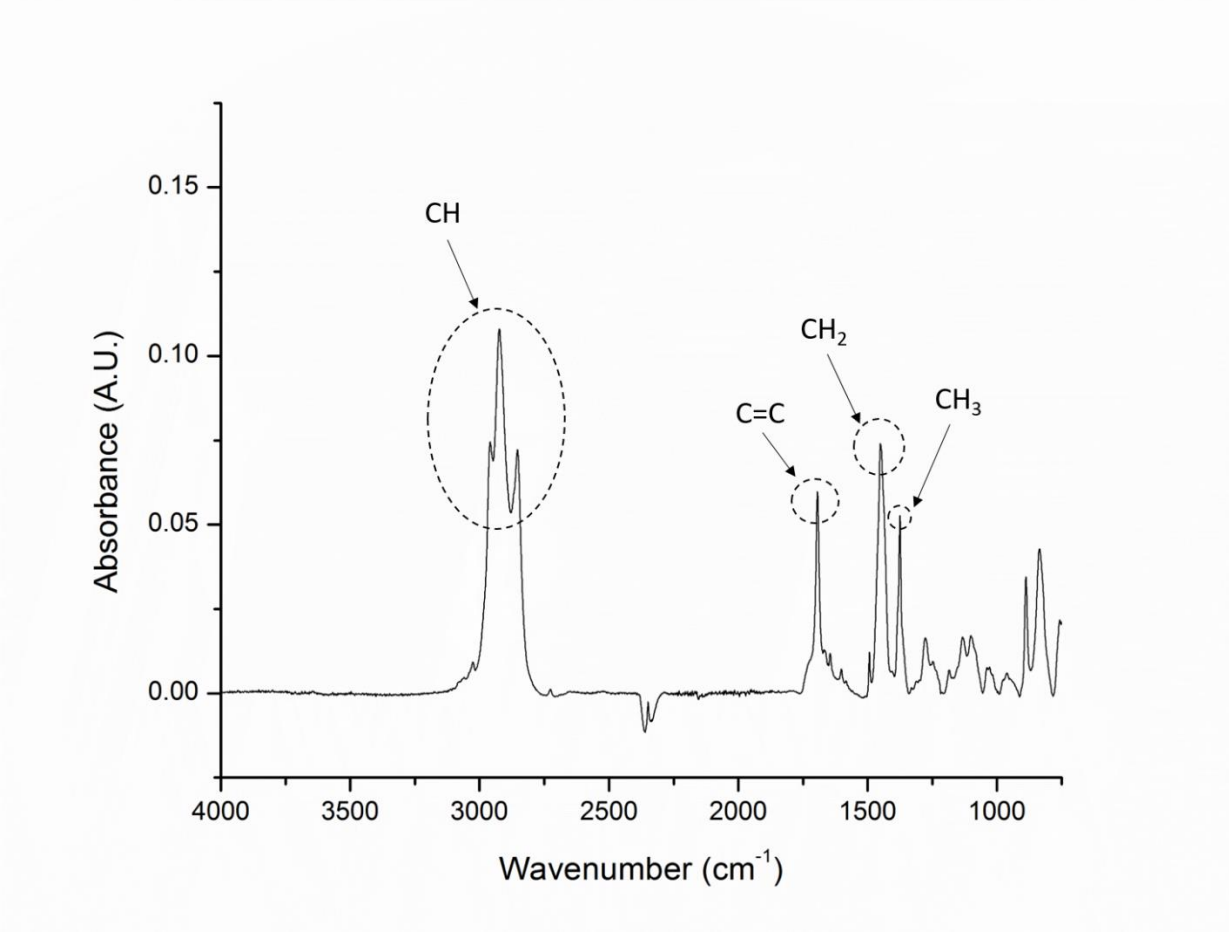

Figure 45. FTIR spectrum of control binder resin, extracted from an unaged vest. The elastomer used to collection this spectrum was isolated from the center part of the middle laminate (number 14) of the body armor. The units of absorbance are arbitrary. The characteristic peaks of the spectrum are represented by arrows.

Previous studies on polystyrene and polyisoprene elastomers have shown that elevated temperatures will induce C-C bond scissions in the backbone of the polymer chains and produce C-centered free radicals through a mechanism similar to that of UHMWPE described in Chapter 2 [111, 112]. These C-center free radicals, in the presence of oxygen, will induce oxidation reactions and ultimately will form carbonyl groups in the polymer, which are easily detected in the IR spectrum at around 1700 cm^{-1} [111-113]. Similar to the FTIR study of UHMWPE discussed in a previous chapter, the spectra of binder samples extracted from different areas of new and NIJ conditioned body armor were collected and the area under the carbonyl peat at 1700 cm^{-1} was calculated by taking the integral of the peak. The percent changes in the area of this peak between the different samples was calculated and the data are shown in Figure 46 and Figure 47. In this set of experiments, the control used was the area under the peak at 1700 cm^{-1} of binder extracted from the center part of the 14^{th} laminate of a new body armor.

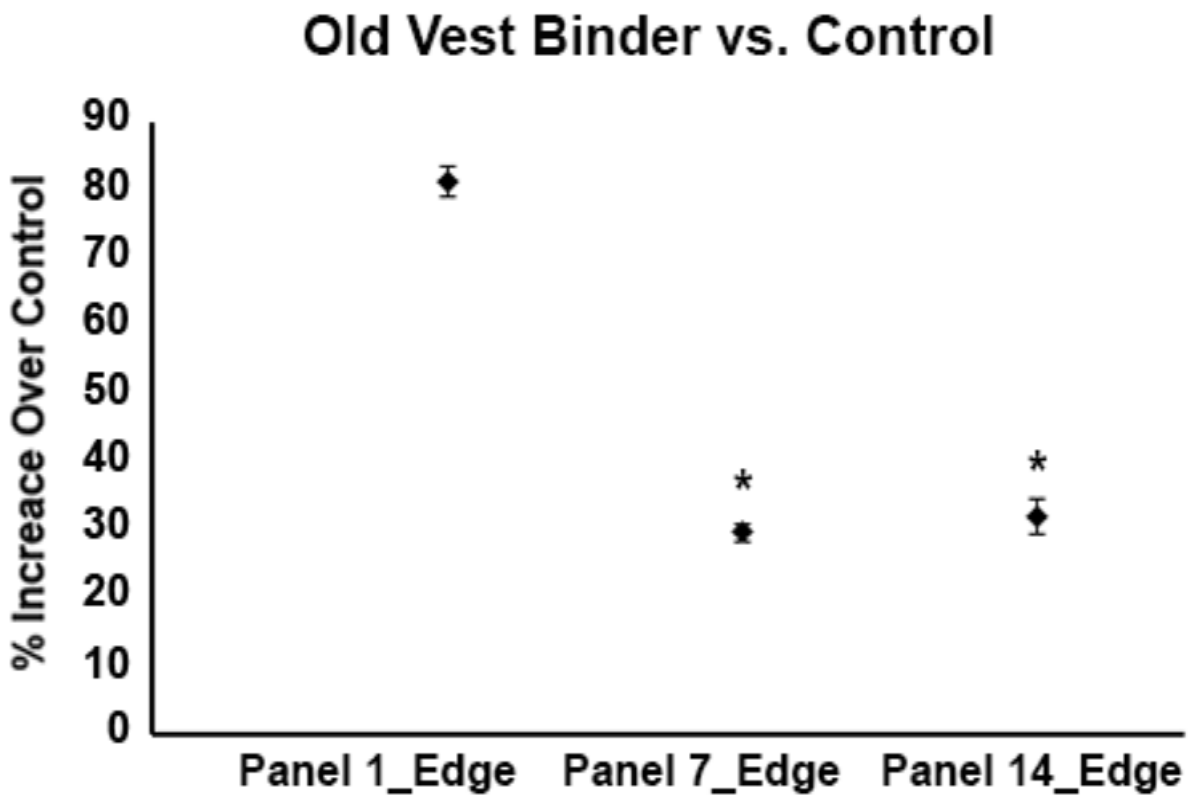

Figure 46. Percent increase in the area under the carbonyl peak at 1700 cm^{-1} of binder extracted from NIJ conditioned vests over the control. Samples from different laminates are compared. For each sample, 3 FTIR spectra were obtained and integrated. *≤0.05, compares each sample with "Panel 1_Edge" by Student's t-test. Data are mean ± S.E.M. (n=3).

The results from Figure 46 demonstrate a significant increase in the carbonyl peak of the binder material of 81.5%±2.2, between the new and the aged vests. Furthermore, moving towards the middle portion of the body armor, oxidation is limited by oxygen diffusion, which significantly decreases the percent increase in the carbonyl peak of the binder samples over the control. Also, samples extracted from the center part and the edges of these laminates were tested. The results are summarized in Figure 47.

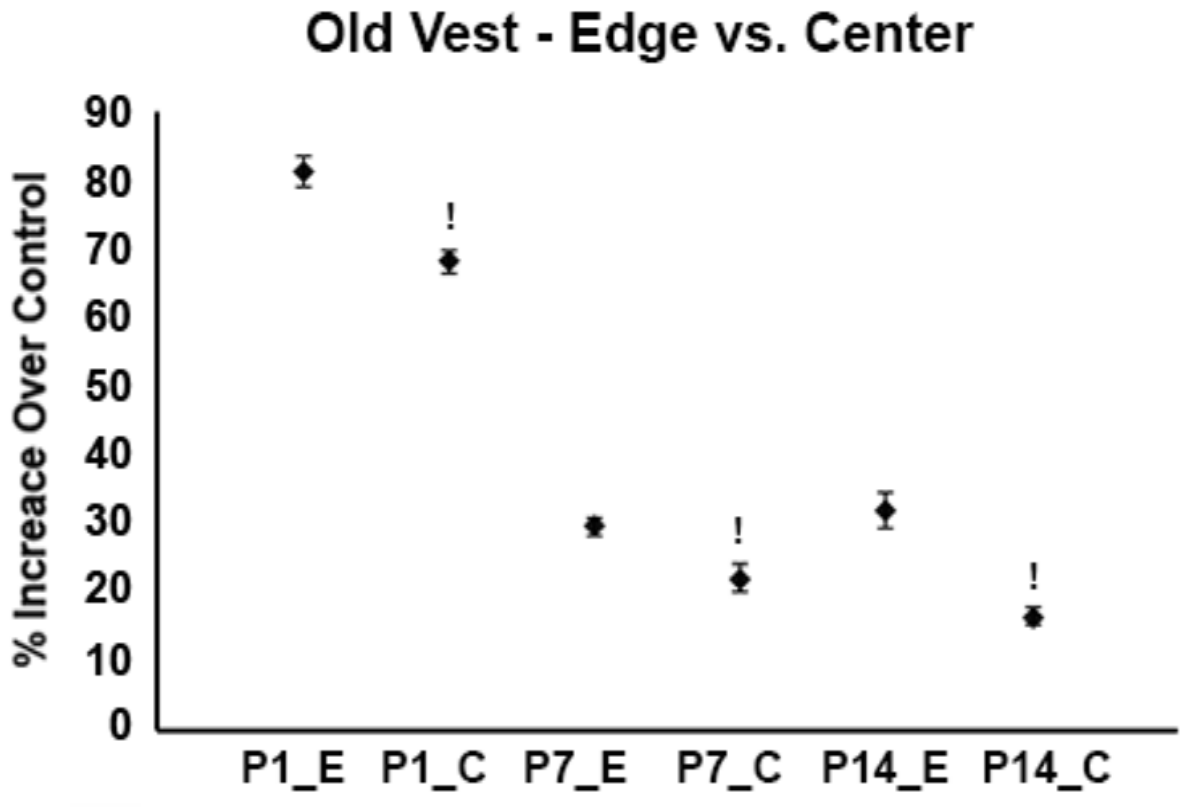

Figure 47. Percent increase in the area under the carbonyl peak at 1700 cm^{-1} of binder extracted from NIJ conditioned vests over the control. Samples from different laminates are compared. For each sample, 3 FTIR spectra were obtained and integrated. *≤0.05, compares each sample with "Panel 1_Edge" by Student's t-test. Data are mean ± S.E.M. (n=3).

Ultimately, a statistically significant decrease in the number of carbonyl groups detected within binder samples from the edges and the center of the laminates was observed. These oxidation results clearly demonstrate that the binder is adversely affected by the accelerating aging conditions used to age the body armor. However, binder material that resides in the inner part of the laminates and the body armor is affected to a lesser extent.

5.4 Characterization of Molecular Weight

When oxidation takes place in polymeric materials, it is accompanied by bond scission reactions that will shorten the length of the polymer chain and result in a decrease of the molecular weight. In this study binder samples were extracted from different laminates as well as different areas on the laminates, and their molecular weight was characterized via GPC analysis. Binder extracted from the center part of the 14th laminate was used as a control. The results showing the average number molecular weight of the material are summarized in Figure 48.

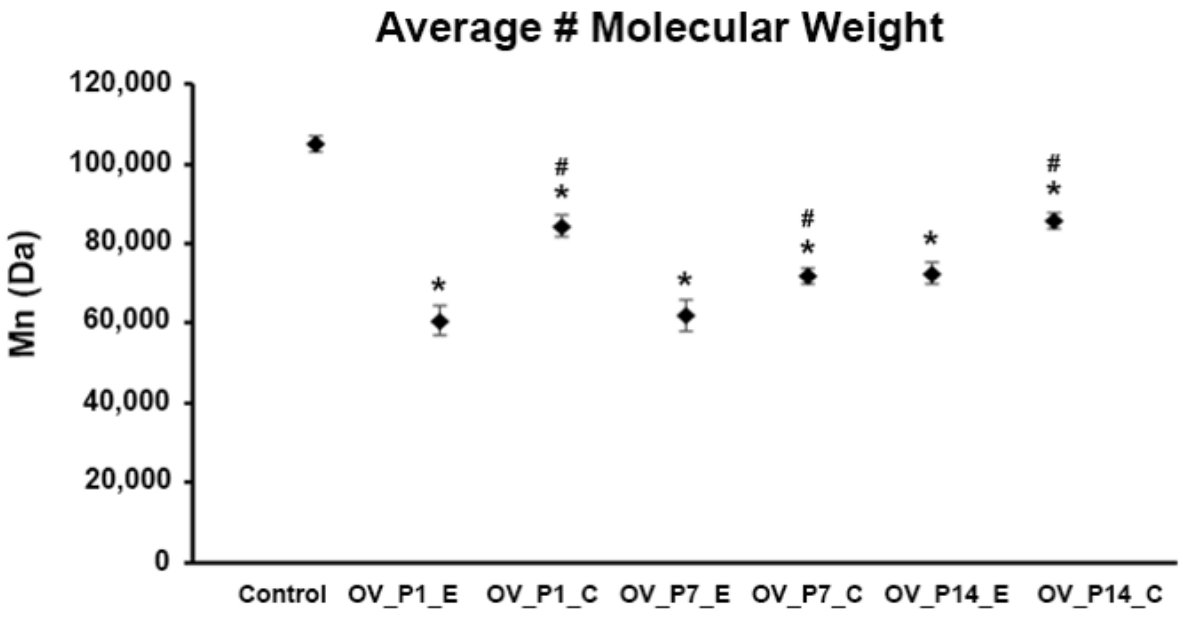

Figure 48. Changes in the number average molecular weight of the binder material after accelerated aging of the body armor via the NIJ protocol. Binder was extracted from the center part and edges of different laminates. The control was binder extracted from the center part of the 1st laminate of a new body armor. *p≤0.05, compares everything to the control; #p≤0.05, compares edge versus center samples, by Student's t-test. Data are means ± S.E.M. (n=3).

These results show that there is a statistically significant decrease in the molecular weight of the binder material compared to the control across the entire mass of the body armor. Also, the is a statistically significant decrease in the molecular weight of the binder material extracted when comparing edge vs. center parts of the laminate, and that is true for all the different laminates tested. Finally, one should note that the oxidation data collected from different areas of different laminates follow the same pattern as the molecular weight results. This leads to the conclusion that the decrease in the molecular weight is a result of the oxidation reactions happening in the polymer.

5.5 Summary

In this chapter the degradation of the binder material extracted from UHMWPE body armor was evaluated. The results demonstrate that the elastomer material used in the body armor characterized in this study is an 18% polystyrene-polyisoprene copolymer. This elastomer material undergoes degradation in a similar way to UHMWPE. Elevated temperatures will induce bond scissions in the backbone of the elastomer. This leads to the formation of C-centered free radicals. These free radicals will react with oxygen to produce peroxy radicals, such as in the case of the polyethylene. The FTIR results prove that carbonyl groups are forming in the binder material due to the oxidative reactions occurring. Additionally, the oxidation was shown to be significantly affected by the diffusion of oxygen into the material. Finally, the GPC results revealed that the molecular weight of the elastomer decreases significantly upon aging. These results are in accordance with the oxidation results, showing that degradation of the binder material is more profound in the outer most regions of the body armor.

Chapter 6: Conclusions and Future Work

6.1 Contribution to Science

6.1.1 UHMWPE as a Model Compound for Certain Biological Compounds

The proposed C-centered free radical degradation mechanisms of the UHMWPE can be used as a model for other biological molecules such as DNA, proteins, fatty acids, and cellulose. Despite their enormous differences in the chemical structures with PE, these molecules undergo degradation through C-centered radicals (R-C•), as in the case of the UHMWPE. In all cases, the C-centered radicals are produced from the rupture of C-C bonds in the backbone of the molecules. Also, because of the reductive nature of these C-centered radicals, they react very rapidly with available molecular oxygen to produce the corresponding peroxy radicals (R-CO_2•) and initiate the first step of the oxidation process:

R-C• + O_2 → R-CO_2•

This work has also shown that these peroxy radicals undergo a series of reactions, which further induce bond scissions in the backbone of the polymeric molecules, and produce oxidation products, such as ketones, esters, and CO. This can apply to a certain extent to biological molecules. Among the reactions of R-CO_2•, is the recombination reaction leading to the production of the unstable tetraoxide (ROOOOR). The decomposition of ROOOOR into ketone has been found as an oxidative product in UHMWPE, proteins, and fatty acids.

6.1.2 Kink Band Formation in UHMWPE Fibers

This work, for the first time, fully characterized kink bands formed in UHMWPE fibers extracted from body armor. These defects have been previously studied in other high strength fibers, such as PPTA and PBO fibers [114, 115]. However, this study shows that compressive forces in UHMWPE, originating from bending of the fibers, result in the formation of kink bands and knuckles. Additionally, kink bands in UHMWPE fibers were characterized by X-ray elemental and IR analysis, and the results showed higher levels of oxidation in the kink bands as compared to other areas of the fibers.

6.1.3 The Synergetic Effects of Mechanical and Oxidative Degradation

This work shows for the first time that the concentration of oxygen is higher in the mechanically-induced kink bands and knuckles compared to other parts of the fibers. This can be explained by the fact that molecular oxygen can diffuse into these areas more easily than other regions, due to the formation of micro-voids in the structure of the fibers. It should also be mentioned that some oxidative intermediates such as tetraoxide decompose to stable and other unstable oxidative products and produce O_2.

$$RCOOOCR \rightarrow RC{=}O + RCOH + O_2$$

$$2ROO \rightarrow RCOOCR + O_2$$

This is specifically important for the areas in the polymer where O_2 from the surrounding environment is difficult to diffuse.

6.1.4 Oxidation Takes Place Mainly in the Amorphous Regions

The DSC results clearly demonstrate that there is no decrease in the total degree of crystallinity in UHMWPE fibers. This may suggest that the oxidation mainly takes place in the amorphous regions and at the interfaces between the crystalline and the amorphous regions. Based on this conclusion, total crystallinity should be closely monitored and maximized during the production of UHMWPE fibers.

6.1.5 The Absence of Unsaturation due to the Presence of Oxygen

It is very common that C-centered radicals in PE undergo disproportionation reaction leading to the formation of the unsaturation according to the following reaction:

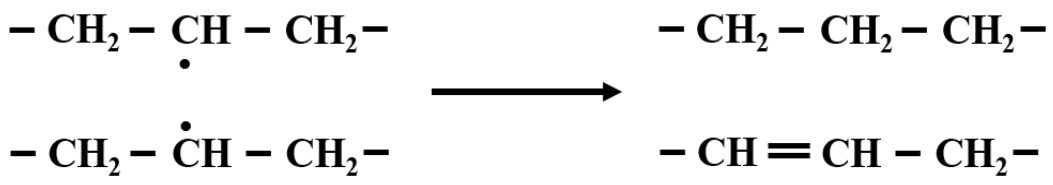

However, no FTIR absorption at around 980 cm^{-1} was detected. This can be explained by the fact that a state of competition reactions has been established between the reaction of C-centered radicals with oxygen, and the disproportionation reaction. It is concluded that the reaction with oxygen is the predominant one, which makes the fiber more prone to oxidation.

6.1.6 Crystal Phase Formation during Manufacturing

The DSC results on the new vest (not aged) fibers show the presence of the monoclinic (136 °C), and the orthorhombic (147 °C) phases. This was further supported by the WAXS results that revealed the preens of monoclinic and orthorhombic diffraction peaks.

6.1.7 Importance of Crystal Morphology of Fibers in Body Armor Applications

The DSC and WAXS data obtained in this study demonstrate that the fibers used in the body armor have different types of crystal structures, including monoclinic and orthorhombic. This leads to the conclusion that the manufacturer used high drawing ratios at various high temperatures to produce these fibers [104]. Drawing ratios and temperature control significantly affects the crystal morphology of fibers. In body armor applications it is of major importance to produce not only highly crystalline fibers, but also fibers with uniform crystal structures. Therefore, the results from this study suggest that a standard protocol should be developed to produce highly crystalline fibers with consistently uniform crystals during manufacturing.

6.2 Future Work

While the work described herein resulted in some very important conclusions about the degradation mechanisms in UHMWPE fibers extracted from body armors and the effects of accelerated aging in the binder material of the armor, there remain many additional areas for future work. First, to better understand the crystal structure of the UHMWPE fibers used in this application we need to conduct more DSC measurments, testing fibers that are not drawn, less drawn, or more drawn that those studied in this work. This will provide some useful information about the melting peak at ~153 °C observed in this study, and whether this peak is associated with the hexagonal phase or not. We expect that un-drawn fibers will not develop a hexagonal melting point during the DSC testing and if also there is no peak formed at ~153 °C for these fibers, this will support our hypothesis that this peak is somehow associated to the hexagonal phase of the material.

Additionally, the molecular weight of the UHMWPE fibers can be characterized before and after aging to support the oxidation data shown in this study. GPC analysis was attempted, but high temperatures are required to retain the polymer in the solution, which make it difficult to measure even with a high temperature GPC. Therefore, viscometry can be used as an alternative. A solvent, such as decahydranapthalene, can be used to solubilize the fibers and then molecular weight will be determined by measuring the flow time from a certain start point to an end point in a viscometer, submerged in an oil bath kept at 135 °C. However, viscometry does not yield the absolute molecular weight value. Instead, it only provides us with a relative measure of the polymer's molecular weight. In order to dissolve UHMWPE fibers in decahydranapthalene a reflux apparatus needs to be assembled. The solution needs to be warmed to 150 °C. Pentaerythritol

tetrakis (3,5-di-tert-butyl-4-hydroxyhydrocinnamate) should be added, as an antioxidant. The viscometer will be first calibrated with pure decahydranapthalene solution at 135 °C. Calculations of molecular weight will be performed in accordance with ASTM D 1601 standard. Lastly, static light scattering measurements coupled to a size separation method can be used as an alternative to evaluate the molecular weight distribution of UHMWPE.

To evaluate the degradation of the UHMWPE fibers due to bond scission, either the molecular weight distribution or oxidation byproducts can be monitored. Fragmentation reactions occurring during the thermal-oxidation can lead to the formation of carbon dioxide, as shown below:

To measure the concentration of CO_2, a gas chromatographer coupled to a mass spectrometer can be connected directly to the conditioning chambers. As oxidation reactions take place, changes in the concentration of CO_2 in the chamber can be measured in situ.

The formation of free radicals in UHMWPE fibers is of major importance according to the oxidation mechanism proposed in this work. Carbon-centered free radicals will be produced mainly in the amorphous areas of the polymer through bond scissions induced by mechanical stress and elevated temperatures. Identifying the species and the concentration of these free radicals is crucial to further support the evidence from the oxidation products in this study, and shed light to the present of anti-oxidants in the fibers. Electron paramagnetic resonance spectroscopy (EPR) can be used to determine the following free radicals: alkyl, allyl, polyenyle, peroxy, and alcoxy free radicals. To this end, fibers should be extracted from NIJ accelerated aged body armor and from laminates conditioned with the folding protocol. The results can be compared to the spectra of free radicals identified by O'Neill et al. [116].

Next, much work still remains to examine in which way oxidative degradation and how the changes in the crystalline morphology of UHMWPE fibers discussed in this work translate to changes in the mechanical properties of the fibers. To measure the mechanical properties of the material an Instron Model 5582 test frame equipped with a 1 kN load cell and pneumatic yarn and cord grips (Instron model 2714-006) will be used to measure the breaking strength of new, aged, and folded UHMWPE fibers. SEM can be performed on the samples before and after, and effort will be put to identify if the break occurred at a kink band or at a random area on the fiber. Also, ultimate tensile strength (UTS) and Young's modulus (E) of single UHMWPE fibers extracted from body armor can be measured.

Peel adhesion tests should be developed and performed to relate the degradation of the binder material characterized in this work to the adhesive properties of the binder and the physical changes at the binder-fiber interface. ASTM standard F88 can be used, which was developed for seal strength testing of flexible barrier materials. The tests will be conducted at an angle of 180°. Laminates need to be cut to an appropriate size, according to the grip dimensions. Grips can be mechanical or pneumatic. The edges of the laminates under examination should be separated and the LDPE films can be clamped in a tensile testing machine. The adhesive properties of the binder can be tested at various rates of grip separation between 200 and 300mm/min. For each measurement the maximum force as the specimen is stressed to separate will be reported. The same protocol can be used to perform fiber pull out tests to evaluate the adhesion of a fiber onto the laminate matrix. In this case the panel should be separated in half first. Then, fibers will be pulled individually from the matrix.

Finally, there is a great amount of heat generated upon the impact of a projectile with the body armor. The local increase in temperature is created by the friction upon impact and its heat

dissipation through the materials, especially the fibers. The heat transfer through the UHMWPE ballistic inserts and the temperature gradient created is not yet measured or modeled.

Bibliography

[1] Tompkins D. Body armor safety initiative: To protect and serve... better. NIJ Journal 2006;254.

[2] Gulmine JV, Janissek PR, Heise HM, Akcelrud L. Degradation profile of polyethylene after artificial accelerated weathering. Polymer Degradation and Stability 2003;79:385-97.

[3] Weon J-I. Effects of thermal ageing on mechanical and thermal behaviors of linear low density polyethylene pipe. Polymer Degradation and Stability 2010;95:14-20.

[4] Guedes RM. Analysis of temperature and aging effects on biomedical ultra-high molecular weight polyethylene's grades using a viscoelastic model. Polymer Testing 2011;30:641-50.

[5] Jahan MS, Durant J. Investigation of the oxygen-induced radicals in ultra-high molecular weight polyethylene. Nuclear Instruments and Methods in Physics Research Section B: Beam Interactions with Materials and Atoms 2005;236:166-71.

[6] NIJ. Status report to the Attorney General of body armomr safety initiative testing and activities. NIJ Special Report 2004.

[7] NIJ. Third status report to the Attorney General on body armor safety initiative testing and activities. NIJ Special Report 2005.

[8] Grujicic M, Arakere G, He T, Bell WC, Cheeseman BA, Yen CF, et al. A ballistic material model for cross-plied unidirectional ultra-high molecular-weight polyethylene fiber-reinforced armor-grade composites. Materials Science and Engineering: A 2008;498:231-41.

[9] Park AD. Ballistic panel. U.S. Patent No. 5,443,883 A; 1995.

[10] Hu X-D, Jenkins SE, Min BG, Polk MB, Kumar S. Rigid-Rod Polymers: Synthesis, Processing, Simulation, Structure, and Properties. Macromolecular Materials and Engineering 2003;288:823-43.

[11] Walley SM, Chapman DJ, Williamson DM, Morley MJ, Fairhead TW, Proud WG. High rate mechanical properties of Dyneema in compression. 2009;2:1133-8.

[12] Richards R. Polyethylene-structure, crystallinity and properties. Journal of Applied Chemistry 1951;1:370-6.

[13] Odian GG. Principles of polymerization. 3rd ed. New York: Wiley; 1991.

[14] Gedde U. Polymer physics: Springer Science & Business Media; 2013.

[15] Talebi S, Duchateau R, Rastogi S, Kaschta J, Peters GWM, Lemstra PJ. Molar Mass and Molecular Weight Distribution Determination Of UHMWPE Synthesized Using a Living Homogeneous Catalyst. Macromolecules 2010;43:2780-8.

[16] Kelly JM. ULTRA-HIGH MOLECULAR WEIGHT POLYETHYLENE*. Journal of Macromolecular Science, Part C: Polymer Reviews 2002;42:355-71.

[17] Painter PC, Coleman MM. Essentials of polymer science and engineering: DEStech Publications, Inc; 2008.

[18] Breslow DS, Newburg NR. Bis-(cyclopentadienyl)-titanium dichloride-alkylaluminum complexes as soluble catalysts for the polymerization of ethylene1, 2. Journal of the American Chemical Society 1959;81:81-6.

[19] Padmanabhan S, Sarma KR, Sharma S, Patel V. Controlled Catalyst Dosing: An Elegant Approach in Molecular Weight Regulation for UHMWPE. Macromolecular Reaction Engineering 2009;3:257-62.

[20] Padmanabhan S, Sarma KR, Rupak K, Sharma S. Synthesis of ultra high molecular weight polyethylene: A differentiate material for specialty applications. Materials Science and Engineering: B 2010;168:132-5.

[21] Sinn H, Kaminsky W. Ziegler-Natta catalysis. Advances in Organometallic Chemistry 1980;18:99-149.

[22] Sinn H, Kaminsky W, Vollmer HJ, Woldt R. “Living polymers” on polymerization with extremely productive Ziegler catalysts. Angewandte Chemie International Edition in English 1980;19:390-2.

[23] Jüngling S, Mülhaupt R. The influence of methylalumoxane concentration on propene polymerization with homogeneous metallocene-based Ziegler-Natta catalysts. Journal of organometallic chemistry 1995;497:27-32.

[24] Harney MB. Examination of Dynamic Processes in Living Ziegler-Natta Polymerization and New Polypropylene Architectures through Bimolecular Control. 2006.

[25] Kurtz SM. The UHMWPE handbook: ultra-high molecular weight polyethylene in total joint replacement: Academic press; 2004.

[26] Kurtz SM, Muratoglu OK, Evans M, Edidin AA. Advances in the processing, sterilization, and crosslinking of ultra-high molecular weight polyethylene for total joint arthroplasty. Biomaterials 1999;20:1659-88.

[27] Kurtz SM. UHMWPE biomaterials handbook: ultra high molecular weight polyethylene in total joint replacement and medical devices: Academic Press; 2009.

[28] Naidu SH, Bixler BL, Moulton MJ. Radiation-induced physical changes in UHMWPE implant components. Orthopedics 1997;20:137-42.

[29] Callister WD, Rethwisch DG. Materials science and engineering: an introduction: Wiley New York; 2007.

[30] Mann G. Encyclopedia of polymer science and engineering. Acta Polymerica 1989;40:137-8.

[31] Li C-S, Zhan M-S, Huang X-C, Zhou H. Degradation behavior of ultra-high molecular weight polyethylene fibers under artificial accelerated weathering. Polymer Testing 2012;31:938-43.

[32] Chin J, Petit S, Forster A, Riley M, Rice K. Effect of artificial perspiration and cleaning chemicals on the mechanical and chemical properties of ballistic materials. Journal of Applied Polymer Science 2009;113:567-84.

[33] Fisch AG, da Silveira N, Cardozo NSM, Secchi AR, dos Santos JHZ, Soares JBP. Direct production of ultra-high molecular weight polyethylene with oriented crystalline microstructures. Journal of Molecular Catalysis A: Chemical 2013;366:74-83.

[34] Barham PJ, Keller A. High-strength polyethylene fibres from solution and gel spinning. Journal of Materials Science 1985;20:2281-302.

[35] Pennings AJ, van der Hooft RJ, Postema AR, Hoogsteen W, ten Brinke G. High-speed gel-spinning of ultra-high molecular weight polyethylene. Polymer Bulletin 1986;16:167-74.

[36] Yao J, Bastiaansen C, Peijs T. High Strength and High Modulus Electrospun Nanofibers. Fibers 2014;2:158.

[37] Smook J, Pennings AJ. Preparation of ultra-high strength polyethylene fibres by gel-spinning/hot-drawing at high spinning rates. Polymer Bulletin 1983;9.

[38] Kanamoto T, Tsuruta A, Tanaka K, Takeda M, Porter RS. Super-drawing of ultrahigh molecular weight polyethylene. 1. Effect of techniques on drawing of single crystal mats. Macromolecules 1988;21:470-7.

[39] Peterlin A. Drawing and extrusion of semi-crystalline polymers. Colloid and polymer science 1987;265:357-82.

[40] Peterlin A. Annealing of drawn crystalline polymers. Polymer Engineering & Science 1978;18:488-95.

[41] Ottani S, Ferracini E, Ferrero A, Malta V, Porter RS. SAXS investigations on uniaxially drawn fibers obtained from polyethylene reactor powder. Macromolecules 1996;29:3292-9.

[42] Ratner S, Weinberg A, Wachtel E, Moret P, Marom G. Phase transitions in UHMWPE fiber compacts studied by in situ synchrotron microbeam WAXS. Macromolecular rapid communications 2004;25:1150-4.

[43] Garcia-Leiner M, Song J, Lesser AJ. Drawing of ultrahigh molecular weight polyethylene fibers in the presence of supercritical carbon dioxide. Journal of Polymer Science Part B: Polymer Physics 2003;41:1375-83.

[44] Berger L, Kausch HH, Plummer CJG. Structure and deformation mechanisms in UHMWPE-fibres. Polymer 2003;44:5877-84.

[45] Hu WG, Schmidt-Rohr K. Characterization of ultradrawn polyethylene fibers by NMR: crystallinity, domain sizes and a highly mobile second amorphous phase. Polymer 2000;41:2979-87.

[46] Fu Y, Chen W, Pyda M, Londono D, Annis B, Boller A, et al. Structure-property analysis for gel-spun, ultrahigh molecular mass polyethylene fibers. Journal of Macromolecular Science, Part B 1996;35:37-87.

[47] Litvinov VM, Xu J, Melian C, Demco DE, Möller M, Simmelink J. Morphology, Chain Dynamics, and Domain Sizes in Highly Drawn Gel-Spun Ultrahigh Molecular Weight Polyethylene Fibers at the Final Stages of Drawing by SAXS, WAXS, and1H Solid-State NMR. Macromolecules 2011;44:9254-66.

[48] Bunn C. Fibers from synthetic polymers. R Hill. Elsevier, Amsterdam; 1953.

[49] Yeh J-T, Lin S-C, Tu C-W, Hsie K-H, Chang F-C. Investigation of the drawing mechanism of UHMWPE fibers. Journal of Materials Science 2008;43:4892-900.

[50] Lee BL, Walsh TF, Won ST, Patts HM, Song JW, Mayer AH. Penetration Failure Mechanismsof Armor-Grade FiberComposites under Impact. Journal of Composite Materials 2001;35:1605-33.

[51] Prevorsek DC, Kwon YD, Chin HB. Analysis of the temperature rise in the projectile and extended chain polyethylene fiber composite armor during ballistic impact and penetration. Polymer Engineering and Science 1994;34:141-52.

[52] Park AD, Park D, Park AJ. Ballistic laminate structure in sheet form. Google Patents; 2006.

[53] Park AD. Ballistic panel. Google Patents; 1995.

[54] Harpell GA, Prevorsek DC, Li HL. Flexible multi-layered armor. U.S. Patent No. 5,175,040 A; 1992.

[55] Schnabel W. Polymer degradation : principles and practical applications. New York: Hanser International; 1981.

[56] Nguyen TQ, Liang QZ, Kausch H-H. Kinetics of ultrasonic and transient elongational flow degradation: a comparative study. Polymer 1997;38:3783-93.

[57] Nguyen TQ, Kausch H-H. Chain extension and degradation in convergent flow. Polymer 1992;33:2611-21.

[58] Forster AL, Rice KD, Riley MA, Messin G, Petit S, Clerici C, et al. Development of soft armor conditioning protocols for NIJ standard-0101.06: Analytical results. National Institute of Standards and Technology 2009.

[59] Stadler FJ, Kaschta J, Münstedt H. Dynamic-mechanical behavior of polyethylenes and ethene-/α-olefin-copolymers. Part I. α′-Relaxation. Polymer 2005;46:10311-20.

[60] Rodriguez F, Cohen C, Ober CK, Archer L. Principles of polymer systems: CRC Press; 2014.

[61] Coote CF, Hamilton JV, McGimpsey WG, Thompson RW. Oxidation of gamma-irradiated ultrahigh molecular weight polyethylene. Journal of applied polymer science 2000;77:2525-42.

[62] Martínez-Morlanes M, Castell P, Alonso PJ, Martinez MT, Puértolas J. Multi-walled carbon nanotubes acting as free radical scavengers in gamma-irradiated ultrahigh molecular weight polyethylene composites. Carbon 2012;50:2442-52.

[63] Cottrell T. The Strength of Chemical Bonds, 2nd edit. Butterworths: London; 1958.

[64] Ivanov VacS. Radiation chemistry of polymers: Vsp; 1992.

[65] Clegg D, Collyer AA. Irradiation effects on polymers. 1991.

[66] Johnson W, Lyons B. Radiolytic formation and decay of trans-vinylene unsaturation in polyethylene: Fourier transform infra-red measurements. Radiation Physics and Chemistry 1995;46:829-32.

[67] Dole M, Milner D, Williams TF. Irradiation of polyethylene. II. Kinetics of unsaturation effects. Journal of the American Chemical Society 1958;80:1580-8.

[68] Shah Jahan M. ESR Insights into Macroradicals in UHMWPE. The 2nd edition of the UHMWPE biomaterials handbook 2009:433-50.

[69] Arnaud R, Moisan JY, Lemaire J. Primary hydroperoxidation in low-density polyethylene. Macromolecules 1984;17:332-6.

[70] Lacoste J, Carlsson D. Gamma-, photo-, and thermally-initiated oxidation of linear low density polyethylene: A quantitative comparison of oxidation products. Journal of Polymer Science Part A: Polymer Chemistry 1992;30:493-500.

[71] Costa L, Luda M, Trossarelli L, Del Prever EB, Crova M, Gallinaro P. Oxidation in orthopaedic UHMWPE sterilized by gamma-radiation and ethylene oxide. Biomaterials 1998;19:659-68.

[72] DeVries K, Smith R, Fanconi B. Free radicals and new end groups resulting from chain scission: 1. y-irradiation of polyethylene. Polymer 1980;21:949-56.

[73] Collier JP, Sperling DK, Currier JH, Sutula LC, Saum KA, Mayor MB. Impact of gamma sterilization on clinical performance of polyethylene in the knee. The Journal of arthroplasty 1996;11:377-89.

[74] Lazár M. Free radicals in chemistry and biology: CRC press; 1989.

[75] Gates BC, Katzer JR, Schuit GC. Chemistry of catalytic processes: McGraw-Hill New York; 1979.

[76] Costa L, Bracco P. Mechanisms of crosslinking, oxidative degradation and stabilization of UHMWPE. UHMWPE Biomaterials Handbook 2009:309.

[77] Pauly S. Permeability and Diffusion Data in Polymer Handbook, edited by J. Brandrup, EH Immergut. Wiley Interscience, New York; 1989.

[78] Michaels AS, Bixler HJ. Solubility of gases in polyethylene. Journal of Polymer Science 1961;50:393-412.

[79] Capaccio G, Ward I. Structural studies of ultrahigh-modulus linear polyethylene using nitric acid etching and gel permeation chromatography. I. Determination of the crystal size distribution. Journal of Polymer Science: Polymer Physics Edition 1981;19:667-75.

[80] Holden P, Orchard G, Ward I. A study of the gas barrier properties of highly oriented polyethylene. Journal of Polymer Science: Polymer Physics Edition 1985;23:709-31.

[81] Daly BM, Yin J. Subsurface oxidation of polyethylene. Journal of biomedical materials research 1998;42:523-9.

[82] Woods RJ, Pikaev AK. Applied radiation chemistry: radiation processing: John Wiley & Sons; 1994.

[83] Lacoste J, Carlsson D, Falicki S, Wiles D. Polyethylene hydroperoxide decomposition products. Polymer degradation and stability 1991;34:309-23.

[84] Costa L, Luda M, Trossarelli L. Ultra-high molecular weight polyethylene: I. Mechano-oxidative degradation. Polymer degradation and stability 1997;55:329-38.

[85] Bolland J. Kinetic studies in the chemistry of rubber and related materials. I. The thermal oxidation of ethyl linoleate. Proceedings of the Royal Society of London A: Mathematical, Physical and Engineering Sciences: The Royal Society; 1946. p. 218-36.

[86] Lundbäck M, Hedenqvist M, Mattozzi A, Gedde U. Migration of phenolic antioxidants from linear and branched polyethylene. Polymer degradation and stability 2006;91:1571-80.

[87] Moss S, Zweifel H. Degradation and stabilization of high density polyethylene during multiple extrusions. Polymer Degradation and Stability 1989;25:217-45.

[88] Oral E, Christensen SD, Malhi AS, Wannomae KK, Muratoglu OK. Wear resistance and mechanical properties of highly cross-linked, ultrahigh–molecular weight polyethylene doped with vitamin E. The Journal of arthroplasty 2006;21:580-91.

[89] Tomita N, Kitakura T, Onmori N, Ikada Y, Aoyama E. Prevention of fatigue cracks in ultrahigh molecular weight polyethylene joint components by the addition of vitamin E. Journal of biomedical materials research 1999;48:474-8.

[90] Peltzer M, Wagner J, Jiménez A. Thermal characterization of UHMWPE stabilized with natural antioxidants. Journal of Thermal Analysis and Calorimetry 2007;87:493-7.

[91] Bladen C, Tzu-Yin L, Fisher J, Tipper J. In vitro analysis of the cytotoxic and anti-inflammatory effects of antioxidant compounds used as additives in ultra high-molecular weight polyethylene in total joint replacement components. Journal of Biomedical Materials Research Part B: Applied Biomaterials 2013;101:407-13.

[92] Chumakov MK. The Novel Use of Nitroxide Antioxidants as Free Radical Scavengers in Ultra-High Molecular Weight Polyethylene (UHMWPE) for Total Joint Replacements. 2010.

[93] Forster AL, Forster AM, Chin JW, Peng J-S, Lin C-C, Petit S, et al. Long-term stability of UHMWPE fibers. Polymer Degradation and Stability 2015;114:45-51.

[94] Mukasey M, Sedgwick J, Hagy D. Ballistic Resistance of Body Armor, NIJ Standard-0101.06. US Department of Justice (www ojp usdoj gov/nij) 2008.

[95] Takahashi T, Miura M, Sakurai K. Deformation band studies of axially compressed poly (p-phenylene terephthalamide) fiber. Journal of Applied Polymer Science 1983;28:579-86.

[96] Edmunds R, Wadee MA. On kink banding in individual PPTA fibres. Composites Science and Technology 2005;65:1284-98.

[97] Hunt GW, Peletier MA, Wadee MA. The Maxwell stability criterion in pseudo-energy models of kink banding. Journal of Structural Geology 2000;22:669-81.

[98] Dobb M, Johnson D, Saville B. Compressional behaviour of Kevlar fibres. Polymer 1981;22:960-5.

[99] Leal AA, Deitzel JM, Gillespie JW. Compressive strength analysis for high performance fibers with different modulus in tension and compression. Journal of composite materials 2009;43:661-74.

[100] Lorenzo-Villafranca E, Tamargo-Martínez K, Molina-Aldareguia JM, González C, Martínez-Alonso A, Tascón JMD, et al. Influence of plasma surface treatments on kink band

formation in PBO fibers during compression. Journal of Applied Polymer Science 2012;123:2052-63.

[101] Teodoru S, Kusano Y, Rozlosnik N, Michelsen PK. Continuous Plasma Treatment of Ultra-High-Molecular-Weight Polyethylene (UHMWPE) Fibres for Adhesion Improvement. Plasma Processes and Polymers 2009;6:S375-S81.

[102] Tashiro K, Sasaki S, Kobayashi M. Structural investigation of orthorhombic-to-hexagonal phase transition in polyethylene crystal: the experimental confirmation of the conformationally disordered structure by X-ray diffraction and infrared/Raman spectroscopic measurements. Macromolecules 1996;29:7460-9.

[103] ASTMF2625. Standard Test Method for Measurement ofEnthalpy of Fusion, Percent Crystallinity, and Melting Pointof Ultra-High-Molecular Weight Polyethylene by Means ofDifferential Scanning Calorimetry. ASTM: West Consho-hocken. PA2010.

[104] Rein DM, Shavit L, Khalfin RL, Cohen Y, Terry A, Rastogi S. Phase transitions in ultraoriented polyethylene fibers under moderate pressures: A synchrotron X-ray study. Journal of Polymer Science Part B: Polymer Physics 2004;42:53-9.

[105] Kwon Y, Boller A, Pyda M, Wunderlich B. Melting and heat capacity of gel-spun, ultra-high molar mass polyethylene fibers. Polymer 2000;41:6237-49.

[106] Devaux E, Cazé C. Composites of UHMW polyethylene fibres in a LD polyethylene matrix. I. Processing conditions. Composites science and technology 1999;59:459-66.

[107] Smith P, Lemstra PJ, Kalb B, Pennings AJ. Ultrahigh-strength polyethylene filaments by solution spinning and hot drawing. Polymer Bulletin 1979;1:733-6.

[108] Ratner S, Weinberg A, Wachtel E, Moret PM, Marom G. Phase Transitions in UHMWPE Fiber Compacts Studied by in situ Synchrotron Microbeam WAXS. Macromolecular Rapid Communications 2004;25:1150-4.

[109] Satoh K, Aoshima H, Kamigaito M. Iron (III) chloride/R-Cl/tributylphosphine for metal-catalyzed living radical polymerization: A unique system with a higher oxidation state iron complex. Journal of Polymer Science Part A: Polymer Chemistry 2008;46:6358-63.

[110] Rozentsvet V, Khachaturov A, Ivanova V. Microstructure of polyisoprene produced by cationic polymerization: NMR spectroscopic study. Polymer Science Series A 2009;51:870-6.

[111] Li G-Y, Koenig J. FT-IR imaging of the thermal oxidation of polyisoprene (PI) rubber at high temperature. Applied spectroscopy 2002;56:1390-6.

[112] Faravelli T, Pinciroli M, Pisano F, Bozzano G, Dente M, Ranzi E. Thermal degradation of polystyrene. Journal of analytical and applied pyrolysis 2001;60:103-21.

[113] Chen F, Qian J. Studies on the thermal degradation of cis-1, 4-polyisoprene. Fuel 2002;81:2071-7.

[114] Chau C, Blackson J, Im J. Kink bands and shear deformation in polybenzobisoxazole fibres. Polymer 1995;36:2511-6.

[115] Deteresa S, Nicolais L. The contribution of thermal stresses to the failure of Kevlar fabric composites. Polymer composites 1988;9:192-7.

[116] O'Neill P, Birkinshaw C, Leahy JJ, Barklie R. The role of long lived free radicals in the ageing of irradiated ultra high molecular weight polyethylene. Polymer Degradation and Stability 1999;63:31-9.